Oxidative Assembly of the Outer Membrane Lipopolysaccharide Translocon LptD/E and Progress towards Its X-Ray Crystal Structure

Citation

Garner, Ronald Aaron. 2014. Oxidative Assembly of the Outer Membrane Lipopolysaccharide Translocon LptD/E and Progress towards Its X-Ray Crystal Structure. Doctoral dissertation, Harvard University.

Permanent link

http://nrs.harvard.edu/urn-3:HUL.InstRepos:13064991

Terms of Use

Share Your Story

The Harvard community has made this article openly available.
Please share how this access benefits you. Submit a story .

Accessibility

Oxidative Assembly of the Outer Membrane Lipopolysaccharide Translocon LptD/E and

Progress towards Its X-Ray Crystal Structure

A dissertation presented

by

Ronald Aaron Garner

to

The Department of Chemistry and Chemical Biology

in partial fulfillment of the requirements

for the degree of

Doctor of Philosophy

in the subject of

Chemistry

Harvard University

Cambridge, Massachusetts

June 2014

Dissertation Advisor: Professor Daniel Kahne   Ronald Aaron Garner

Oxidative Assembly of the Outer Membrane Lipopolysaccharide Translocon LptD/E and

Progress towards Its X-Ray Crystal Structure

Abstract

Lipopolysaccharide (LPS) is the glycolipid that comprises the outer leaflet of the Gram-negative outer membrane (OM). Because it is essential in nearly all Gram-negative species, and because it is responsible for making these bacteria impervious to many types of antibiotics, LPS biogenesis has become an important area of research. While its biosynthesis at the cytoplasmic face of the inner membrane (IM) is well studied, the process by which it is removed from the IM, transported across the aqueous periplasmic compartment, and specifically inserted into the outer leaflet of the OM is only beginning to be understood. This transport process is mediated by the essential seven-protein LPS transport (Lpt) complex, LptA/B/C/D/E/F/G. The OM portion of the exporter, LptD/E, is a unique plug-and-barrel protein complex in which LptE, a lipoprotein, sits inside of LptD, a β-barrel integral membrane protein. LptD is of particular interest, as it is the target of an antibiotic in *Pseudomonas aeruginosa*.

Part I of this thesis investigates how the cell forms the two non-consecutive disulfide bonds that connect LptD's C-terminal β-barrel to its N-terminal soluble domain. These disulfides, one of which is almost universally conserved among Gram-negatives, are essential for cell viability. Here, we show that an intermediate oxidation state with non-native disulfide bonds accumulates in the absence of LptE and in strains defective in either LptE or LptD. We then

demonstrate that this observed intermediate is on-pathway and part of the native LptD oxidative folding pathway. Using a defective mutant of DsbA, the protein that introduces disulfide bonds into LptD, we are able to identify additional intermediates in the LptD oxidative folding pathway. We ultimately demonstrate that the disulfide rearrangement that activates the LptD/E complex occurs following an exceptionally slow β-barrel assembly step and is dependent on the presence of LptE.

Part II describes work towards obtaining X-ray crystal structures of the LptD N-terminal domain and LptD/E complex. Expression construct and purification optimization enabled the production of stable LptD/E in quantities that make crystallography feasible. Numerous precipitants, detergents, and additives were screened, ultimately resulting in protein crystals that diffract to a resolution of 3.85 Å.

Table of Contents

Acknowledgements

First and foremost I must thank my advisor, Professor Daniel Kahne, for his mentorship and support. He has helped me grow as a scientist and played a critical role in the development of this thesis. He has also assembled a friendly, supportive group of graduate students and post-doctoral researchers who make his laboratory a wonderful place to work. In particular, I would like to thank Shu Sin Chng for welcoming me into the laboratory when I first began graduate school. He taught me the basics of protein biochemistry and got me started on what would eventually become my thesis. He was also a close collaborator for much of this thesis, and I thank him for his help and support in making this work possible. Next, I would like to thank Goran Malojcic, who in addition to being one of my closest friends in lab, was an essential collaborator for the crystallography projects discussed in this thesis. I would also like to thank Mingyu Xue, with whom I collaborated on the disulfide bond rearrangement project. His work was complementary to my own and allowed us to develop a more complete understanding of the system we were studying. I would also like to thank all of the current and former members of the Kahne laboratory for their help and support throughout the years. In particular, David Sherman, Joe Wzorek, Suguru Okuda, Luisa Gronenberg, Elizaveta Freinkman, Dorothee Andres, Carolin Doering, and Alex George have all either provided me with materials or offered valuable scientific discussion during my time in the Kahne laboratory. In addition to group members, I thank Helen Corriero and Mike Quinn; without them, our laboratory would cease to function.

I would also like to thank my Graduate Advisory Committee for their help throughout the years. Alan Saghatelian was helpful and supportive of my research during its formative years. Jonathan Beckwith was a collaborator for much of my thesis research, and as such, he offered

List of Abbreviations

ABC	ATP-binding cassette
ACP	Acyl carrier protein
ADP	Adenosine diphosphate
AMPPNP	Adenylyl imidodiphosphate
ATP	Adenosine triphosphate
β-ME	β-Mercaptoethanol
Bam	β-Barrel assembly machine
C_8E_4	n-octyltetraoxyethylene
C_8E_5	n-octylpentaoxyethylene
CHAPSO	3-[(3-cholamidopropyl)dimethylammonio]-2-hydroxy-1-propanesulfonate
CMP	Cytidine monophosphate
DDM	n-dodecyl-β-D-maltopyranoside
DMPC	1,2-dimyristoyl-*sn*-glycero-3-phosphocholine
DTT	Dithiothreitol
EM	Electron microscopy
ESI-MS	Electrospray ionization-mass spectroscopy
Fos-12	n-dodecylphosphocholine
Gal	D-Galactose
Glc	D-Glucose
GlcN	D-glucosamine
GlcNAc	*N*-Acetyl-D-glucosamine
Hep	L-glycero-D-*manno*-heptose
HEPES	4-(2-hydroxyethyl)-1-piperazineethanesulfonic acid
IAM	Iodoacetamide
IM	Inner membrane
IPTG	Isopropyl-β-D-1-thiogalactopyranoside
Kdo	3-deoxy-D-*manno*-oct-2-ulosonic acid
LDAO	n-dodecyl-*N*,*N*-dimethylamine-*N*-oxide, or n-lauryldimethylamine-*N*-oxide
Lol	Localization of lipoproteins
LPS	Lipopolysaccharide
Lpt	Lipopolysaccharide transport
MME	Monomethyl ether
NEM	*N*-ethylmaleimide
OAc	Acetate
OG	n-octyl- β-D-glucoside
OM	Outer membrane
OMP	Integral outer membrane protein
pBPA	Para-benzoylphenylalanine
PEG	Polyethylene glycol
PL	Phospholipid
PMSF	Phenylmethylsulfonyl fluoride
POTRA	Polypeptide transport-associated

SDS-PAGE	Sodium dodecyl sulfate polyacrylamide gel electrophoresis
SEC	Size exclusion chromatography
SeMet	L-selenomethionine
TCA	Trichloroacetic acid
TLR4	Toll-like receptor 4
Tris	2-amino-2-hydroxymethyl-propane-1,3-diol
UDP	Uridine diphosphate
UMP	Uridine monophosphate
WT	Wild-type
ZW3-14	Anzergent 3-14 (n-tetradecyl-*N*,*N*-dimethyl-3-ammonio-1-propanesulfonate)

List of Figures

Chapter 1: Introduction

1.1. Introduction

The cell envelope that surrounds Gram-negative bacteria is a double membrane structure in which the cytoplasm is enclosed by a phospholipid inner membrane (IM) that is separated from an outer membrane (OM) by an aqueous compartment known as the periplasm. The periplasm contains peptidoglycan, a polymer network that helps determine the cell's shape and protects it from osmotic stress[1,2]. The OM faces the extracellular space and acts as a barrier that protects the cell from factors such as antibiotics and hydrophobic small molecules, making Gram-negative bacteria generally more resistant to antibiotics than Gram-positive bacteria[3,4]. In contrast to the IM, the OM is an asymmetric membrane in which the inner, periplasm-facing leaflet is comprised of phospholipid, while the outer, extracellular space-facing leaflet is comprised of lipopolysaccharide (LPS). LPS, a glycolipid that is essential in most Gram-negative species, is generally credited as the source of the OM's relative impermeability[3,4]. The biogenesis of LPS begins with its synthesis in the inner leaflet of the IM and is followed by its translocation across the IM, subsequent maturation in the periplasmic leaflet of the IM, and transport from the IM, across the periplasm, to its final location in the outer leaflet of the OM. Transport across the periplasm is facilitated by the seven protein lipopolysaccharide transport (Lpt) complex, LptA/B/C/D/E/F/G.

This thesis focuses on the two proteins that comprise the OM portion of the Lpt complex, LptD and LptE. Chapter 2 describes the research that elucidated the oxidative assembly pathway for the OM LPS translocon, LptD/E, and this pathway's significance in LPS transport. Chapters

3 and 4 describe the progress that has been made towards obtaining the X-ray crystal structures of individual domains of LptD and of the two-protein LptD/E complex, respectively.

This chapter provides an overview of what is currently known regarding the structure, function, and biogenesis of the OM. Transport and assembly of the protein components of the OM are discussed with an emphasis on the transport and assembly of β-barrel integral OM proteins (OMPs). This is followed by a discussion of LPS that addresses its structure, biosynthesis, translocation across the IM, tailoring in the periplasm, and ultimate transport to the OM outer leaflet. Specific attention is paid to the Lpt complex and its components.

1.2. The outer membrane is an asymmetric permeability barrier

The primary function of the OM is to establish a permeability barrier that enables the cell to maintain favorable intracellular conditions even in harsh extracellular environments. While typical membrane bilayers are impermeable to polar solutes, the OM is additionally impermeable to lipophilic molecules[3]. This property of the OM is attributed to LPS; in fact, the presence of LPS causes the OM to be approximately two orders of magnitude less permeable to lipophilic substances than an equivalent phospholipid (PL) membrane bilayer[5,6]. The impermeability of the LPS-containing OM is due to its lack of fluidity. LPS contains numerous saturated lipid chains and is able to interact with neighboring LPS molecules via bridging divalent cations, forming a gel-like structure with very low fluidity[3].
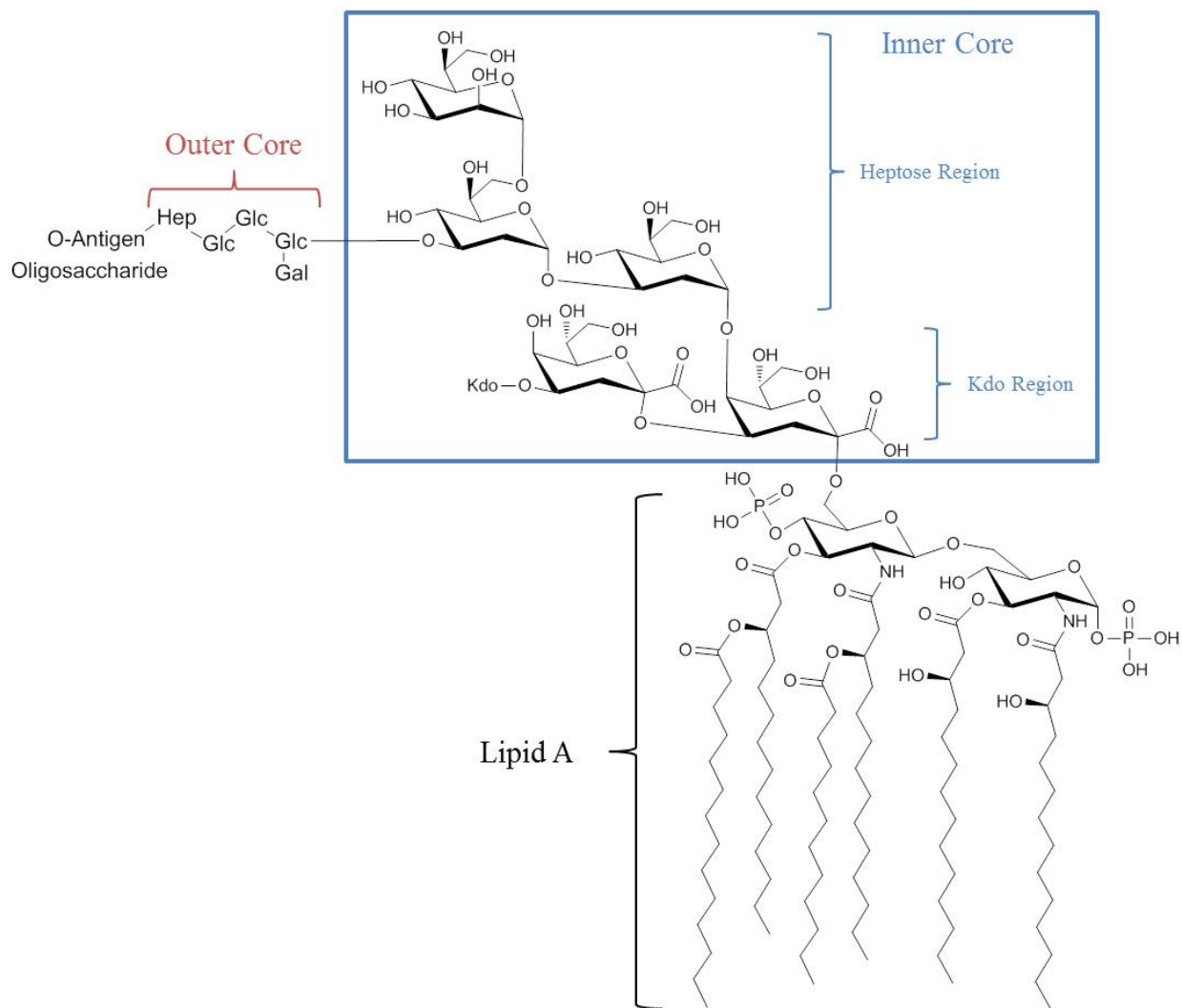
Figure 1. The general structure of LPS. Lipid A represents the membrane anchoring unit, which is connected to two monomers of Kdo to give the minimal form of LPS needed for viability, Re-LPS. Kdo is connected to a heptose region to form the remainder of the inner core. The second heptose is connected to the outer core oligosaccharide, altogether known as Ra-LPS. Ra-LPS is connected to the O-antigen oligosaccharide by the outer core. Gal, D-galactose; Glc, D-glucose; Hep, L-glycero-D-*manno*-heptose; Kdo, 3-deoxy-D-*manno*-oct-2-ulosonic acid.

Lipid A, a β-1,6 glucosamine disaccharide that is phosphorylated at positions 1 and 4'

and hexa-acylated via modifications at positions 2, 3, 2', and 3' (Figure 1), forms the lipidic

portion of LPS that anchors it into the membrane. Two monomers of Kdo (3-deoxy-D-*manno*-

oct-2-ulosonic acid) are attached to position 6' of the glucosamine disaccharide to form the

minimal unit of LPS that is necessary for *Escherichia coli* viability[7]. Additional sugars are often

present as core regions or as part of the highly variable O-antigen. The inner core region is

composed of an essential Kdo region and a heptose region. Kdo_2-Lipid A, without any additional

saccharides, is also known as Re-LPS. The inner core is connected to the outer core, as described

in Figure 1. LPS containing the core oligosaccharides, but not the O-antigen oligosaccharide, is

known as Ra-LPS[7]. The additional sugars of the core and O-antigen regions are not generally

required for viability, but may help the cells to survive in certain environments[4]. One proposed

function of the variable O-antigen sugars is to evade recognition by the immune system[7], as LPS

activates the innate immune system via toll-like receptor 4 (TLR4)[8,9]. This property of LPS is

also why it is commonly known as endotoxin.

A defining feature of the OM is its asymmetry; its outer leaflet almost exclusively

contains LPS while its inner leaflet is comprised of PL. This was first suggested by Mühlradt and

Golecki in 1975 when electron microscopy (EM) of *Salmonella typhimurium* OMs labeled with

ferritin-conjugated antibodies against LPS showed that the label was only present on the outer

leaflet of the membrane[10]. Shortly thereafter, Kamio and Nikaido reported that the head groups

of phosphatidylethanolamine, a PL, were inaccessible to modification by either *Bacillus cereus*

phospholipase C or cyanogen bromide activated dextran in whole *S. typhimurium* cells[11]. Taken

together, these results suggest that the outer leaflet of the OM exclusively contains LPS while the

inner leaflet exclusively contains PL. Subsequent research, such as the observation that nearly all

LPS in intact *S. typhimurium* cells can be oxidized by galactose oxidase, has further established the asymmetric structure of the OM[12].

In addition to lipids, the OM contains two broad classes of proteins: lipoproteins and integral outer membrane proteins (OMPs). Lipoproteins are post-translationally modified at their N-termini with three lipid chains that anchor them to the membrane, and they exist only on the periplasmic surface of the OM[13]. These proteins are known to be involved in binding to peptidoglycan[14], OM stability[15], and OM biogenesis[16]. In contrast to lipoproteins, OMPs assume a β-barrel fold that is inserted into the OM and extends from the periplasm to the extracellular space. This fold consists of a number of amphiphilic β-strands that form a continuous β-sheet in which one β-strand at the end of the β-sheet curves back around to the other side of the β-sheet to form a cylindrical barrel such that all peptide backbone hydrogen bonds are internally satisfied. The amphiphilic nature of the individual β-sheets results in a β-barrel in which the exterior is hydrophobic and the interior is hydrophilic. OMPs can feature additional N-terminal and C-terminal domains, extensive extracellular loops that connect their β-strands, and β-barrels that can vary in size from 8 to as many as 24 β-strands[17]. These features enable OMPs to be quite diverse, even though they share the same general β-barrel structure. OMPs serve a variety of purposes which generally enable the cell to be selectively permeable in order to carry out cellular functions without compromising the protection afforded by the OM. Such functions include passive nutrient exchange, either by non-specific porins or by substrate specific channels such as maltoporin, secretion of proteins and other molecules, membrane biogenesis, and even active uptake of specific substrates such as iron and vitamin B_{12}[3].

1.3. Outer membrane biogenesis

As discussed earlier, the outer membrane is a complex, asymmetric structure that is composed of LPS, PL, lipoproteins, and β-barrel OMPs. The assembly of the OM presents a challenge that the cell must overcome; since there is no source of energy in the periplasm, all OM components must be synthesized in the cytoplasm and subsequently transported to the OM. This is especially challenging because the components of the OM are amphiphilic and must cross the aqueous periplasmic compartment. In recent years, the protein systems responsible for the transport of lipoproteins, OMPs, and LPS have been identified and aspects of their mechanisms have been elucidated. At this point, however, it is unclear how PL is transported to the OM. No protein machinery has been identified as being responsible for its transport, although the conserved *mla* genes have been found to function in the retrograde transport of PL from the OM[18]. The PL composition of the OM is different from that of the IM in that it is enriched in phosphatidylethanolamine and saturated fatty acids, which suggests selectivity in PL transport[19-21]. LPS, but not PL, transport continues in *E. coli* spheroplast cells, suggesting that the two processes either occur via separate pathways or have different requirements for transport[22]. PL transport has also been shown to be bidirectional[23,24] and dependent on the proton motive force, but not ATP, protein, or lipid synthesis[25]. Together, these observations suggest the existence of an undiscovered mechanism of PL transport.

1.3.1. Lipoprotein trafficking to the outer membrane

Lipoproteins, like OMPs and soluble periplasmic proteins, are translated in the cytoplasm as pre-proteins with an N-terminal signal peptide that directs them for secretion through the IM, in an unfolded state, by the Sec translocon[26]. After secretion, pre-lipoproteins are lipidated via a

three-step process that is triggered by recognition of a lipobox consensus sequence located near the signal peptide cleavage site. First, the enzyme Lgt forms a thioether linkage between a molecule of diacylglycerol and the cysteine residue that will ultimately become the N-terminal most amino acid of the mature protein. Next, LspA removes the signal peptide, and then Lnt acylates the amino group of the N-terminal cysteine. The ultimate result is a mature lipoprotein that is anchored to the outer leaflet of the IM by three fatty acyl chains that are attached to the most N-terminal residue of the protein[27].

Following maturation, lipoproteins can either be retained in the periplasmic leaflet of the IM or exported to the periplasmic leaflet of the OM. The sorting of lipoproteins is dependent upon the residues present at positions 2 and 3 following the N-terminal Cys at position 1[28,29]. The most important factor for retention in the IM is the presence of Asp at position 2[28]. Other amino acids in position 2 can also trigger retention of model substrates, but generally only Asp is found in *E. coli* proteins[27,30]. Depending on its identity, the amino acid in position 3 can either act synergistically with Asp at position 2 to promote retention (such as Asp, Asn, Glu, or Gln) or antagonistically to promote trafficking to the OM (such as Lys and His)[31].
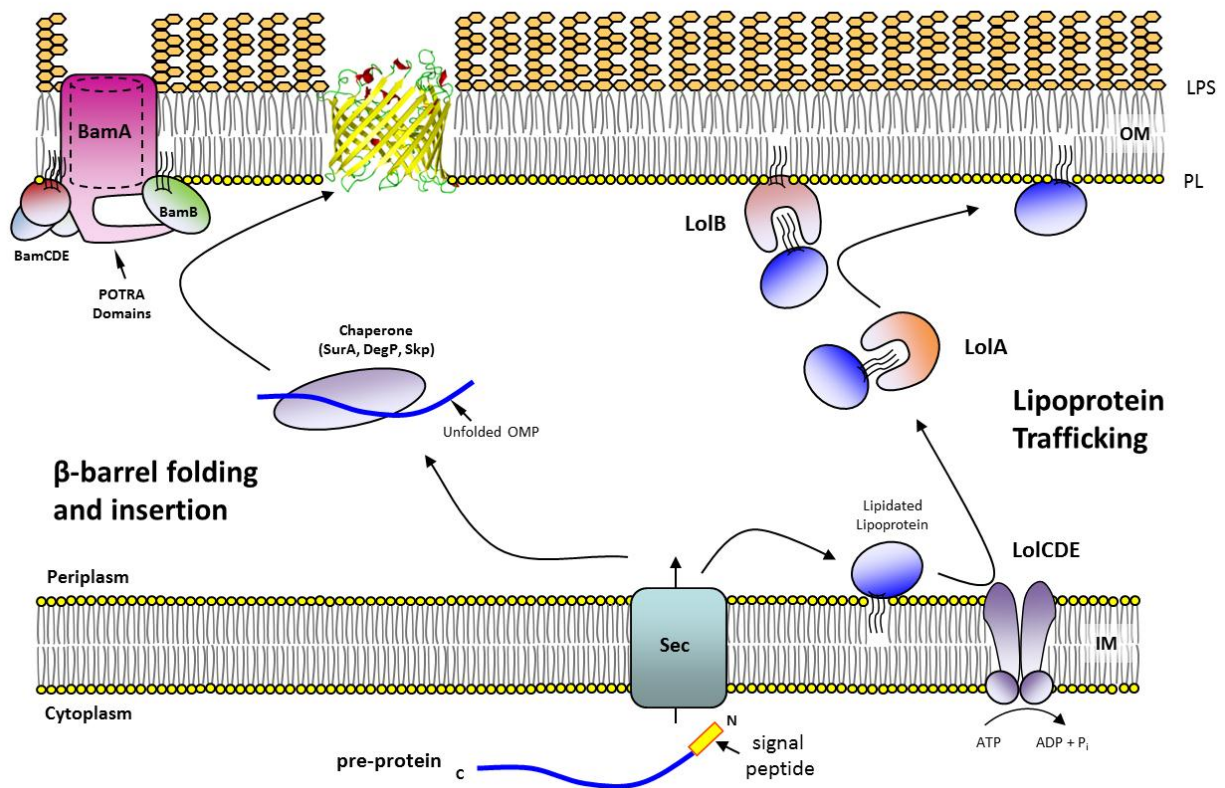
Figure 2. Biogenesis of outer membrane lipoproteins and OMPs. OMPs and lipoproteins are both translated as pre-proteins in the cytoplasm that are secreted across the IM by the Sec translocon. OMPs remain unfolded following translocation and are carried by chaperone proteins across the periplasm, where they are assembled into the membrane by the BamA/B/C/D/E complex. Lipoproteins are inserted into the periplasmic leaflet of the IM following translocation. They are removed from the membrane by LolC/D/E and passed off to LolA, which chaperones them to LolB. LolB then catalyzes their insertion into the inner leaflet of the OM.

The removal of mature lipoproteins from the IM and their subsequent transport and insertion into the OM is catalyzed by the essential five-protein Lol (localization of lipoproteins) system (Figure 2)[27]. The first component of the system was identified following the observation that lipoprotein release from *E. coli* spheroplasts only occurs in the presence of concentrated

periplasmic exacts. These results suggested that there was a soluble periplasmic factor that was

necessary for the release of lipoproteins from the IM. This factor was identified to be LolA,

which forms a water-soluble complex with lipoproteins in order to chaperone them across the

periplasm[32]. Following this work, it was noted that the LolA-lipoprotein complex could transfer

lipoprotein into the OM but not the IM. This led to the identification of LolB, a lipoprotein that

interacts with the LolA-lipoprotein complex in order to facilitate release of the lipoprotein from

LolA and its insertion in the OM[33]. It was also observed that LolA is capable of removing

lipoproteins that are imbedded in the IM but not those imbedded in the OM, and its ability to do

so was found to be ATP-dependent[34]. This led to the identification of the LolCDE complex.

These proteins form an ATP binding cassette (ABC) transporter with a stoichiometry of (1:2:1

LolC:LolD:LolE)[35]. LolD serves as the nucleotide binding portion of the transporter with LolC

and LolE together forming the eight helix transmembrane portion of the transporter[27]. LolCDE

recognizes lipoproteins and hydrolyzes ATP in order to facilitate their removal from the IM and

transfer to LolA. Reconstitution of the Lol system in proteoliposomes revealed that LolCDE was

the protein factor that recognizes the second and third residues of the lipoprotein to determine

whether to retain it in the IM or transfer it to LolA for transport to the OM[36]. LolCDE also fails

to accept incompletely matured lipoproteins[37,38]. This system has been determined to be the

general pathway used in *E. coli* for lipoprotein trafficking[39].

The structures of LolA and LolB reveal that the two proteins share a similar hydrophobic

pocket that is likely to bind the hydrophobic portion of lipoproteins[40]. This has led to the

proposal of a "mouth-to-mouth" model of transfer in which a predicted hydrophobic cavity in

LolC aligns with the hydrophobic cavity in LolA in order to transfer the lipoprotein cargo from

LolCDE to LolA. LolA subsequently aligns its hydrophobic cavity with that of LolB in order to

transfer the lipoprotein to it[41]. In terms of energy, the Lol pathway uses LolCDE to hydrolyze ATP in order to generate a high energy LolA-lipoprotein intermediate that can favorably donate its lipoprotein to LolB to form the lower energy LolB-lipoprotein complex. This effectively couples the energy of cytosolic ATP to the distal process of inserting lipoproteins into the OM[41,42]. The downhill nature of this process also prevents the reverse process and ensures that lipoproteins are retained in the OM once placed there.

1.3.2. Transport and assembly of β-barrel outer membrane proteins

Like lipoproteins and periplasmic proteins, OMPs are translated in the cytosol as pre-proteins that bear N-terminal signal peptides. As with lipoproteins, these signal peptides trigger secretion via the Sec translocon through an ATP driven process[26]. Following translocation, the nascent OMP is released from the IM following cleavage of the signal peptide by a signal peptidase. The OMP is then kept in a folding competent state by association with a periplasmic chaperone, such as SurA, Skp, or DegP[43,44]. SurA is thought to form a distinct pathway from Skp/DegP, which are thought to be more important for stress response and rescue of misfolded proteins[45,46]. The nascent OMP is chaperoned to the outer membrane where it interacts with the β-barrel assembly machine (Bam complex), which folds and inserts the β-barrel of the OMP into the OM (Figure 2)[43]. The Bam complex is comprised of five individual proteins, BamA/B/C/D/E, and is required for assembly of nearly all OMPs[43,47]. BamA is an essential β-barrel containing OMP that was initially implicated in β-barrel assembly when it was observed that its depletion in *Neisseria meningitidis* led to the accumulation of misfolded OMPs in the periplasm[48]. Initial speculation that BamA was also involved in LPS transport was disproven[49,50] and the observed effects of BamA depletion on LPS trafficking are thought to be due to the fact

that LptD, an essential OMP required for LPS trafficking, requires BamA for proper assembly[51]. It is worth noting that BamA and LptD are the only β-barrel proteins that are known to be essential in *E. coli*. BamA in Gram-negative organisms contains five polypeptide transport-associated (POTRA) domains at its N-terminus and a β-barrel domain at its C-terminus[52]. The X-ray crystal and NMR structures of the POTRA domains have been solved and show that they adopt similar folds, each consisting of a single three-stranded β-sheet that is folded over by a pair of antiparallel helices[53,54]. The crystal structure showed interactions between pairs of POTRA domains via interactions between edges of β-sheets, which led to the proposal of a β-strand augmentation mechanism of β-barrel assembly, whereby POTRA domains assist the folding of β-barrels by complementing the β-strands of the nascent OMP as they assemble into a barrel[53]. Four lipoproteins, BamB, BamC, BamD, and BamE, join BamA in comprising the Bam complex in *E. coli*. Of these, only BamD is essential. BamA interacts with BamB via POTRA domains 2-4 and with BamC/D/E via POTRA domain 5[43].

Protein folding catalyzed by purified Bam components has been reconstituted in proteoliposomes. These studies revealed that the Bam complex functions much more efficiently when all four lipoproteins are present. It also revealed that no source of energy was necessary, just a soluble, chaperone-stabilized or urea-denatured OMP[55]. Subsequent work has demonstrated that the reconstituted system can undergo multiple rounds of protein folding and that certain lipoproteins alone are sufficient to assemble BamA[56,57].

The structure of BamA was recently reported, with the authors noting several features in the structure that suggest a mechanism for BamA-mediated β-barrel assembly[58]. First, they observed an interior cavity that is exposed in one structure, but closed in another, suggesting two possible conformations that might occur during β-barrel assembly. They also noted that the

11

exterior of the BamA β-barrel features a narrowed hydrophobic surface that is hypothesized to disrupt the membrane to facilitate β-barrel insertion. There is also a narrowed contact between the first and last β-strands of the β-barrel, which they suggest is a possible point at which the β-barrel might open to allow access to the membrane. The significance of these observations has yet to be established, and the mechanism of the Bam complex remains an active area of research.

1.3.3. Lipopolysaccharide biogenesis in the inner membrane

Since LPS is essential in nearly all Gram-negative bacteria and unique to bacteria, its biosynthesis has strong potential as an antibiotic target. As a result, it has been extensively studied, is well understood, and has largely been reconstituted *in vitro*[7,59]. Broadly speaking, the process begins in the cytoplasm with the synthesis of Kdo_2-Lipid A and is followed by addition of the remaining core oligosaccharides. The nascent Ra-LPS is flipped into the periplasmic leaflet of the IM, where it is decorated with the O-antigen oligosaccharide, concluding its biosynthesis, before trafficking to the OM.
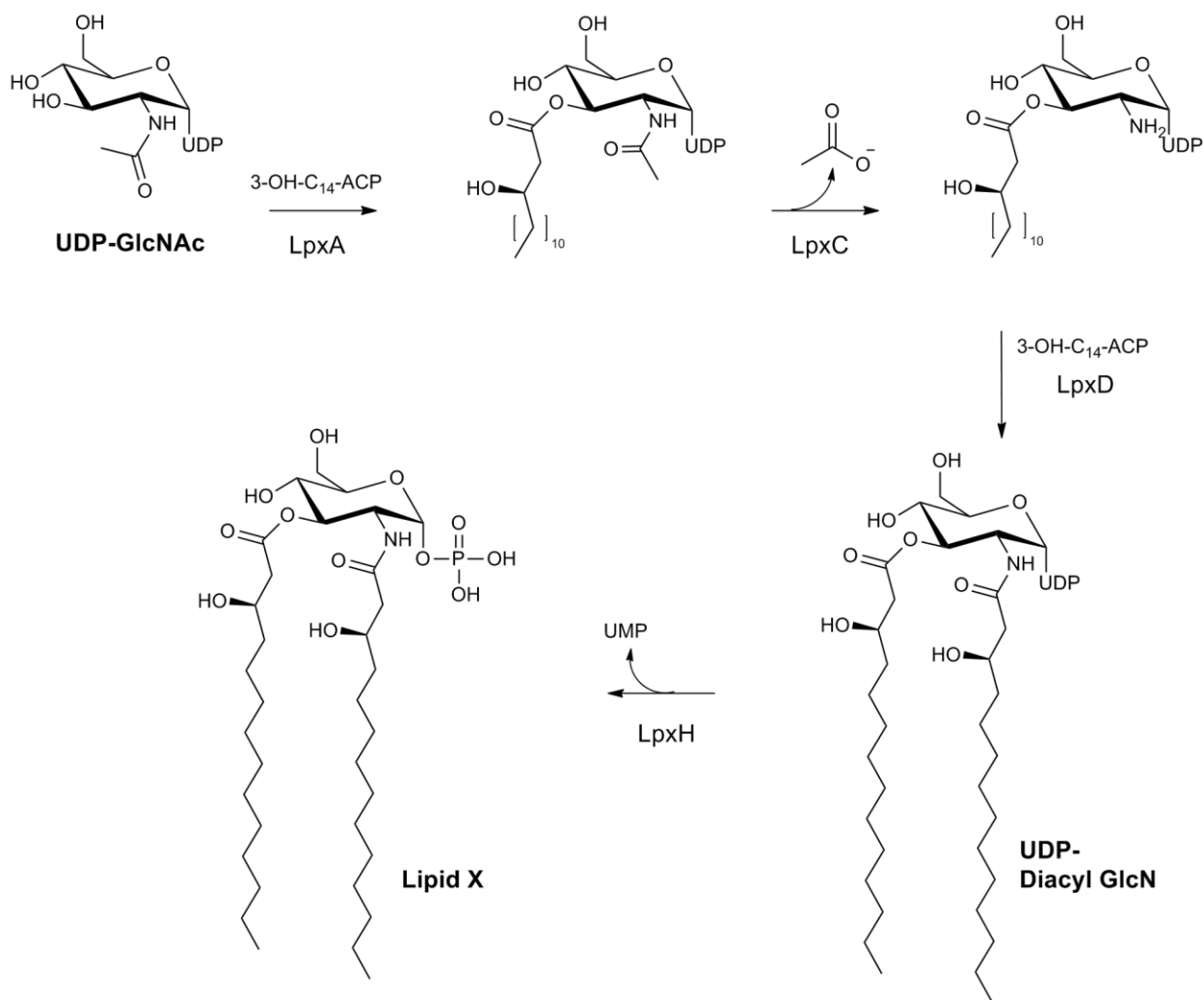
Figure 3. The biosynthetic pathway of LPS biosynthetic intermediates Lipid X and UDP-diacyl GlcN.

Kdo$_2$-Lipid A is produced in the cytoplasmic leaflet of the IM in the multistep process described in Figure 3 and Figure 4[7]. The first step in its biosynthesis begins with transfer of *R*-3-hydroxymyristate onto UDP-*N*-acetylglucosamine (UDP-GlcNAc) in a thermodynamically unfavorable process catalyzed by LpxA[59-61]. LpxC then hydrolyzes the acetyl group in a favorable process that constitutes the first committed step of LPS biosynthesis[61-63]. Another *R*-3-hydroxymyristate moiety is added to the newly revealed amine by LpxD to give UDP-2,3-diacylglucosamine[64]. In some portion of UDP-2,3-diacylglucosamine, the phosphoanhydride

13

bond of UDP is hydrolyzed by LpxH to give the intermediate Lipid X (2,3-diacylglucosamine-1-

phosphate) and UMP (Figure 3)[65,66]. Subsequently, a molecule of Lipid X and UDP-2,3-

diacylglucosamine are condensed by LpxB to form the β-1,6 linked glucosamine disaccharide

that is characteristic of LPS[67]. The resulting intermediate is phosphorylated by LpxK at the 4'

position using ATP to give Lipid IV_A[68,69]. Lipid IV_A is modified twice by WaaA, which utilizes

two molecules of CMP-Kdo to add two units of Kdo to the 6' position of the Lipid IV_A

glucosamine disaccharide[70,71]. LpxL and LpxM catalyze the final two acyl transfer reactions that

yield Kdo_2-Lipid A, the hexa-acylated species that forms the minimal LPS needed for viability.

LpxL adds laurate to the β-hydroxyl group of the 2' lipid[72], and LpxM adds myristate to the β-

hydroxyl group of the 3' lipid (Figure 4)[73]. It is worth noting that since these enzymes are

selective for the Kdo_2 containing intermediate, Lipid A is never actually formed as an

intermediate during LPS biosynthesis, despite being the complete membrane anchoring unit.

While Kdo is generally recognized as being required for cell viability, certain suppressor strains

have been generated that can rescue Kdo-depleted *E. coli,* though these and other minimal LPS

mutants tend to display OM defects and exhibit stress responses[74-76].
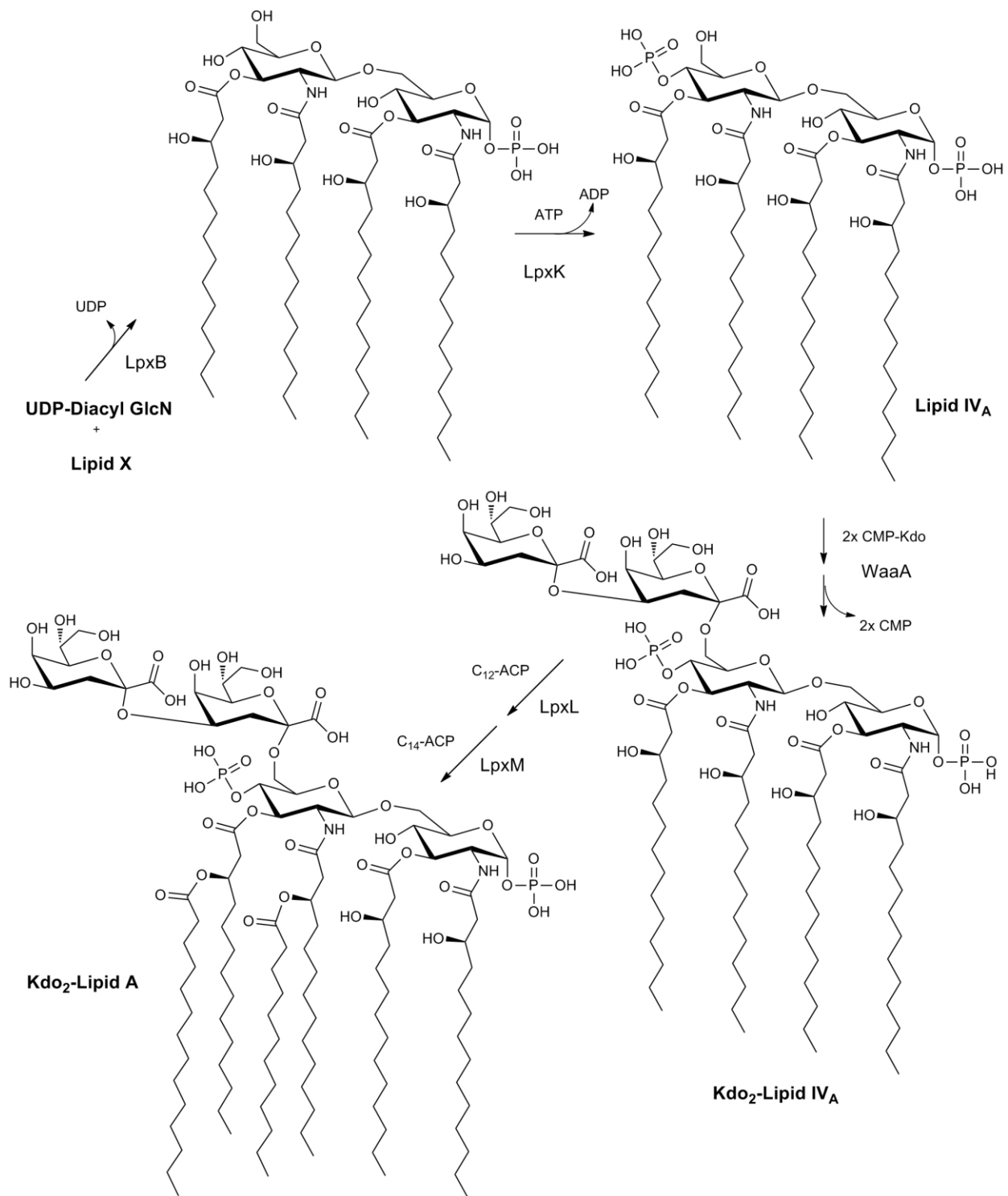
Figure 4. Biosynthetic pathway of Kdo$_2$-Lipid A beginning with intermediates described in Figure 3.

While Kdo_2-Lipid A is sufficient for viability in *E. coli*, LPS typically features additional sugars in the form of a core oligosaccharide and O-antigen oligosaccharide. Like Lipid A biosynthesis, the installation of the core oligosaccharide occurs on the cytoplasmic leaflet of the IM, where it is carried out by a series of membrane-associated glycosyltransferases[77]. In contrast to Lipid A, the core oligosaccharide tends to be less conserved. The inner core is more conserved than the outer core and typically contains Kdo and Hep (L-glycero-D-*manno*-heptose), while the outer core commonly contains D-glucose and D-galactose in addition to the types of sugars found in the inner core[77]. The genes responsible for core oligosaccharide assembly are found in the *gmhD*, *waaQ*, and *kdtA* operons[78]. The *gmhD* operon encodes the genes needed for synthesis and transfer of Hep[79]. The *kdtA* operon encodes genes needed for Kdo installation[80]. The *waaQ* operon encodes additional genes that are responsible for the synthesis and assembly of the outer core sugars[77]. Like Ra-LPS, the precursors to the O-antigen oligosaccharide are synthesized on the cytoplasmic leaflet of the IM, where they are assembled by glycosyltransferases from sugar-nucleotide substrates and anchored to the membrane by an undecaprenyl phosphate moiety[77]. O-antigen precursors are flipped to the periplasmic face of the IM by Wzx, where they are polymerized by Wzy and Wzz[81]. The genes responsible for the synthesis, polymerization, and flipping of the O-antigen oligosaccharide to the periplasm are encoded by the *rfb* gene cluster[4]. The *gmhD* operon also encodes the ligase, WaaL, that is responsible for the addition of the O-antigen polysaccharide to Ra-LPS (core-Lipid A)[81,82]. WaaL acts in the periplasm, following flipping of Ra-LPS from the inner leaflet of the IM.

Numerous modifications to both the sugar and lipid regions of Lipid A have been reported. Functions of these modifications include resisting cationic antimicrobial peptides,

evading immune recognition, and adapting to stressful extracellular environments[77]. These modifications are often mediated by the PmrA-PmrB two-component system, which regulates virulence and responds to stresses such as high Fe^{3+} and low Mg^{2+}, or by the PhoP-PhoQ two-component system, which also responds to low Mg^{2+} and is involved in virulence[79,83-86]. Activation of the *arn* operon ultimately results in the transfer of 4-amino-4-deoxy-α-L-arabinose onto the Lipid A 4'-position phosphate[77,87-89]. Modification of the phosphate group at the 1-position with phosphoethanolamine is also triggered by the PmrA-PmrB two-component system[77]. These modifications both aid in resistance to certain antimicrobial peptides and are implicated in virulence[90]. The 1- and 4'- phosphates are cleaved by phosphatases in some species, which is associated with virulence[91]. A number of enzymes are known that modify the lipid portion of Lipid A via acylation, deacylation, and hydroxylation. PagP transfers a palmitate moiety to the β-position of the 2-position lipid chain, resulting in a hepta-acylated Lipid A derivative[92]. PagL is a lipase that 3-O-deacylates Lipid A[93]. LpxO introduces *S*-2-hydroxy modifications to the myristate attached to β-hydroxyl of the 3'-myristate[94].

Following the synthesis of core-Lipid A, but prior to the addition of the O-antigen oligosaccharide, LPS is flipped from the inner leaflet of the IM to the outer leaflet of the IM. This process features a high activation barrier and is facilitated by the ABC transporter MsbA[95]. MsbA was first reported as a multicopy suppressor of an LpxL temperature-sensitive mutant and *lpxL* deletion[96]. Further studies observed that in LpxL temperature-sensitive mutants, hexa-acylated LPS is predominantly observed at the OM even after several generations at a non-permissive temperature. In these cells, however, significantly higher amounts of tetra-acylated LPS are observed at the OM when extra copies of *msbA* are present, establishing a role for MsbA in LPS transport[97]. This suggests that extra copies of *msbA* suppress loss of LpxL function

because MsbA is inefficient at transporting tetra-acylated LPS species. Subsequently, a temperature-sensitive mutant of MsbA was found to lead to accumulation of Lipid A in the cytoplasmic leaflet of the IM, as judged by its lack of modification by periplasmic enzymes, which firmly established that MsbA is the IM LPS flippase[95]. MsbA was purified and its activity was reconstituted in proteoliposomes. In this assay, it was found that hexa-acylated species, such as Kdo_2-Lipid A, stimulated MsbA activity, while tetra-acylated species, such as Lipid IV_A, did not[98]. This is consistent with the observation that MsbA is inefficient at transporting tetra-acylated LPS species[97].
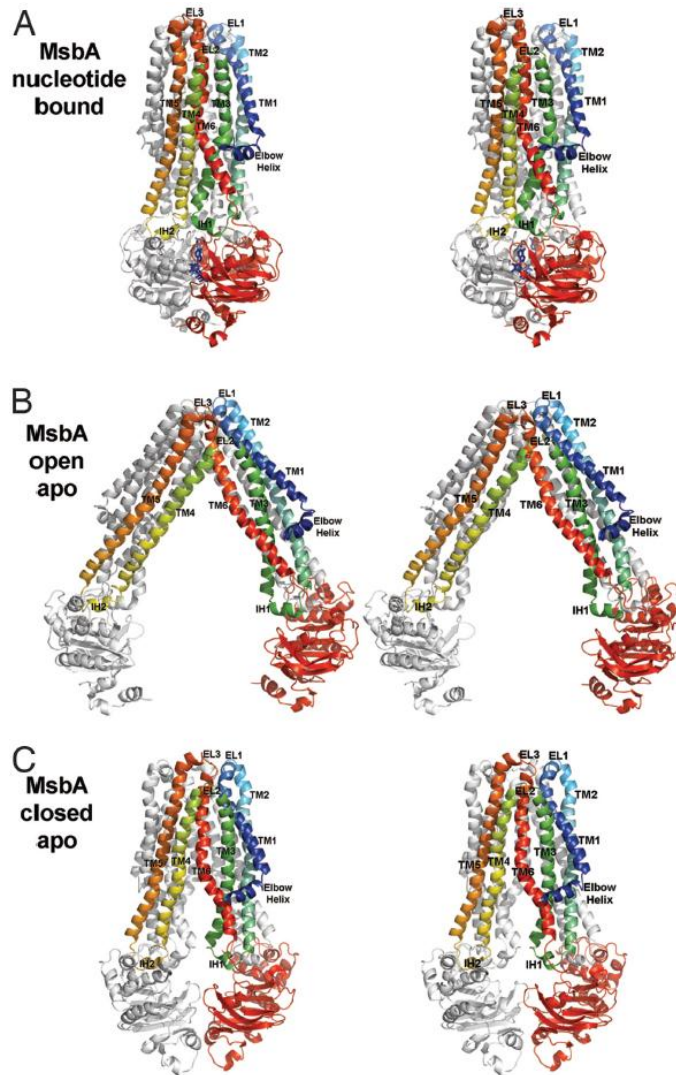
Figure 5. Stereo view of the X-ray crystal structure of the MsbA homodimer in three conformations. MsbA exhibits large structure rearrangements between the nucleotide bound (A), open apo (B), and closed apo (C) states. Figure taken directly from Ward et al[99]. Copyright 2007, National Academy of Sciences, USA.

The X-ray crystal structures of MsbA from several related species were found to crystallize in a number of conformations that, when taken together, suggest that large structural rearrangements occur during the ATP binding and hydrolysis cycle (Figure 5)[99]. MsbA from *E. coli* crystallized in an apo-state that is open to the cytoplasm. MsbA from *Vibrio cholera*

crystallized in an apo-state that features a closed, cytoplasm-facing conformation. MsbA from *S. typhimurium* crystallized with bound AMPPNP in an outward facing conformation. These structures suggest a model in which LPS binding to MsbA's open, inward facing apo-state (as in Figure 5B) triggers a structural rearrangement in which the transmembrane domains come together to produce a closed, inward facing apo-state (as in Figure 5C). Subsequent nucleotide binding would then induce a conformational change that produces the outward facing conformation (as in Figure 5A) that would allow LPS access to the outer leaflet. Hydrolysis of the nucleotide would presumably allow the cycle to repeat[99]. Extensive studies of MsbA using electron paramagnetic resonance (EPR) spectroscopy have proven consistent with this model and help validate the relevance of the crystal structures[100,101].

1.3.4. Lipopolysaccharide biogenesis: transport to the outer membrane

Once fully mature and present at the outer leaflet of the IM, LPS must be transported across the aqueous periplasm to the outer leaflet of the OM, where it functions to establish a permeability barrier. This transport is facilitated by the trans-envelope Lpt complex (Figure 6), which is comprised of LptA/B/C/D/E/F/G, all of which are essential in most Gram-negative organisms, including *E. coli*.
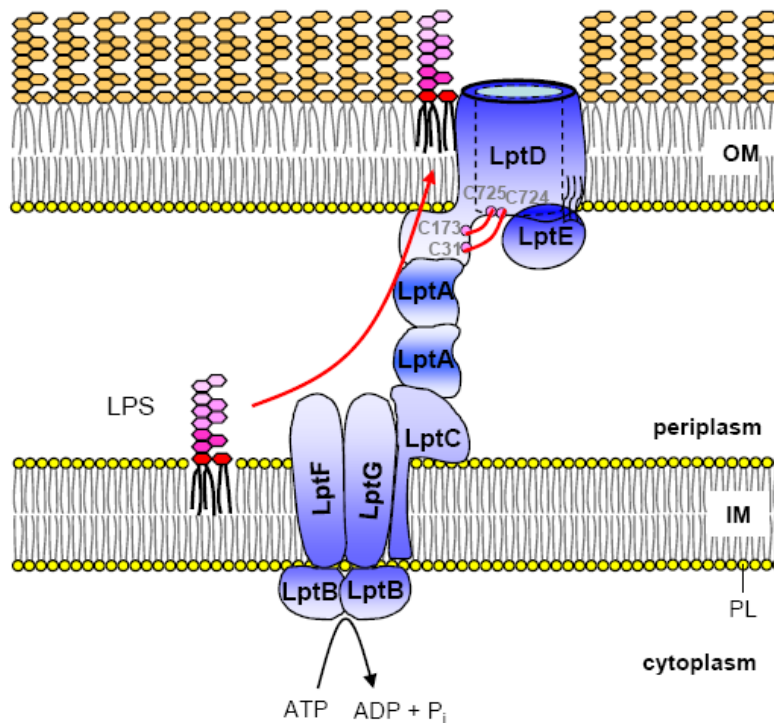
Figure 6. The trans-envelope Lpt complex removes LPS from the periplasmic leaflet of the IM and inserts it directly into the outer leaflet of the OM.

LptB$_2$CFG are the IM portion of the Lpt complex, where they form an ABC transporter in which LptF and LptG provide the transmembrane domains and two molecules of LptB provide the nucleotide binding domains[102]. LptC is a single pass transmembrane protein that contains a periplasmic OstA domain that is homologous to domains found in LptA and LptD. LptA is a soluble periplasmic protein that interacts with the OstA domains of LptC and LptD to create a periplasm-spanning bridge[103]. LptD and LptE form a tight complex and represent the OM portion of the Lpt complex. LptD contains a soluble, N-terminal OstA domain and a membrane spanning, C-terminal β-barrel domain[104,105]. LptE is a lipoprotein that forms a plug inside the LptD β-barrel[106].

1.3.4.1 Identification of the Lpt proteins

LptD, the first Lpt protein to be identified, was reported in 1989 by Sampson et al. following a genetic selection for mutations that increased outer membrane permeability and allowed large maltodextrins to cross the OM in the absence of the LamB maltoporin[107]. One of the reported mutations, LptD4213 (Δ330-352), elicited a particularly strong phenotype that resulted in sensitivity to a variety of detergents and antibiotics. This work also established LptD to be essential in *E. coli*. Braun and Silhavy later showed that LptD depletion led to mislocalization of outer membrane proteins and lipids, establishing its role in envelope biogenesis[108]. Bos et al. further refined the role of LptD to LPS biogenesis by showing that loss of LptD in *N. meningitidis* resulted in loss of LPS at the cell surface, as judged by PagL labeling and inaccessibility to extracellular neuraminidase[51]. While most Gram-negative species require LPS for viability, it is not essential in *N. meningitidis*, which enabled its deletion by Bos et al.[109] Other species in which LPS is not essential include *Acinetobacter baumanii[110]*, *Moraxella catarrhalis[111]*, and *Helicobacter pylori[112]*. Wu et al. used affinity purification techniques to purify LptD, and in doing so, co-purified LptE. Depletion of either LptD or LptE prevented labeling of LPS by PagP, establishing that both proteins are essential for LPS transport[104].

LptA and LptB were first identified by random transposon mutagenesis as being essential in *E. coli*[113]. Subsequent research revealed that genes encoded in the same locus as *lptA* and *lptB* were responsible for synthesis of Kdo, hinting at a role for LptA and LptB in OM biogenesis[114]. Sperandeo et al. soon showed that mutants depleted of LptA and/or LptB are defective in LPS transport to the OM and proposed a model in which LptB is the nucleotide-binding domain of an ABC transporter that hydrolyzes ATP in order to remove LPS from the membrane and pass it to LptA[115]. The observation that the *lptA* gene overlapped with another gene, *lptC*, led to the

identification of LptC, and subsequent research confirmed that it was required for LPS transport to the OM[116].

Given that LptB was believed to form the nucleotide-binding domain of an ABC transporter, and since the single transmembrane helix of LptC is not sufficient to provide the transmembrane domains of an ABC transporter, it was known that at least one Lpt protein remained to be discovered. Using this knowledge, LptF and LptG were identified by a bioinformatics approach that scanned the genome of a Gram-negative endosymbiont, *Blochmannia floridanus,* for essential genes of unknown function[102]. LptF and LptG were then shown to be essential for LPS transport and were proposed to be the missing transmembrane domains of the IM ABC transporter.

1.3.4.2. The Lpt proteins form a trans-envelope complex

Following the identification of the seven Lpt proteins, questions remained concerning the mechanism of LPS transport. Of principal interest was the architecture of the system as a whole. Two primary hypotheses existed, one in which LptA acts as a periplasmic chaperone that binds LPS and shuttles it across the periplasm in a manner analogous to LolA's handling of lipoproteins, and another in which LptA forms a periplasmic bridge that connects the IM ABC transporter to the OM translocon, LptD/E, to form a continuous, trans-envelope complex[16]. Several pieces of evidence initially suggested a trans-envelope model. First, it was observed that LPS transport continues in spheroplasts, while lipoprotein transport does not, which suggests that LPS transport does not occur via a soluble periplasmic chaperone like lipoprotein transport[22]. Second, the elucidation of the LptA X-ray crystal structure revealed crystal contacts between neighboring molecules that form end-to-end stacked fibrils with a continuous hydrophobic

groove running throughout (Figure 7)[117]. This form of contact provided a mechanism by which

LptA could form a periplasm-spanning bridge that could accommodate the movement of LPS.

Given the homologous OstA domains found in LptD and LptC, it also provided a mechanism for

how such a bridge could connect the IM and OM portions of a putative trans-envelope complex.

When the X-ray crystal structure of the LptC OstA domain was solved, it revealed a β-jellyroll

fold similar to that of LptA (Figure 8)[118]. This supported the theory that LptA and LptC interact

in an end-to-end fashion similar to that observed in the LptA crystal structure.
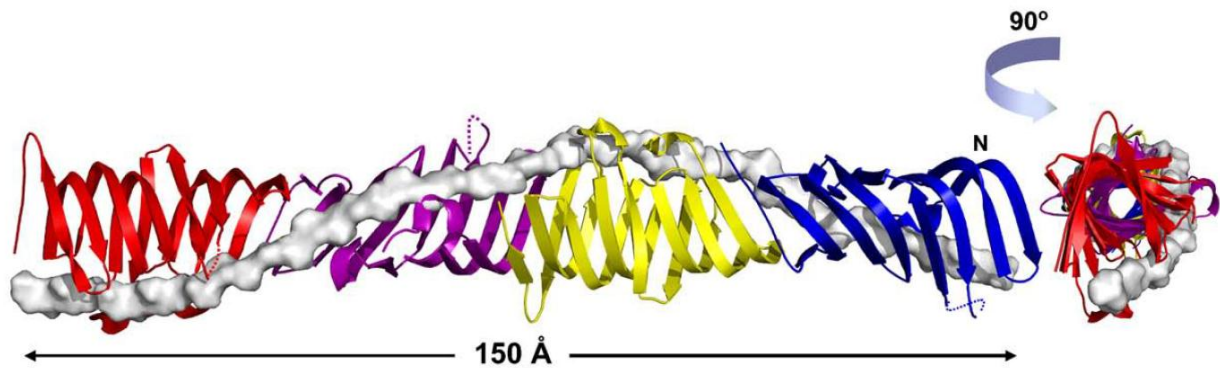
Figure 7. The X-ray crystal structure of LptA reveals a β-jellyroll fold in which neighboring

molecules form end-to-end stacked fibrils that feature a continuous hydrophobic groove. Figure

taken directly from Suits et al[117]. Copyright 2008, Elsevier.
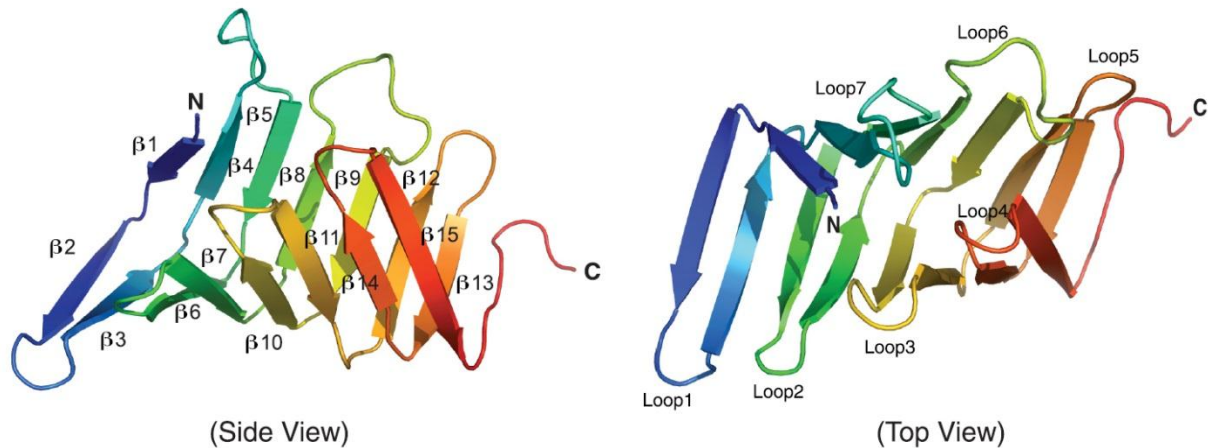
Figure 8. The X-ray crystal structure of the LptC periplasmic domain shows a β-jellyroll fold similar to that of LptA. Figure taken from Tran et al[118]. Copyright 2010, American Society for Biochemistry and Molecular Biology.

Chng, Gronenberg, and Kahne demonstrated in 2010 that all seven Lpt proteins can be co-purified by affinity purification using a His-tag on LptC, establishing that all of the Lpt proteins interact with one another. Using sucrose gradient fractionation, they were also able to show that all of the Lpt proteins co-fractionate to a distinct membrane fraction, termed OM_L, which contains both IM and OM components[119]. From these data, it was concluded that the Lpt proteins form a membrane-spanning, trans-envelope complex. Direct interaction between LptC and LptA was also observed, supporting the trans-envelope model[120]. Freinkman et al. further established the existence of the trans-envelope bridge and provided evidence that supported an end-to-end stacking model in which the OstA domains of LptC, LptA, and LptD interact in much the same way as was observed in the LptA crystal structure. By placing the photo-crosslinking unnatural amino acid *p*-benzoylphenylalanine (pBPA) at specific locations in LptA, LptD, and

LptC, they were able to observe UV-induced crosslinks between LptA and LptC and between LptA and LptD that were consistent with the model shown in Figure 9[103].
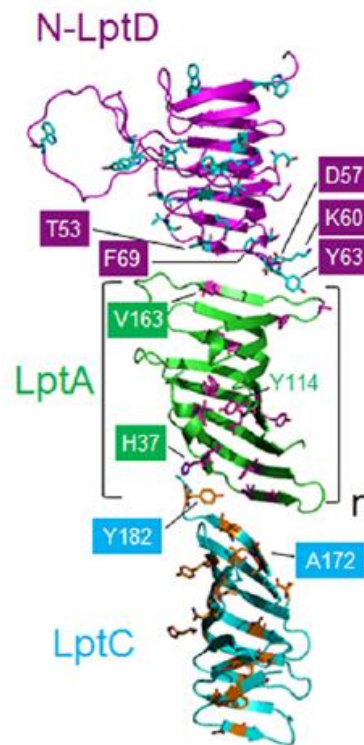
Figure 9. Proposed structure of the Lpt trans-envelope bridge. When pBPA is placed at the indicated positions in N-LptD, LptA, or LptC, UV-induced crosslinking can be observed between the mutagenized protein and its contact partner. The N-LptD structure is a predicted structure. Figure taken directly from Freinkman et al[103]. Copyright 2012, American Chemical Society.

1.3.4.3. Studies investigating the inner membrane complex, LptB/F/G/C

Because of its enzymatic activity, the ATPase function of the IM ABC transporter is the most obvious target for inhibition of the Lpt complex. The ATPase activities of both LptB and LptB$_2$FGC have been reconstituted *in vitro* and have proven useful in screening for LptB

inhibitors[121,122]. The X-ray crystal structure of LptB was recently reported, and residues critical for catalytic activity and transmembrane domain binding were identified[123].

Okuda, Freinkman, and Kahne were able to trap LPS transport intermediates on LptA and LptC using site-specific crosslinking facilitated by pBPA. They were able to show that multiple rounds of ATP hydrolysis are necessary to observe said crosslinking, demonstrating that the energy needed for LPS transport comes from ATP hydrolysis by the IM ABC transporter. From these data, they proposed a model in which LPS is pushed through the trans-envelope bridge in a continuous stream, powered by ATP hydrolysis[124].

1.3.4.4. Studies investigating the outer membrane translocon, LptD/E

Further characterization of the LptD/E complex established that it exists as a stable 1:1 complex that can be overexpressed and purified. It was found that LptD interacts with LptE via its C-terminal β-barrel domain, but that both the N-terminal and C-terminal domains are necessary for cell viability. Furthermore, it was shown that the LptD C-terminal β-barrel domain protects LptE from trypsin digestion, which led to the hypothesis that LptE is a plug that is situated inside of the LptD β-barrel[105]. Other studies utilized pBPA-mediated site-specific crosslinking to further establish the plug-and-barrel model by showing that various positions on all sides of LptE make contact with LptD. One specific crosslink was determined to be to a predicted extracellular loop of LptD. Removal of this loop, $LptD_{\Delta529-538}$, results in an increased OM permeability phenotype similar to the one observed in LptD4213. These studies also led to the proposal of a direct insertion model of LPS insertion into the outer leaflet of the OM, meaning that LPS is never placed in the inner leaflet of the OM, but instead is transported directly from the LptD β-barrel lumen to the cell surface[106].

LptD in *E. coli* contains four cysteine residues at positions 31, 173, 724 and 725, and they were known to form disulfide bonds[108]. Ruiz et al. performed an exhaustive characterization of the oxidation state of LptD; by constructing all possible combinations of single, double, triple, and quadruple mutations of cysteine to serine, and by using non-reducing SDS-PAGE to observe the disulfide bonds that form in each mutant *in vivo*, they were able to determine that mature LptD is fully oxidized and contains two intramolecular disulfide bonds between C31 and C724 and between C173 and 725[125]. Both of these disulfide bonds connect the N-terminal periplasmic domain to the C-terminal β-barrel domain, suggesting that they may play some role in orienting the two domains relative to one another. Ruiz et al. also established the essentiality of these disulfide bonds; neither individual disulfide is necessary for viability so long as at least one of the two is present[125]. They also found that the periplasmic oxidase DsbA is important, but not absolutely required, for LptD oxidation, consistent with previous identification of LptD as a substrate for DsbA[125,126]. They found no requirement for DsbC, a disulfide bond isomerase, in LptD oxidation, but noted that LptE depletion results in a loss of proper LptD oxidation. The same effect was not observed for LptF/G depletion, suggesting a specific role for LptE in the assembly of LptD[125].

The *lptE6* mutant allele, in which LptE amino acids 116-120 (YPISA) are mutated to YRA, was isolated during a screen for mutations that increase OM permeability. The *lptE6* allele was found to interfere with LptD oxidation, and suppressor mutations to *lptE6* were isolated in *bamA* and *lptD*; therefore, it was proposed that LptE must play some role in LptD assembly at the Bam complex[127]. Similarly, suppressors to *lptD4213* have been isolated in *bamA* and *bamB*[128,129]. Taken together, these findings suggest that LptE and LptD interact together at the Bam complex during LptD/E biogenesis.

In 2010, a peptidomimetic antibiotic was reported whose target appears to be LptD in *Pseudomonas* spp. The antibiotic was found to crosslink to LptD *in vivo*; furthermore, resistance mutations were found to arise in the N-terminal domain of LptD. Specifically, tandem duplication of nucleotides 628 to 645, corresponding to duplication of amino acids 210-215 (LRDKGM) were found to confer resistance to the drug (numbering refers to *P. aeruginosa lptD*)[130]. Interestingly, this duplication lies immediately downstream of amino acids 207-209 (GNV), which are three of the most highly conserved residues in *lptD* homologues. The mechanism of this antibiotic and the significance of this resistance mutation are not yet understood.

1.4. Perspectives

Bacterial resistance to antibiotic drugs is an escalating problem that severely threatens our society[131]. This issue is particularly pronounced in Gram-negative organisms for which treatments are already limited due to the relative impermeability of the OM. Consequently, the identification of new antibiotic drugs and antibiotic targets is imperative. Biogenesis of the Gram-negative outer membrane provides an attractive target because of its essential nature, the fact that its disruption causes sensitivity to otherwise ineffective drugs, and because of its accessible location at the cell surface. Several molecules have been identified that validate OM biogenesis as a drug target, such as inhibitors of LpxC[132,133], LptB[121,122], and the peptidomimetic drug believed to target LptD[130]; however, our understanding of OM biogenesis is far from complete, and as such, there are still a number of open questions. Perhaps most striking is that we know virtually nothing regarding phospholipid trafficking to the OM, and while the

molecular components involved in OMP and LPS trafficking have likely all been identified, the mechanisms by which they function are poorly understood.

The remaining chapters of this dissertation focus on furthering our understanding of the biogenesis and mechanism of LptD/E. Chapter 2 documents research that led to the elucidation of the oxidative assembly pathway of LptD/E that culminates in a disulfide bond rearrangement that activates the LPS translocon. Chapters 3 and 4 document efforts to determine the X-ray crystal structure of the LptD/E complex. Chapter 3 details the more limited goal of obtaining a crystal structure for just the N-terminal, periplasmic domain of LptD, while chapter 4 chronicles the ongoing effort to obtain a crystal structure for the two-protein complex. As a whole, the research described herein has contributed to our knowledge of LPS transport and could ultimately help address questions regarding the mechanism by which LptD and LptE handle LPS and facilitate its insertion into the outer leaflet of the OM.

Chapter 2: Disulfide Rearrangement Triggered by Translocon Assembly Controls

Lipopolysaccharide Export

This chapter is adapted from: Chng, S. S., Xue, M., Garner, R. A., Kadokura, H., Boyd, D., Beckwith, J., Kahne, D. Disulfide rearrangement triggered by translocon assembly controls lipopolysaccharide export. *Science* **337**, 1665-1668, (2012). Reprinted with permission from AAAS.

Collaborators: Shu Sin Chng, Mingyu Xue, Hiroshi Kadokura, Dana Boyd, Jonathan Beckwith, Daniel Kahne.

2.1. Introduction

The essential, two-protein LptD/E complex forms the OM portion of the trans-envelope Lpt complex and exists as a unique plug-and-barrel arrangement in which the lipoprotein LptE is situated inside of the β-barrel domain of LptD[105,106,119]. Additionally, the N-terminal periplasmic domain (amino acids 25-202; *E. coli* numbering) of LptD is connected to its C-terminal β-barrel domain (amino acids 203-784; *E. coli* numbering) by two long range, non-consecutive disulfide bonds between C31 and C724 and between C173 and C725[105,125]. The plug-and-barrel arrangement, coupled with the interdomain disulfide linkages, likely presents a challenging protein-folding problem. It also remains unknown how the cell coordinates assembly of the LptD/E complex with the rest of the trans-envelope complex. To understand the assembly of the LptD/E complex, we investigated the biogenesis of LptD.

Such work is made possible by the fact that different disulfide-bonded states of LptD can be visualized and distinguished from one another using SDS-PAGE. Wild-type (WT) cells contain only fully oxidized LptD that contains the C31-C724 and C173-C725 disulfide bonds, hereafter referred to as **[1-3][2-4]**-LptD because the linkages exist between the first and third and between the second and fourth cysteine residues. **[1-3][2-4]**-LptD migrates more slowly than reduced LptD when analyzed by SDS-PAGE, and other disulfide-bonded species of LptD migrate at unique speeds[125].

2.2. Results and Discussion

2.2.1. Observation of a non-native disulfide-bonded LptD species

Since LptE is required for proper oxidation of LptD, we looked for intermediate LptD species in a strain reported to make low levels of LptE at certain points during its growth phase[105]. OM fragments were isolated from both WT and LptE-limiting strains and were analyzed by SDS-PAGE followed by α-LptD and α-LptE immunoblot under both reducing (with β-mercaptoethanol, β-ME) and non-reducing (without β-ME) conditions (Figure 10). A novel LptD species was observed in the LptE-limiting strain (labeled intermediate 1). This species migrates slightly faster than reduced LptD, and it only exists in the absence of β-ME, suggesting that it contains at least one disulfide bond.
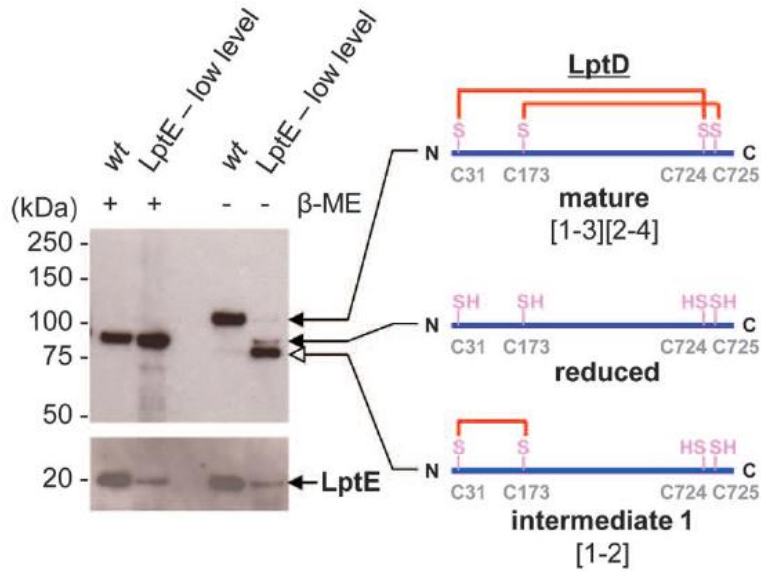
Figure 10. Observation of a non-native disulfide-bonded LptD species under LptE-limiting conditions. α-LptD and α-LptE immunoblots of OM fragments obtained from WT and LptE-limiting strains at early log phase, during which LptE levels are low in the LptE-limiting strain. Where indicated, β-ME was used to reduce disulfide bonds.

In order to assign the disulfide connectivity of the species observed in Figure 10, we performed immunoblot analysis of OM fragments obtained from WT cells bearing plasmids encoding LptD with various cysteine to serine mutations (Figure 11). LptD$_{SSCC}$, which is only capable of forming a **[3-4]** disulfide, migrated indistinguishably from reduced LptD (LptD$_{SSCC}$ is LptD with its first and second Cys residues mutated to Ser). The species that each contain one interdomain disulfide, LptD$_{SCSC}$ and LptD$_{CSCS}$, which are only capable of forming the **[2-4]** and **[1-3]** disulfides, respectively, both migrate more slowly than reduced LptD. Only LptD$_{CCSS}$, which can only form the **[1-2]** disulfide, was shown to migrate faster than reduced LptD, establishing that the LptD species that is observed when LptE is limiting is **[1-2]**-LptD.
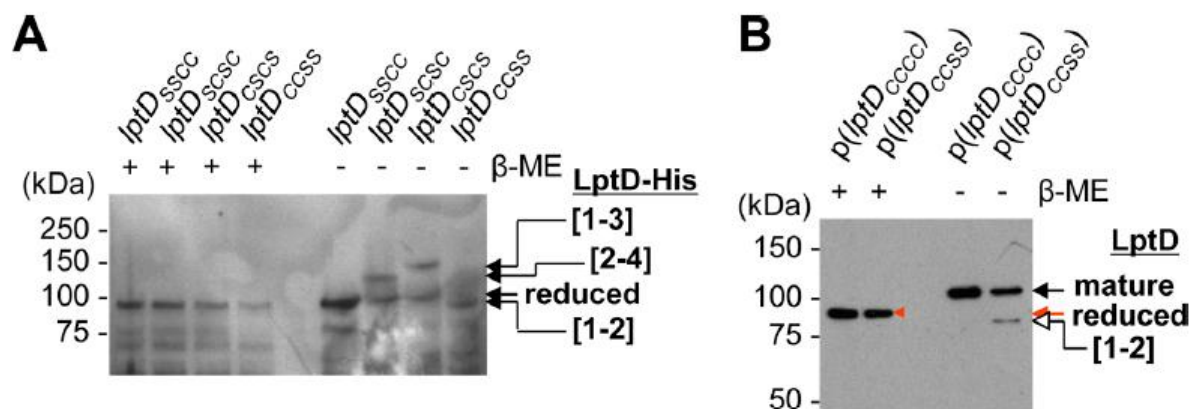
Figure 11. Assignment of the novel LptD species as **[1-2]**-LptD. (A) α-His immonoblot of OM fragments obtained from WT cells expressing LptD$_{SSCC}$-His, LptD$_{SCSC}$-His, LptD$_{CSCS}$-His, or LptD$_{CCSS}$-His (LptD$_{SSCC}$ is LptD with the first and second Cys residues mutated to Ser, etc.). (B) α-LptD immunoblot of OM fragments obtained from WT cells and WT cells expressing a plasmid encoded copy of *lptD$_{CCSS}$*. Where indicated, β-ME was used to reduce disulfide bonds.

2.2.2. Accumulation of [1-2]-LptD in strains with defective LptD or LptE

In order to test how LptD biogenesis is affected in strains bearing defective copies of either *lptD* or *lptE*, we performed immunoblot analysis of OM fragments isolated from WT, *lptDΔ330-352* (*lptD4213*)[107], *lptEΔ100-101/P99R* (*lptE6*)[127], and *lptDΔ529-538*[106] strains (Figure 12). In each of these mutants, significant amounts of intermediate 1 (**[1-2]**-LptD) accumulates in the OM, suggesting that all of these mutants cause defects in LptD biogenesis. Since **[1-2]**-LptD is not functional[125], this observation could explain the OM defects observed in each of these mutations.
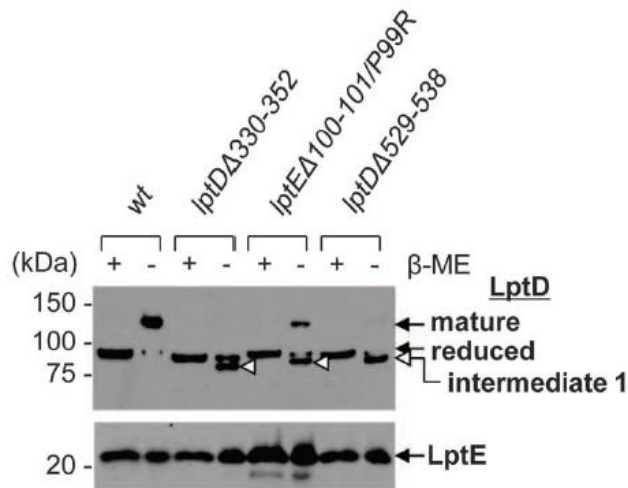
Figure 12. Accumulation of **[1-2]**-LptD in strains defective in *lptD* or *lptE*. α-LptD and α-LptE immunoblots of OM fragments isolated from WT, *lptDΔ330-352*, *lptEΔ100-101/P99R*, and *lptDΔ529-538* strains. The white arrowhead indicates the position of intermediate 1 (**[1-2]**-LptD). Where indicated, β-ME was used to reduce disulfide bonds.

2.2.3. [1-2]-LptD is an intermediate in the LptD assembly pathway

In order to determine whether or not **[1-2]**-LptD is an intermediate along the *in vivo* LptD assembly pathway or a dead-end, off-pathway product, we pulse labeled 3x-FLAG tagged LptD with [^{35}S]-methionine and monitored its maturation following a cold methionine chase (Figure 13). **[1-2]**-LptD was prominent at the beginning of the pulse-chase experiment, and after about thirty minutes, it is almost completely converted to **[1-3][2-4]**-LptD, establishing that it is an intermediate in LptD assembly.
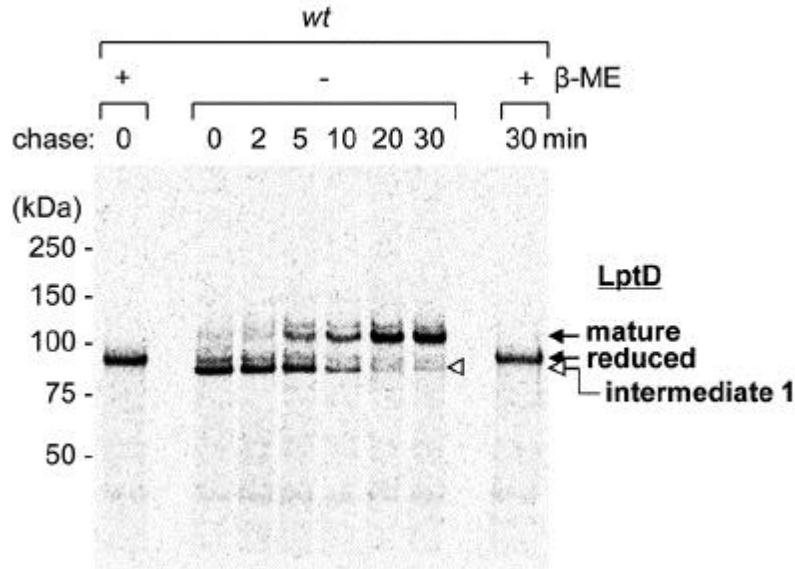
Figure 13. **[1-2]-**LptD is an on-pathway, *in vivo* intermediate in the LptD assembly pathway. WT cells expressing 3x-FLAG tagged LptD were pulse labeled with [^{35}S]-methionine and chased with cold methionine. Samples were taken at various time points, alkylated with N-ethylmaleimide, immunoprecipitated with α-FLAG antibody, and analyzed by SDS-PAGE/autoradiography. The white arrowhead indicates the position of intermediate 1. Where indicated, β-ME was used to reduce disulfide bonds.

2.2.4. Folding of the LptD β-barrel occurs prior to disulfide rearrangement

Next, we performed a version of the pulse-chase experiment that preserved the folded state of the LptD β-barrel domain to determine when folding of the β-barrel occurs in relation to the formation and rearrangement of the **[1-2]** disulfide bond (Figure 14). The pulse-chase was conducted as in Figure 13, but the samples were processed in a non-denaturing fashion and were not heated, unless indicated in Figure 14, prior to analysis via seminative SDS-PAGE. The folding state of LptD can be assessed from this experiment by looking for heat-modifiability in the migration speed of the protein; the folded β-barrel is observed to migrate more rapidly than

the denatured protein. The resulting gel shows that at initial time points, only unfolded, reduced

LptD and unfolded **[1-2]**-LptD are present. As the chase progresses, both species become lost,

and two new folded species appear. The faster-migrating of these bands corresponds to folded

[1-2]-LptD, as judged by an unheated LptD$_{CCSS}$ control that can only form the **[1-2]** disulfide

bond, and it chases away as the experiment progresses. The other faster-migrating species is the

exclusive species present at later time points, leading to its assignment as folded **[1-3][2-4]**-

LptD. Heat modifiability of both of these faster-migrating bands is consistent with these

assignments. Taken together, this experiment enables us to conclude that the disulfide

rearrangement that forms mature LptD occurs after β-barrel assembly. Additionally, since folded

[1-2]-LptD does not accumulate substantially during the chase, we conclude that folding, not

disulfide rearrangement, is the slow step in LptD assembly.
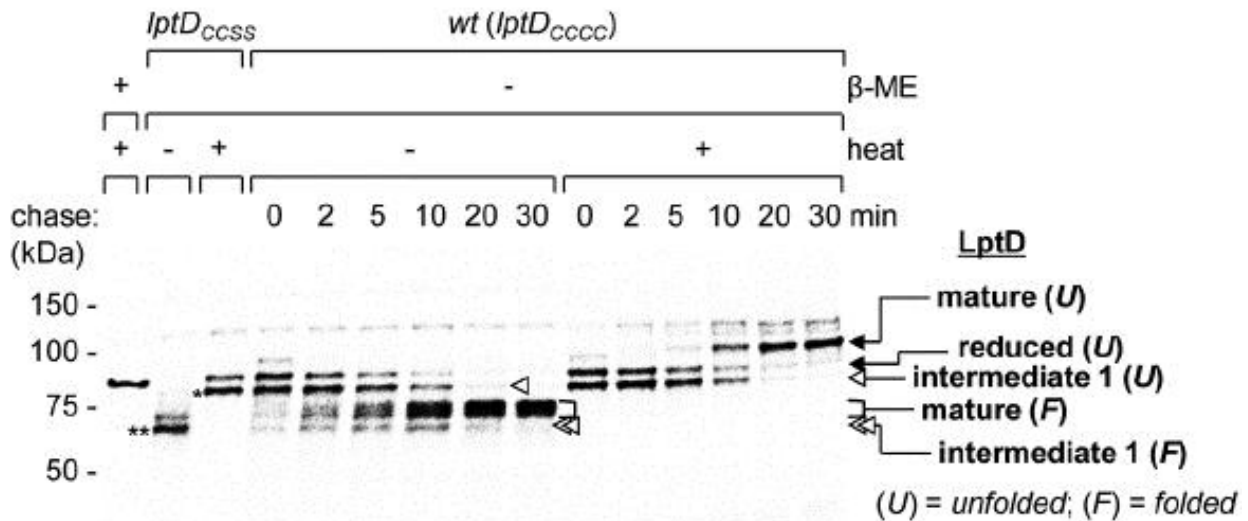
Figure 14. Disulfide rearrangement occurs after assembly of the LptD β-barrel domain. The

pulse-chase experiment described in Figure 13 was performed, but the samples were processed in

a non-denaturing manner and were not heated (unless indicated) prior to analysis by seminative

SDS-PAGE/autoradiography. The white arrowhead marks the position of intermediate 1; the double white arrowhead marks the position of folded intermediate 1; the single and double asterisks mark the positions of the unfolded and folded **[1-2]**-LptD$_{CCSS}$ controls, respectively. Where indicated, β-ME was used to reduce disulfide bonds.

2.2.5. The roles of DsbA and DsbC in LptD biogenesis

LptD is known to be a substrate of DsbA[126], and it is known that DsbA, but not DsbC, is important for proper oxidation of LptD[125]. To determine the roles of DsbA and DsbC in LptD assembly, we analyzed isolated OM fragments from WT, *ΔdsbA*, and *ΔdsbC* strains grown in either rich (LB) or minimal medium (M63/Glc) (Figure 15A). At steady state, *ΔdsbA* cells grown in rich medium contain both mature **[1-3][2-4]**-LptD and an additional species, intermediate 2. Intermediate 2 migrates at the same speed as oxidized LptD$_{SCSC}$, enabling us to assign it as being **[2-4]**-LptD. **[2-4]**-LptD, but not **[1-3][2-4]**-LptD, was observed when *ΔdsbA* cells were grown in minimal medium, suggesting that the mature LptD observed in *ΔdsbA* cells grown in rich medium is the result of a non-specific oxidant that is present in the medium. WT cells and *ΔdsbC* cells are able to exclusively produce **[1-3][2-4]**-LptD in either rich or minimal medium. Pulse-chase experiments were also conducted in both the *ΔdsbA* and *ΔdsbC* backgrounds. In the *ΔdsbA* pulse-chase experiment, by 60 minutes, the pulse-labeled LptD's oxidation state resembled the makeup observed at steady state (Figure 15B and C). In this experiment, almost exclusively reduced LptD is present, with a trace of **[2-4]**-LptD (Figure 15). In the *ΔdsbC* pulse-chase experiment, the rate of LptD maturation is significantly slower than in the WT strain; by ~20 min, LptD is almost completely oxidized in the WT strain, but in the *ΔdsbC* background, an hour is necessary before complete conversion is observed (Figure 16A). We propose that the role of

DsbC is to reduce a **[3-4]** disulfide that also exists in the **[1-2]**-LptD species such that disulfide

rearrangement can occur. To test this theory, the same pulse-chase experiment was conducted in

the *ΔdsbC* background, but with LptD$_{CCSC}$-3xFLAG instead of LptD$_{CCCC}$-3xFLAG (Figure 16B).

In this experiment, formation of a **[3-4]** disulfide is impossible, removing the need for DsbC to

reduce it to enable disulfide rearrangement. Consistent with this hypothesis, we observed that

rearrangement of **[1-2]**-LptD to **[2-4]**-LptD returned to a rate consistent with the WT strain,

suggesting that DsbC's role in LptD assembly is to reduce a **[3-4]** disulfide prior to disulfide

rearrangement.
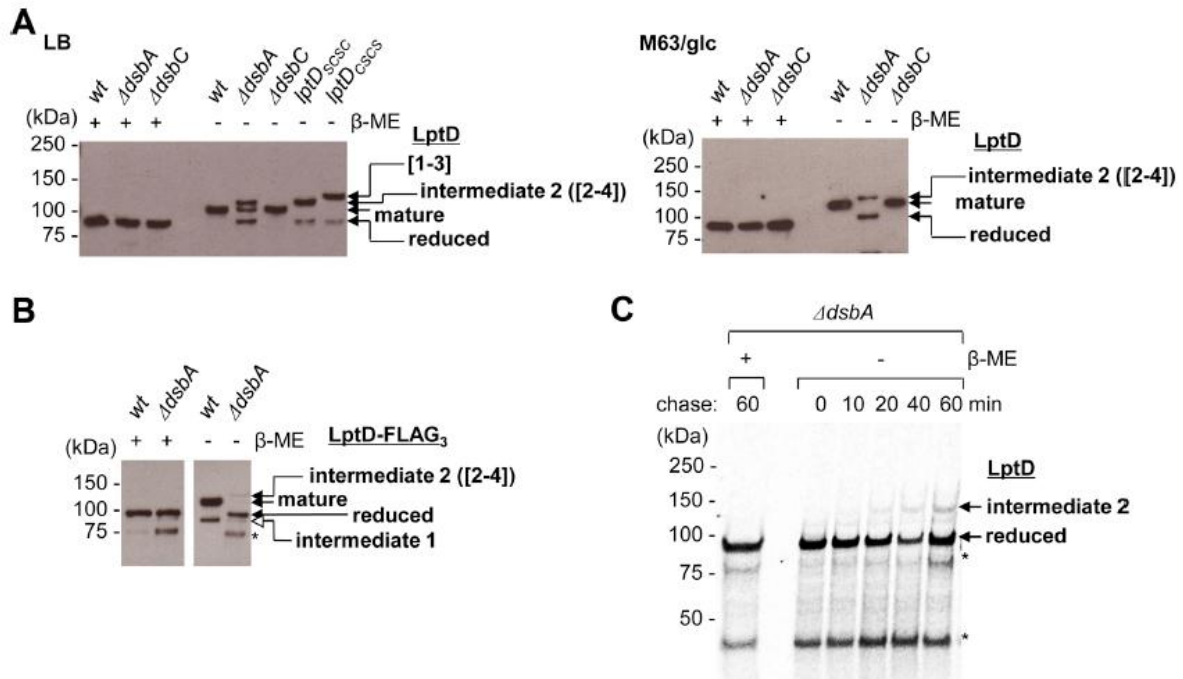
Figure 15. DsbA is required for formation of **[1-2]**-LptD. (A) α-LptD immunoblot analysis of

OM fragments isolated from WT, *ΔdsbA*, and *ΔdsbC* strains grown in either rich (LB) or

minimal medium (M63/Glc). Intermediate 2 is identified as being **[2-4]**-LptD using the indicated

lptD$_{CSCS}$ and *lptD$_{SCSC}$* controls. (B) α-FLAG immunoblot analysis of OM fragments isolated from

WT or *ΔdsbA* cells containing pET23/42*lptD-3xFLAG* grown in minimal medium. (C) [^{35}S]-

Methionine pulse-chase, as in Figure 13, but conducted in a *ΔdsbA* background. Bands marked with an asterisk are LptD degradation products. Where indicated, β-ME was used to reduce disulfide bonds.
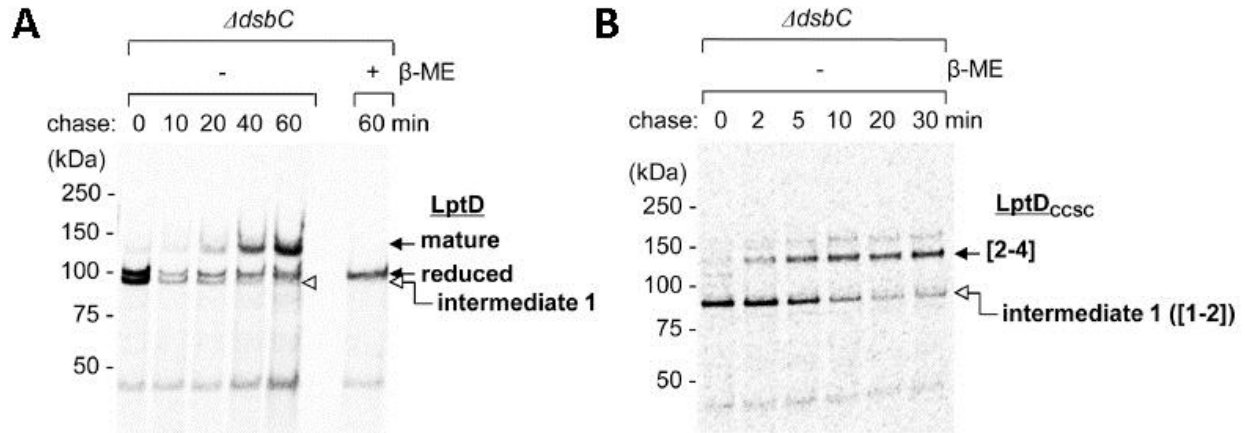
Figure 16. DsbC acts as a reductant during LptD assembly. (A) [^{35}S]-Methionine pulse-chase experiment, as in Figure 13, conducted in a *ΔdsbC* background. (B) [^{35}S]-Methionine pulse-chase experiment, as in (A), but conducted using LptD$_{CCSC}$-3xFLAG instead of LptD$_{CCCC}$-3xFLAG. Where indicated, β-ME was used to reduce disulfide bonds.

To further explore the role of DsbA in LptD assembly, we used DsbA$_{P151T}$, a point mutant in DsbA that forms slow-to-resolve mixed-disulfide adducts with its substrates[126]. α-FLAG immunoprecipitation followed by α-FLAG and α-DsbA immunoblot analysis was conducted on WT and *dsbA$_{P151T}$* strains bearing pET23/42*lptD-3xFLAG*, and two DsbA-LptD adducts were observed (Figure 17A). The first species, adduct A, migrated slightly faster than **[1-3][2-4]**-LptD, while the second species, adduct B, migrated more slowly than **[1-3][2-4]**-LptD. In order to establish the identity of these species, we performed the same analysis on *dsbA$_{P151T}$* strains bearing a variety of pET23/42*lptD-3xFLAG* plasmids in which the encoded *lptD* genes contained all possible single and double cysteine to serine mutations (Figure 17C). The adducts

40

were only detected when C31 was present, suggesting that both adducts are mixed disulfides

between C31 and DsbA. Since adduct A is observed in double mutants in which no other

disulfides are possible, we conclude that it must be **[1-DsbA]-**LptD. Adduct B is observed in

LptD$_{CCSC}$, which is known to exist as **[2-4]-**LptD[125], allowing us to conclude that adduct B is **[2-**

4][1-DsbA]-LptD. In this experiment, a third adduct is observed in LptD$_{CCCS}$, which is known to

exist as **[2-3]-**LptD[125], allowing us to conclude that this species is **[2-3][1-DsbA]-**LptD; this

species is not observed in cells with WT *lptD*.
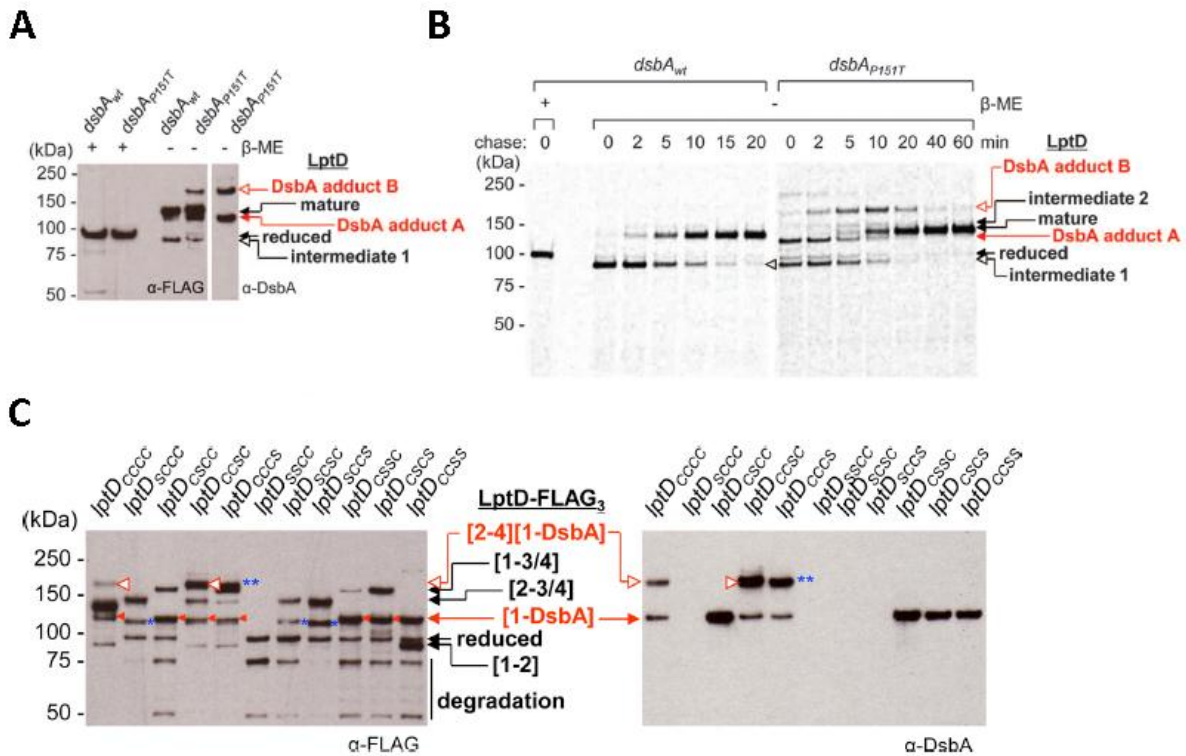
Figure 17. DsbA-mediated oxidation forms the **[1-2]** and **[1-3]** disulfide bonds in LptD. (A) α-

FLAG and α-DsbA immunoblot analysis following α-FLAG immunoprecipitation from WT and

dsbA$_{P151T}$ cells. Two DsbA-LptD adducts are detected, labeled A and B and indicated in red. (B)

[^{35}S]-Methionine pulse-chase experiment using WT and *dsbA$_{P151T}$* cells. New species

corresponding to the DsbA-LptD adducts from (A) are observed. DsbA adduct A appears first and chases away, while DsbA adduct B appears later and chases away. (C) α-FLAG and α-DsbA immunoblot analysis following α-FLAG immunoprecipitation from *dsbA*$_{P151T}$ strains bearing plasmid encoded *lptD*$_{CCCC}$-*3xFLAG*, *lptD*$_{SCCC}$-*3xFLAG*, *lptD*$_{CSCC}$-*3xFLAG*, *lptD*$_{CCSC}$-*3xFLAG*, *lptD*$_{CCCS}$-*3xFLAG*, *lptD*$_{CSSC}$-*3xFLAG*, *lptD*$_{CSCS}$-*3xFLAG*, and *lptD*$_{CCSS}$-*3xFLAG*. **[2-4][1-DsbA]-**LptD, open arrowhead**; [1-DsbA]-**LptD, closed arrowhead; **[2-3][1-DsbA]-**LptD, double asterisk; LptD degradation product, single asterisk.

We performed a pulse-chase experiment in the *dsbA*$_{P151T}$/pET23/42*lptD-3xFLAG* background and were able to observe both of the **[1-DsbA]-**LptD and **[2-4][1-DsbA]-**LptD mixed-disulfide adducts (Figure 17B). **[1-DsbA]-**LptD is evident from the beginning of the experiment, and it chases away, presumably to form **[1-2]-**LptD by ~5-10 minutes. **[2-4][1-DsbA]-**LptD begins to appear at around 2-5 minutes, as **[1-2]-**LptD begins to chase away, and it begins to disappear at around 10-20 minutes as **[1-3][2-4]-**LptD becomes predominant.

2.2.6. Discussion

Taken together, the experimental observation of these six LptD intermediates allows us to establish a pathway for LptD oxidative assembly (Figure 18). Pre-LptD is translated in the cytoplasm with its signal peptide and then secreted across the IM by the Sec machine and processed by the signal peptidase. Following secretion, reduced LptD is oxidized by DsbA, via the **[1-DsbA]-**LptD mixed-disulfide intermediate, to form **[1-2]-**LptD. Evidence also suggests that a **[3-4]** disulfide might also exist in this species, but this has not been firmly established. Following this initial oxidation, unfolded **[1-2]-**LptD is processed by the Bam complex to give a folded β-barrel. The mechanism of this assembly, as well as LptE's role in it, remains poorly

understood. Following folding, **[1-2]**-LptD undergoes a disulfide rearrangement to form **[2-4]**-LptD. Evidence suggests that this step might be preceded by reduction of the possible **[3-4]** disulfide by DsbC. It is worth noting that this rearrangement is the step at which the OM LPS translocon becomes active, since a single interdomain disulfide linkage is sufficient for function[125]. The folded, active **[2-4]**-LptD species is oxidized again by DsbA at the OM, via a **[2-4][1-DsbA]**-LptD mixed-disulfide intermediate, to mature **[1-3][2-4]**-LptD. This species, which is the exclusive form of LptD present in steady-state WT cells, forms the OM portion of the complete Lpt complex.
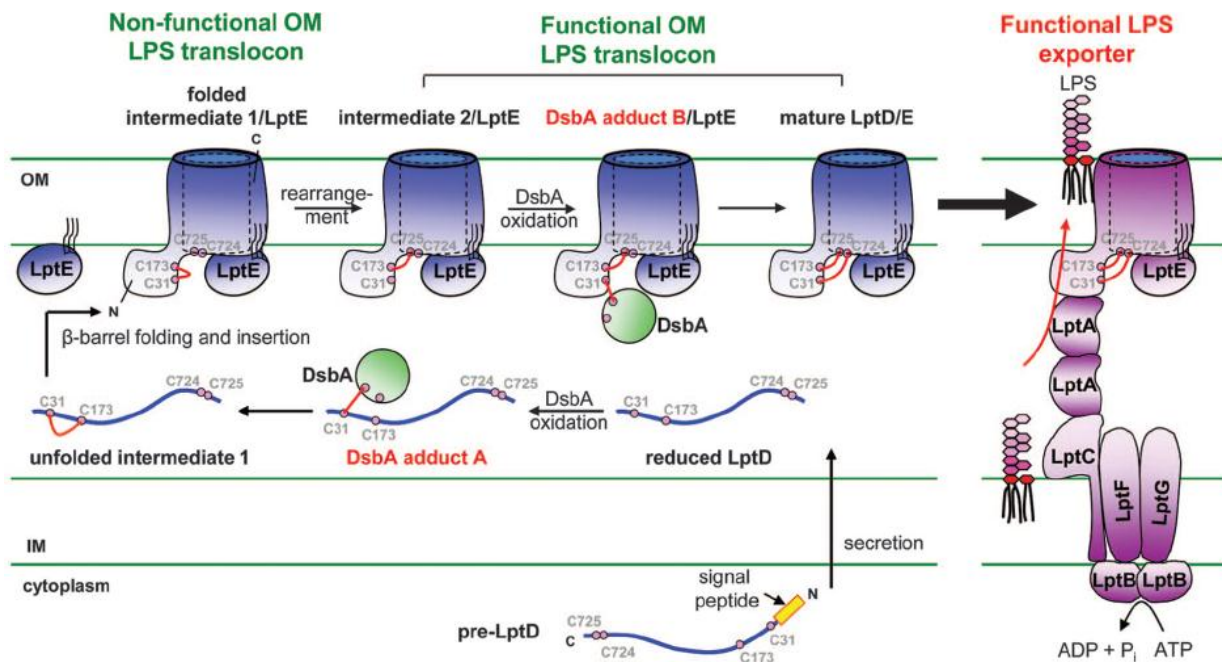
Figure 18. Schematic showing the oxidative assembly pathway of LptD, including the six experimentally observed LptD intermediates.

It is particularly noteworthy that the formation of the **[2-4]** disulfide represents the first active form of the complex because it is the more conserved of the two LptD disulfides and is present in more than 95% of >1000 surveyed non-identical LptD homologs (Figure 19). The **[1-**

3] disulfide is much less conserved, suggesting that the **[2-4]** disulfide plays a critical structural role in the function of the translocon.

Cysteine motifs in LptD	Cys_{31}	Cys_{173}	Motifs at $Cys_{724/5}$	
			CysCys/CysXaaCys	Single Cys
Present	236	1028	491	526
Missing	820	28	39	
Total	1056			

Figure 19. Cysteines 173 and 724/5 from *E. coli* LptD are highly conserved and are present in >95% of 1056 surveyed non-identical LptD homologs.

The disulfide rearrangement from an assembled **[1-2]-**LpD/LptE complex to an activated **[2-4]-**LptD/LptE complex provides a mechanism to guarantee that both LptD and LptE have been properly assembled together into a complex before they are activated. This model is supported by the observation that mutants defective in either LptD or LptE fail this check and remain in the **[1-2]** state (Figure 12). This is also consistent with the observation that **[1-2]-**LptD that accumulates in the LptE-limiting strain during growth phases when LptE is limited (as in Figure 10) is not seen when LptE levels are restored (Figure 20). From this, we conclude that activation of the LptD/E complex, via the disulfide rearrangement, is controlled by proper assembly of the LptD/E complex. It is also worth noting that the oxidation state of LptD is, in this way, controlled by LptE, which is not an oxidoreductase.
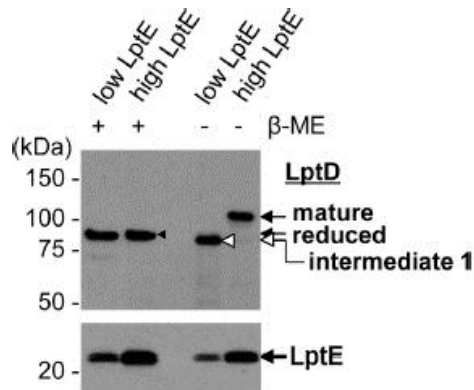
Figure 20. Restoration of LptE restores proper LptD oxidation in an LptE-limiting strain. α-LptD and α-LptE immunoblots of OM fragments isolated from an LptE-limiting strain that expresses low levels of LptE during early-log phase ("low LptE") and higher levels of LptE during mid-log phase ("high LptE"). Intermediate 1, **[1-2]-**LptD, is indicated with an open arrowhead; reduced LptD is indicated with a solid arrowhead.

It has also been previously observed that proper oxidation of LptD is necessary for its association with LptA[103]. Therefore, the disulfide rearrangement provides a mechanism that ensures that only correctly assembled LptD/E species are incorporated into the trans-envelope complex. Perhaps this prevents the formation of non-functional LPS transporters or prevents inappropriate targeting of LPS.

These findings also reveal that β-barrel assembly for LptD is the rate-limiting step in its maturation and is remarkably slow, taking about 20 minutes (about a third of a cell cycle under these conditions). In contrast, LamB assembly is several orders of magnitude faster[134]. This delay in assembly might reflect a difficulty in assembling the complex plug-and-barrel structure that LptD/E is believed to adopt. This slow assembly might also present a target for inhibition of OM biogenesis, and could possibly be the mechanism by which the reported peptidomimetic antibiotic[130] functions.

2.3. Materials and methods

2.3.1. Bacterial strains and growth conditions

For most experiments, the wild type strain used is MC4100 [*F⁻ araD139 Δ(argFlac)* *U169 rpsL150 relA1 flbB5301 ptsF25 deoC1 ptsF25 thi*]. The LptE-limiting strain used that makes varying levels of LptE according to growth phase is AM689 [*MC4100 ara⁺ lptE::kan* *λ$_{att}$(P$_{BAD}$-lptE)*][104]. The *lptDΔ330-352* (*lptD4213*), *lptEΔ100-101/P99R* (*lptE6*) and *lptDΔ529-538* mutant strains used are NR698[107], GC190 [*MC4100 ara⁺ ΔlptE2::kan pBAD18lptE6*][127] and MC4100 *ΔlptD2::kan* pET23/42*lptDΔ529-538*[106], respectively. The *ΔdsbA* and *ΔdsbC* strains used are NR1216 and NR1217[125], respectively. For experiments involving the *dsbA$_{P151T}$* mutant, the wild type strain used is HK295, a MC1000 derivative [*F⁻ Δara714 galU galK Δ(lac)X74 rpsL* *thi*] and the *dsbA$_{P151T}$* mutant used is HK348 [HK295 *zin::Tn10 dsbA$_{P151T}$*][126]. Luria-Bertani (LB) broth and M63/glucose minimal broth and agar were prepared as described previously[135]. Arabinose (0.2% w/v) was added for the growth of AM689[104] and GC190[127]. Growth of strains was carried out at 37°C unless explicitly indicated. When appropriate, kanamycin (25 µg/ml) and carbenicillin (50 µg/ml) were added. Amino acids were added at 50 µg/ml when indicated.

2.3.2. Plasmid construction

To construct pET23/42*lptD-FLAG$_3$*, a cassette containing the coding sequence of the FLAG$_3$ tag was inserted into pET23/42*lptD-His*[104] to replace the original His$_8$ tag. Briefly, the entire pET23/42*lptD-His* template was amplified by PCR (using primers 5'-
AGATCATGATATCGACTATAAAGACGATGATGACAAATAATTGATTAATACCTAGG
CTGC-3' and 5'-

ATAGTCGATATCATGATCTTTGTAGTCGCCGTCGTGATCTTTATAATCGCGCGCCAA

GGC-3') and the resulting PCR product mixture was digested with DpnI for >1 h at 37°C.

NovaBlue (Novagen) cells were transformed with 1 µl of digested PCR product and plated onto

LB plates containing 50 µg/ml carbenicillin. For each construct, plasmids from six colonies were

isolated and sequenced.

To generate LptD Cys mutant constructs containing the FLAG$_3$ tag, pET23/42*lptD$_{XXXX}$-His* constructs were first made via site-directed mutagenesis using relevant primers[125] and

pET23/42*lptD-His*[104] as the initial template. Briefly, the entire template was amplified by PCR

and the resulting PCR product mixture digested with DpnI for >1 h at 37°C. NovaBlue

(Novagen) cells were transformed with 1 µl of digested PCR product and plated onto LB plates

containing 50 µg/ml carbenicillin. For each construct, plasmids from six colonies were isolated

and sequenced. The resulting pET23/42*lptD$_{XXXX}$-His* constructs were used in the same protocol

above to generate pET23/42*lptD$_{XXXX}$-FLAG$_3$* constructs.

2.3.3. Growth of AM689 for OM analysis

10 ml cultures were grown overnight at 30°C in LB broth containing 0.2% arabinose.

Cultures were pelleted and washed twice in equal an volume of LB broth. Fresh LB cultures (1.5

l) containing 0.2% arabinose were inoculated with the washed cells to an initial OD$_{600}$ of ~0.01

and were grown at 30°C until OD$_{600}$ reaches ~0.25 (~4 h) and ~0.5 (~5 h). The amount of cells

equivalent to that in a 500 ml culture of OD$_{600}$ ~0.5 was pelleted by centrifugation at 5000 x g

for 20 min and subjected to OM analysis (see below).

2.3.4. Isolation of OM for analysis of LptD oxidation states

Strains MC4100, AM689, NR1216, NR1217, NR698, GC190 and MC4100 *ΔlptD2::kan*
pET23/42*lptDΔ529-538* were used for OM analysis. These strains contain a single copy of *lptD*
expressed from the chromosome or plasmid. Strains MC4100 containing p($lptD_{CCCC}$) or
p($lptD_{CCSS}$) (pET23/42*lptD* or pET23/42*lptD$_{CCSS}$*, respectively[125]), MC4100, NR1216, HK295
and HK348 containing pET23/42*lptD-FLAG$_3$* were also used for OM analysis experiments.
These strains contain two copies of *lptD*, one expressed from the chromosome and the other
expressed from pET23/42. OM analysis is performed as previously described[125]. Briefly, cells
were pelleted by centrifugation at 5000 x *g* for 20 min and then resuspended in 5 ml Tris-B
buffer (10 mM Tris-HCl, pH 8.0) containing 20% (w/w) sucrose, 1 mM phenylmethylsulfonyl
fluoride (Sigma), 50 μg/ml DNase I (Sigma) and 50 mM iodoacetamide (IAM, Sigma). Cells
were lysed by a single passage through a French Press (Thermo Electron) at 8,000 psi. ~8 ml of
cell lysate was layered onto a two-step sucrose gradient (top – 4 ml Tris-B buffer containing 40%
(w/w) sucrose, bottom – 1 ml Tris-B buffer containing 65% (w/w) sucrose) and centrifuged at
39,000 rpm for 16 h in a Beckman SW41 rotor in an ultracentrifuge (Model XL-90, Beckman).
OM fragments (~0.5 ml) were isolated from the 40%/65% interface by puncturing the side of the
tube with a syringe. 1 ml of 20 mM Tris-HCl, pH 8.0 was added to the OM fragments to lower
the sucrose concentration to below 20% (w/w). The OM fragments were then pelleted in a
microcentrifuge at 18,000 x *g* for 30 min and then resuspended in 200-250 μl TBS (20 mM Tris-
HCl, 150 mM NaCl) containing 5 mM IAM. Protein concentration of these OM preparations
were determined using Bio-Rad DC protein assay after precipitating in 10% trichloroacetic acid
(TCA) and resolubilizing in TBS containing 2% SDS. The same amount of OM (based on

protein content) for each strain was analyzed by non-reducing SDS-PAGE and immunoblotted using antibodies directed against LptD and LptE.

2.3.5. Pulse-chase analysis

Strains MC4100, NR1216, HK295 and HK348 containing pET23/42*lptD-FLAG₃* were used in pulse-chase experiments. Pulse-chase experiments were essentially carried out according to published protocols[136]. Briefly, a 5 ml culture was grown to OD_{600} ~0.5 in M63/glucose minimal media supplemented with eighteen amino acids (minus methionine and cysteine) at 37°C. The culture was pulse-labeled with [^{35}S]-methionine (100 µCi/ml final concentration) (American Radiolabeled Chemicals) for 2 min and then chased with cold methionine (5 mM) at 37°C. At the indicated time point during the chase, a 800 µl culture aliquot was transferred to a 1.5 ml tube containing 80 µl of TCA (70% in water) and incubated on ice for 20 min. Precipitated proteins were pelleted at 18,000 x *g* for 10 min at 4°C, washed with 700 µl ice-cold acetone, and then solubilized in 80 µl 100 mM Tris-HCl, pH 8.0 containing 1% SDS and 20 mM *N*-ethylmaleimide (NEM, Sigma). The sample was sonicated for 30 s to aid solubilization. Following that, 800 µl of ice-cold IP buffer (50 mM Tris-HCl, pH 8.0 containing 150 mM NaCl, 2% Triton X-100, 1 mM EDTA) was added and the sample was centrifuged at 18,000 x *g* for 10 min at 4°C. 700 µl of the supernatant was transferred to another 1.5 ml tube containing 2.5 µl of anti-FLAG® M2 magnetic beads (Sigma). The beads were washed and pre-equilibrated with 3 x 1 ml IP buffer before use. The mixture was incubated on a rotary shaker for 1 h at 4°C, and the beads were washed with 3 x 800 µl of ice-cold high salt buffer (50 mM Tris-HCl, pH 8.0 containing 1 M NaCl, 1% Triton X-100, 1 mM EDTA) and 1 x 800 µl ice-cold 10 mM Tris-HCl, pH 8.0 using a magnetic separation rack (New Englands Biolabs). 60 µl 2X SDS non-reducing

sample buffer was then added to the beads and the mixture heated for 10 min at 100°C to elute

the bound proteins. 15 μl of eluted sample was applied to SDS-PAGE directly. For reduction of

disulfide bonds, 0.5 μl β-mercaptoethanol (β-ME, Sigma) was added to 20 μl eluted sample and

heated for 5 min at 100°C before loading. 4-20% Tris-HCl polyacrylamide gels were used

(running conditions: 150 V for 120 min). The gel was then dried and exposed to phosphor

storage screens for autoradiography.

2.3.6. Seminative pulse-chase analysis

Strain MC4100 containing pET23/42*lptD-FLAG$_3$* was used in seminative pulse-chase

experiments. A 5 ml culture was grown to OD_{600} ~0.5 in M63/glucose minimal media

supplemented with eighteen amino acids (minus methionine and cysteine) at 30°C. The culture

was pulse-labeled with [^{35}S]-methionine (100 μCi/ml final concentration) (American

Radiolabeled Chemicals) for 2 min and then chased with cold methionine (5 mM) at 37°C. At

the indicated time point during the chase, an 800 μl culture aliquot was transferred to a 1.5 ml

tube and pelleted at 18,000 x *g* for 1 min at 4°C. The cell pellet was resuspended in 100 μl lysis

buffer (20 mM Tris-HCl, pH 8.0 containing 150 mM NaCl, 1% SDS, 0.5 mg/ml lysozyme, 1

mM phenylmethylsulfonylfluoride (PMSF, Sigma), 1 mM EDTA and 40 mM NEM). After

incubation for 2.5 min at room temperature, 1 ml of ice-cold IP-2 buffer (50 mM Tris-HCl, pH

8.0 containing 150 mM NaCl, 2% n-octyl-β-glucoside (OG, Anatrace), 1 mM EDTA) was added

and the sample was centrifuged at 18,000 x *g* for 30 min at 4°C. 950 μl of the supernatant was

transferred to another 1.5 ml tube containing 2.5 μl of anti-FLAG® M2 magnetic beads (Sigma).

The beads were washed and pre-equilibrated with 3 x 1 ml IP-2 buffer before use. The mixture

was incubated on a rotary shaker for 2 h at 4°C, and the beads were washed with 4 x 800 μl of

ice-cold wash buffer (50 mM Tris-HCl, pH 8.0 containing 1 M NaCl, 2% OG, 1 mM EDTA)

using a magnetic separation rack (New England Biolabs). 30 µl of ice-cold elution buffer (50

mM Tris-HCl, pH 8.0 containing 150 mM NaCl, 2% OG, 1 mM EDTA, 250 µg/ml $FLAG_3$

peptide (Sigma)) was then added to the beads and the mixture incubated for 10 min at 4°C to

elute the bound proteins. An equal volume of 2X SDS non-reducing sample buffer was added

and the sample split into two – one applied to seminative SDS-PAGE directly and the other

heated for 10 min at 100°C before loading. 10% Tris-HCl polyacrylamide gels were used

(Running conditions: 150 V for 75 min, 4°C). The gel was then dried and exposed to phosphor

storage screens for autoradiography.

2.3.7. Bioinformatics

The list of non-identical LptD sequences was collected by BLAST. Using the *E. coli*

LptD sequence as a start, an initial BLAST hit list was collected. The weak hits were then used

as the new reference sequence to BLAST search for more LptD sequences. By doing this

recursively for over 20 rounds, thousands of LptD sequences were collected. This initial list was

then filtered to remove identical sequences and partial genes (usually containing deletions on one

or the other end of the gene). The final list contains 1056 non-identical LptD sequences.

2.3.8. Antibodies

Monoclonal α-His conjugated to horseradish peroxidase was purchased from Qiagen.

Monoclonal α-FLAG conjugated to horseradish peroxidase was purchased from Sigma. α-

LptD[47], α-LptE[105], and α-DsbA[137] antisera were already described.

Chapter 3: Screening of N-LptD Crystallization Conditions

Collaborators: Goran Malojcic, Shu Sin Chng, Daniel Kahne

3.1 Introduction

There are a number of questions about the mechanism and biogenesis of LptD that could be addressed with the aid of an X-ray crystal structure, but as of yet, none have been reported. It is unlikely that a crystal structure of LptD alone is obtainable since LptE is required for LptD expression and likely performs an integral structural role in stabilizing LptD[105,106]. Crystallization of LptD/E is an ambitious goal given the inherent difficulty associated with crystallizing membrane proteins, and it will be discussed further in Chapter 4. This chapter will discuss work towards the more straight-forward goal of obtaining a crystal structure of the soluble LptD N-terminal domain by itself (N-LptD; amino acids 25-203, 19771 Da, *E. coli* LptD numbering including signal sequence).

While having a crystal structure of the full-length LptD/E complex would be ideal, there are a number of questions that could be addressed by looking at only the structure of the N-terminal domain. As discussed in Chapter 1, LptD is the target of a peptidomimetic antibiotic, and resistance to this drug is conferred by a tandem duplication of amino acids 210-215 (LRDKGM) in the LptD N-terminal domain (numbering from *P. aeruginosa* LptD, including the signal sequence)[130]. The mechanism of action for the drug and the mechanism by which this duplication affords resistance are unknown, but insight into these mechanisms could be provided by examining the structure of N-LptD. Additionally, this duplication lies just downstream of

G207, N208, and V209, which are three of the most highly conserved residues in LptD homologs (see Figure 21). The proximal location of the resistance mutation to this nearly universally conserved stretch of amino acids suggests some, as of yet unknown, functional role for this portion of LptD. It is also worth mentioning that the peptidomimetic drug is only known to affect *Pseudomonas* spp., but not other Gram-negative organisms, including *E. coli.* The reason for this selectivity is not understood. Sequence alignments of LptD from *P. aeruginosa* and *E. coli* show that *P. aeruginosa* LptD contains a large (~90 amino acid) extension at the N-terminus that does not overlap with LptD from *E. coli*. This additional portion of *P. aeruginosa* LptD is predicted to be unstructured and contains two cysteine residues in addition to the four conserved cysteine residues that align with *E. coli* LptD. Comparison of N-LptD structures from these two species and from the drug resistant mutant might offer insights into both the drug's mechanism and N-LptD's role in LPS trafficking.

```
Kpn        ------------------------------------------------------------
EC         ------------------------------------------------------------
PA         ADQFDCKVSATGGWDCSPLQNANANLPPRPAHTATSVSTAAAGSSVSGSGGETVEAEPTQ 60
acinetob   ---------------------------------------------------NDSASSVDNK 10


Kpn        -----------------------------ADLATQCMLGVPSYDRPLVEGRPGDLPVT 29
EC         -----------------------------ADLASQCMLGVPSYDRPLVQGDTNDLPVT 29
PA         RLVTESGGRALKSRSADYSHLDWIPREKLTAAQLAEIGPYCGGSYIEPVRPGMDDGAPSD 120
acinetob   KLKESIQKAYPGQEFFEQYYVEKSSPEAQVRDTRSLSSAFCTGTWITPISP-TTQAVPAD 69
                                            :         ::   *:          *


Kpn        INADHAKGNYP------DNAVFTGNVDINQGNSRLRADEVQLHQQQAAGQAQPVRTVDAL 83
EC         INADHAKGDYP------DDAVFTGSVDIMQGNSRLQADEVQLHQKEAPGQPEPVRTVDAL 83
PA         ESPTYVSAKASRYEQEKQIATLAGDVVLRQGSMQVEGDEANLHQLENRG-------ELV 172
acinetob   QATSVVTADYAHYNP-NGDSELEGNVLIDQQGRSIRANKVTIDRTQTYAN-------AE 120
              .   .... .        : : *.* : * .  :..::. :.:  :  .


Kpn        GNVHYDDNQVILKGPKAWSNLNTKDTNVWQGDYQMVGRQGRGTADLMKQRGENRYTILEN 143
EC         GNVHYDDNQVILKGPKGWANLNTKDTNVWEGDYQMVGRQGRGKADLMKQRGENRYTILDN 143
PA         GNVKLRDKGMLVVGDHAQVQLDNGEAQVDNAEYVIHKAHARG-SALYAKRSENAIIMLKD 231
acinetob   GNVQLAQAGLLAQSDQINYNLKTQQGDLKNSFYISEQQHAHGHAEQIQRTSP-TEIILRN 179
           ***: :  ::  . :   :*.. : :: :. *      :.:* :    : .      :* :


Kpn        GSFTSCLPGSD-TWSVVGSEVIHDREEQVAEIWNAR
EC         GSFTSCLPGSD-TWSVVGSEIIHDREEQVAEIWNAR
PA         GTYTRCEPSSN-AWTLKGNNVKLNPATGFGTATNAT
acinetob   ATYTTCPPEQKPTWRLEAKEIKLNQDTGRGTTKNTK
           .::* * * .. :* : ..:: :    .   *:
```

Figure 21. Multiple sequence alignment of the LptD N-terminal domain from four *lptD* homologs. The location of the amino acids duplicated in the *P. aeruginosa* drug resistance mutation is highlighted. Kpn, *Klebsiella pneumonia*; EC, *E. coli*; PA, *P. aeruginosa*; acinetob, *A. baumannii*.

The structure of N-LptD could also provide insight into the functional significance of the disulfide bond rearrangement that activates the LptD/E complex (see Chapter 2). N-LptD contains Cys31 and Cys173, which form the disulfide linkage in the inactive **[1-2]-**LptD species that exists as an intermediate during LptD biogenesis and accumulates in LptD/LptE defective mutants. It might be possible to crystallize N-LptD with and without cysteine residues in order to observe how the presence of the **[1-2]** disulfide affects the conformation of the N-terminal domain. This could provide a structural understanding of disulfide-mediated association with LptA and offer clues as to how the oxidation state of LptD affects its function.

As discussed in Chapter 1, N-LptD is predicted to be structurally homologous to both LptA and LptC and is known to interact with LptA during the formation of the trans-envelope bridge[103]. The structures of both LptA and LptC have been reported and are shown in Figure 7 and Figure 8, respectively[117,118]. Both LptA and LptC assume a twisted β-jellyroll fold, and N-LptD is predicted to do the same. The predicted secondary structure of N-LptD is consistent with this prediction and suggests that N-LptD consists of a large number of short β-strands (Figure 22). The first 26 to 27 residues of N-LptD are predicted to be unstructured (numbering is of mature N-LptD, lacking the signal peptide), and Cys31 is located within this region. This is consistent with reports that DsbA acts non-specifically upon cysteine residues that are located in unstructured regions[138], and is also in line with the observation in Chapter 2 that DsbA acts twice upon this single residue to initially introduce the **[1-2]** intermediate disulfide bond and subsequently the **[1-3]** disulfide following disulfide rearrangement.

A protocol for the overexpression and purification of N-LptD has been reported[105], which provided a starting point for crystallization efforts. From there, we optimized the purification procedure and expression construct and screened for crystallization conditions in order to obtain diffracting crystals.
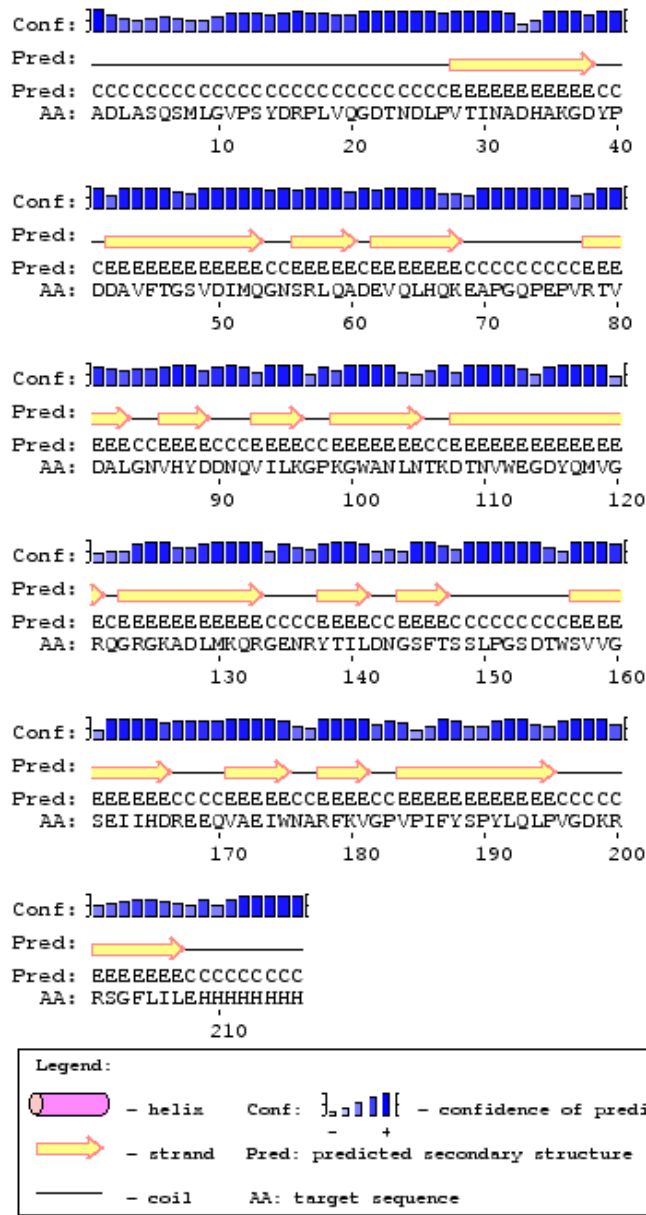
Figure 22. N-LptD predicted secondary structure. The prediction was obtained using the *E. coli* N-LptD-His$_8$ sequence and the PSIPRED v3.3 Protein Sequence Analysis Workbench (available at bioinf.cs.ucl.ac.uk/psipred/). The sequence used for this analysis was that of the mature N-

LptD protein lacking the signal peptide, and as such, the numbering of residues in this figure does not include amino acids 1-24 that make up the signal peptide.

3.2. Results and Discussion

3.2.1. Overexpression and purification of N-LptD-His$_8$ and N-LptD$_{SS}$-His$_8$

N-lptD-His$_8$ was overexpressed with its signal sequence, and the resulting protein was purified from the periplasm as reported[105]. Additionally, a construct in which Cys31 and Cys173 are mutated to serine, *N-lptD$_{SS}$-His$_8$*, was also overexpressed and the resulting protein was purified. The purified samples were analyzed by size exclusion chromatography (SEC) (Figure 23 and Figure 24) and SDS-PAGE (Figure 25). Mostly pure protein was obtained in reasonable yield from each construct (roughly 0.8 to 1.25 mg per liter of culture), but several impurities were notable. Two high molecular weight contaminants were apparent, especially in the construct containing cysteines (referred to as N-LptD$_{CC}$-His$_8$ for clarity). These are observed as the two distinct bands that migrate at roughly 60 kDa and 75 kDa (Figure 25). Given the molecular weight of these species, they are likely the cause of the peak that elutes at roughly 13 ml in Figure 23A. These species are suspected of being N-LptD oligomers, which is supported by the observation that peak fractions collected from SEC of N-LptD$_{CC}$-His$_8$ (collected fractions indicated by the red lines in Figure 23A) gave rise to the peak at 13 ml when analyzed again by SEC (Figure 23B), suggesting that there could be equilibration between monomeric and oligomeric N-LptD in solution. These contaminants were less evident in N-LptD$_{SS}$-His$_8$, but were still present (Figure 25). They are likely the cause of the shoulder observed during N-LptD$_{SS}$-His$_8$ SEC (Figure 24). These proposed oligomers do not contain disulfide bonds, as they are observed in reducing conditions and in a cysteine-free construct.

A
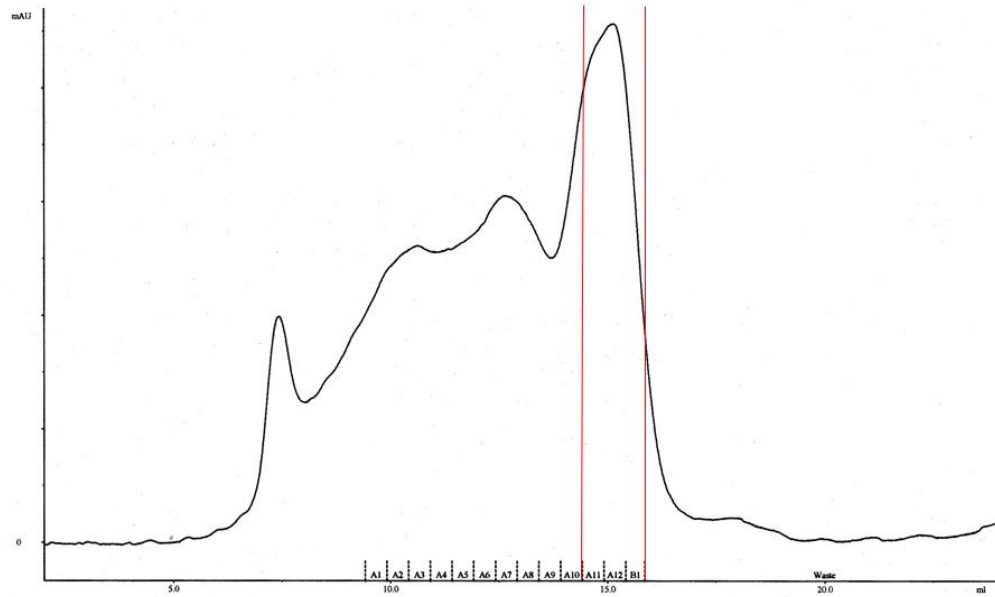
B
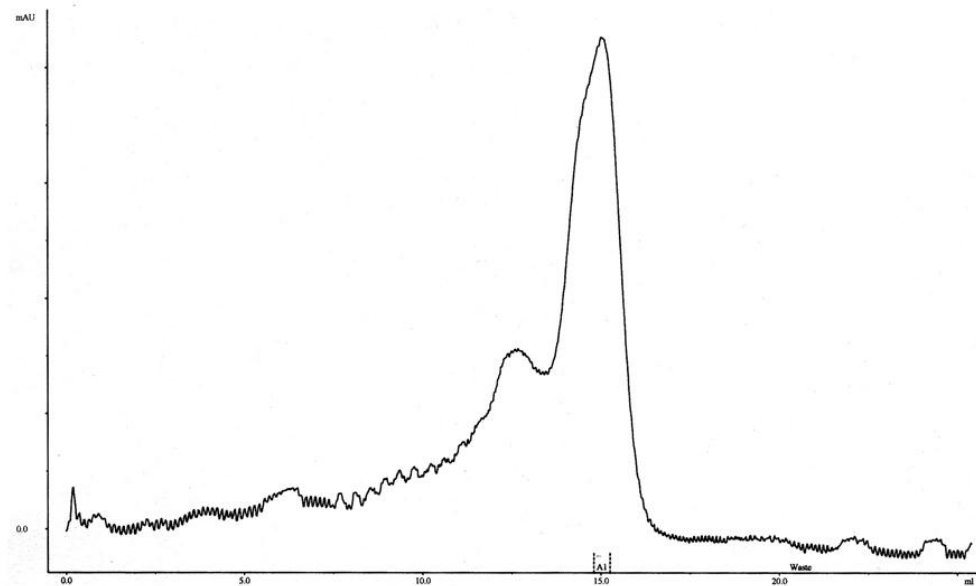
Figure 23. Size exclusion chromatograms of N-LptD$_{CC}$-His$_8$. (A) Size exclusion chromatogram following affinity purification of N-LptD$_{CC}$-His$_8$. (B) Chromatogram in which three fractions (A11-B1, indicated with red vertical lines) from (A) were collected and re-analyzed by size exclusion chromatography.
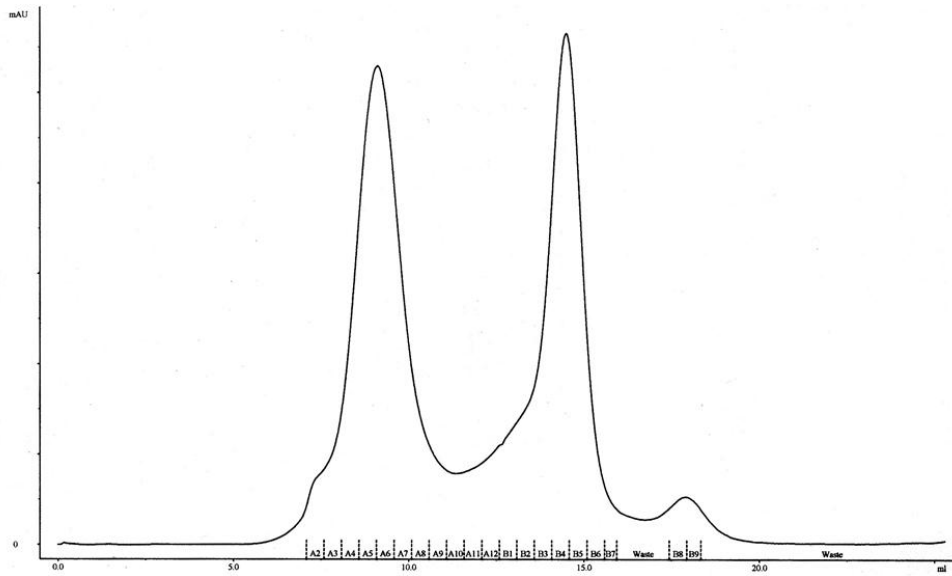
Figure 24. Size exclusion chromatogram of N-LptD$_{SS}$-His$_8$. The chromatogram was obtained

following affinity purification, as in Figure 23A. Pooled fractions B4-B6 were analyzed in

Figure 25.
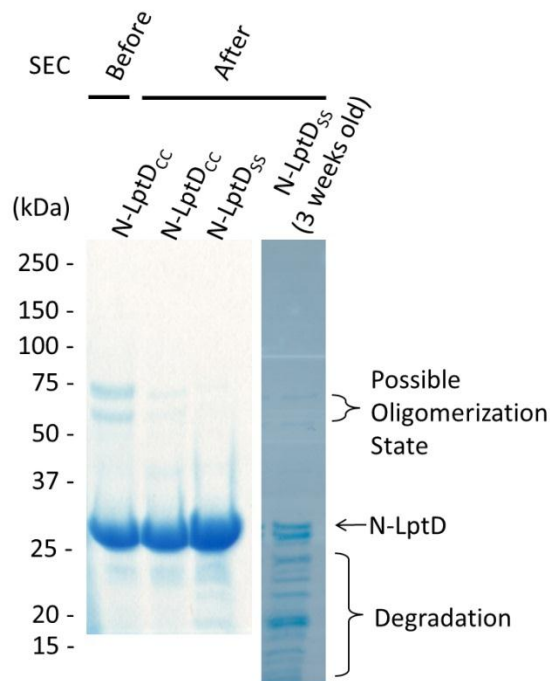
Figure 25. SDS-PAGE analysis of purified N-LptD$_{CC}$-His$_8$ and N-LptD$_{SS}$-His$_8$. Lane 1 contains

N-LptD$_{CC}$-His$_8$ following affinity purification but prior to size exclusion chromatography (SEC).

Lane 2 is an analysis of the pooled eluate fractions obtained from SEC of the sample in lane 1. Lane 3 contains N-LptD$_{ss}$-His$_8$ following SEC purification. Lane 4 is of the same sample as lane 3, but after three weeks of storage at 4°C. All samples were reduced with β-ME prior to analysis.

The other contaminants that appear in the purified protein are bands that appear at a lower molecular weight than N-LptD. These bands are likely degradation products. This is supported by the observation that N-LptD$_{SS}$-His$_8$ that has been stored at 4°C for three weeks undergoes nearly complete decomposition into a ladder of lower molecular weight bands (Figure 25, lane 3 vs. lane 4).

3.2.2. Optimization of the expression construct

Protease protection experiments were conducted with N-LptD$_{CC}$-His$_8$ and N-LptD$_{SS}$-His$_8$ in order to identify a minimal expression construct to use in crystallization screening (Figure 26). In these experiments, these two constructs were digested with various amounts of trypsin or subtilisin and analyzed by SDS-PAGE. Ideally, one would see a protease-stable, truncated fragment that might be useful as a construct for crystallization. In this case, no such stable fragment was observed, and complete loss of the protein occurs with increasing protease concentration.
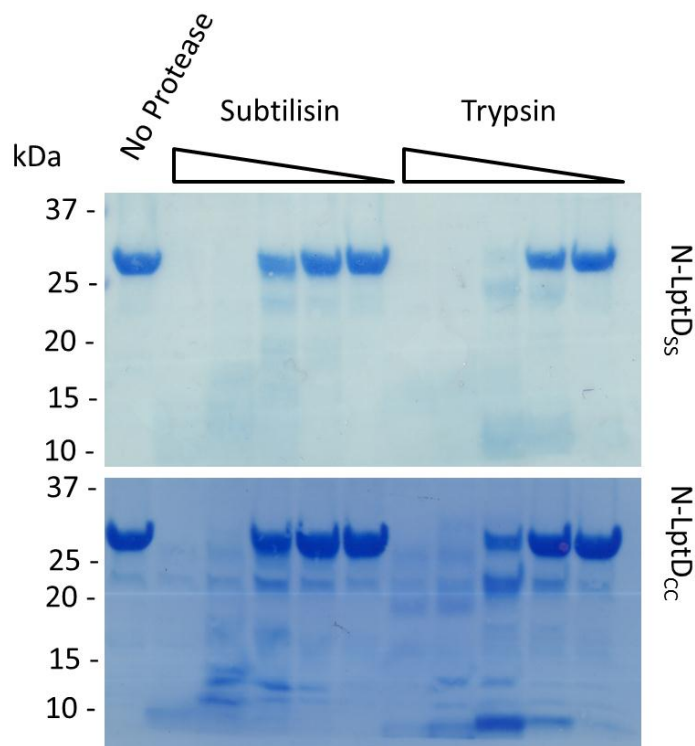
Figure 26. Limited protease digestion of N-LptD$_{CC}$-His$_8$ and N-LptD$_{SS}$-His$_8$. Each lane was loaded with a sample from a reaction in which 1 mg/ml N-LptD$_{XX}$-His$_8$ was digested with some amount of either subtilisin or trypsin at 37°C for one hour. Lane 1 contained no protease. The samples loaded on lanes 2, 3, 4, 5, and 6 were digested with 4000, 800, 160, 32, and 6.4 ng/ml of subtilisin, respectively. The samples loaded into lanes 7-11 were digested with the same concentrations as in lanes 2-6, but trypsin was used instead of subtilisin. All samples are reduced with β-ME.

The predicted secondary structure of N-LptD predicts that the first 26-27 amino acids are unstructured (Figure 22), and since unstructured regions are typically detrimental to protein crystallization, we decided to truncate *N-lptD* from its N-terminus to remove these residues. Five constructs were assembled by site-directed mutagenesis of *N-lptD$_{SS}$-His$_8$* and tested for overexpression (Figure 27). Of these, only *N-lptD$_{C173S, ΔD26-G45}$-His$_8$* overexpressed well and

produced sufficient amounts of protein. These constructs were made in the cysteine-free

construct as to prevent the introduction of unpaired cysteines that could lead to disulfide bonded

oligomers and because the cysteine-free construct seemed to give a cleaner SEC chromatogram

than the construct with cysteines (Figure 23 vs. Figure 24).

Figure 27. N-terminal N-LptD truncation constructs. The indicated truncations were made in *N-lptD$_{SS}$-His$_8$*. Expression level is indicated, and numbering for each deletion refers to *E. coli* LptD containing its signal peptide.

N-lptD$_{C173S, \Delta D26-G45}$-His$_8$ was overexpressed and the resulting protein was purified. The

yield was similar to that obtained from overexpression of *N-lptD$_{CC}$-His$_8$/N-lptD$_{SS}$-His$_8$*. When

analyzed by SEC, the purified protein produced a chromatogram similar to the one obtained from

N-LptD$_{SS}$-His$_8$ (Figure 28A). The purified sample, when analyzed by electrospray ionization-

mass spectroscopy (ESI-MS), shows a single peak of mass 18963.9388 Da (expected mass,

18963.6 Da) (Figure 28B). This construct produces the cleanest and most stable N-LptD protein

to date.
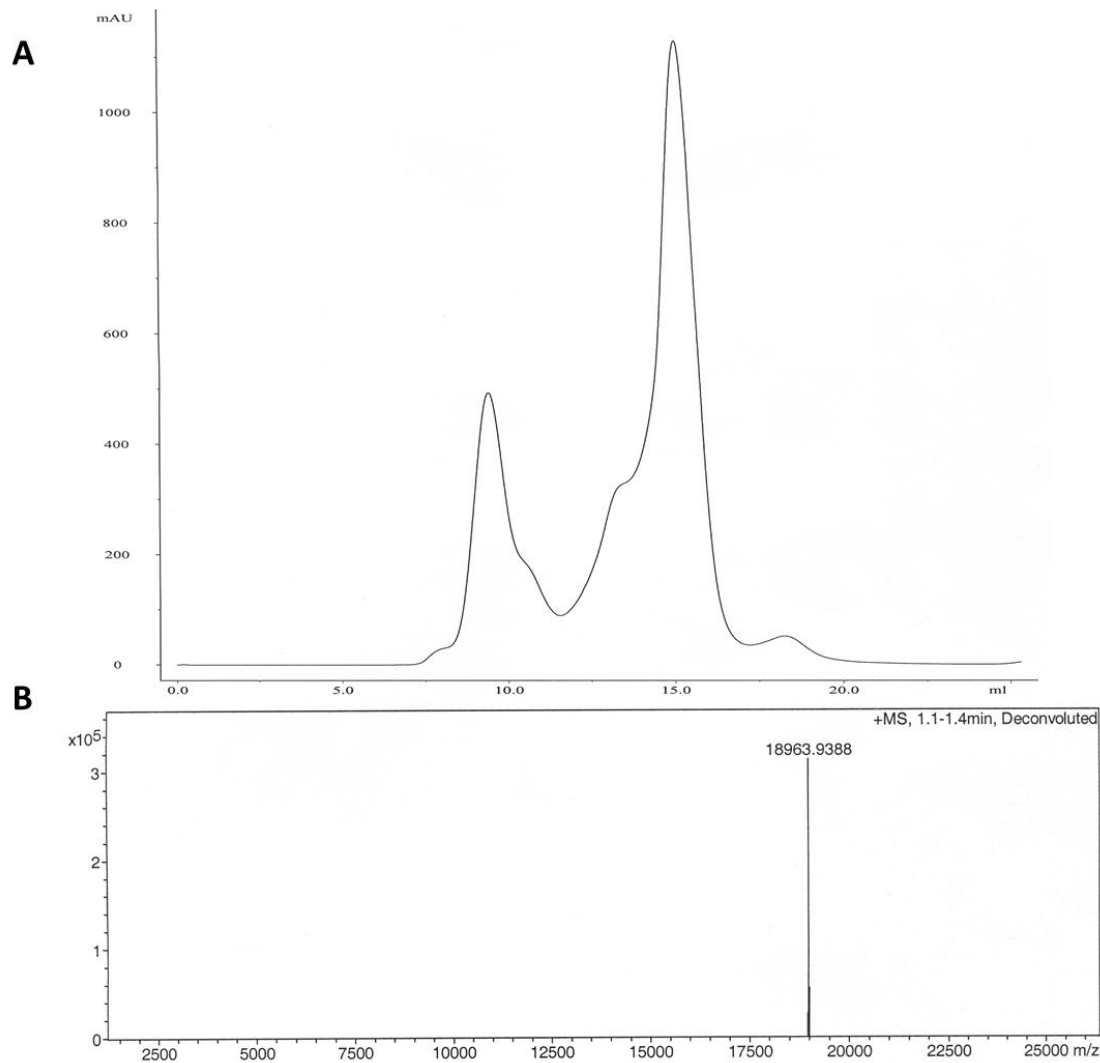
Figure 28. Analysis of purified N-LptD$_{C173S, \Delta D26-G45}$-His$_8$. (A) Size exclusion chromatogram. (B) Deconvoluted ESI-MS spectrum.

3.2.3. Screening of N-LptD crystallization conditions

Both N-LptD$_{SS}$-His$_8$ and N-LptD$_{C173S, \Delta D26-G45}$-His$_8$ have been extensively screened for conditions that produce protein crystals. N-LptD$_{SS}$-His$_8$ has been screened at protein concentrations of 30, 20, and 10 mg/ml using Clear Strategy Screen I and Clear Strategy Screen II (Molecular Dimensions) at 4°C and 18°C. All of these combinations of temperature, protein

concentration, and precipitant condition were also screened using N-LptD$_{SS}$-His$_8$ in which the lysine residues had been reductively methylated[139]. No crystals were observed from any of these conditions.

N-LptD$_{C173S, \Delta D26\text{-}G45}$-His$_8$ was screened both with and without lysine methylation, at 10 mg/ml, at 4°C and 18°C, using JCSG+ (Qiagen), ProComplex (Qiagen), ComPAS (Qiagen), Clear Strategy Screen I (Molecular Dimensions), and Clear Strategy Screen II (Molecular Dimensions). Very small microcrystals were detected in a number of wells containing methylated protein (Figure 29). These crystals grew slowly over time, consistent with protein crystal growth patterns. The crystals were exceptionally small and not of sufficient size to test for diffraction. Each of the conditions described in Figure 29 was repeated on a larger scale (2 µl vs. 300 nl droplet), but crystals failed to grow. Seeding of these crystals was not possible due to their size.
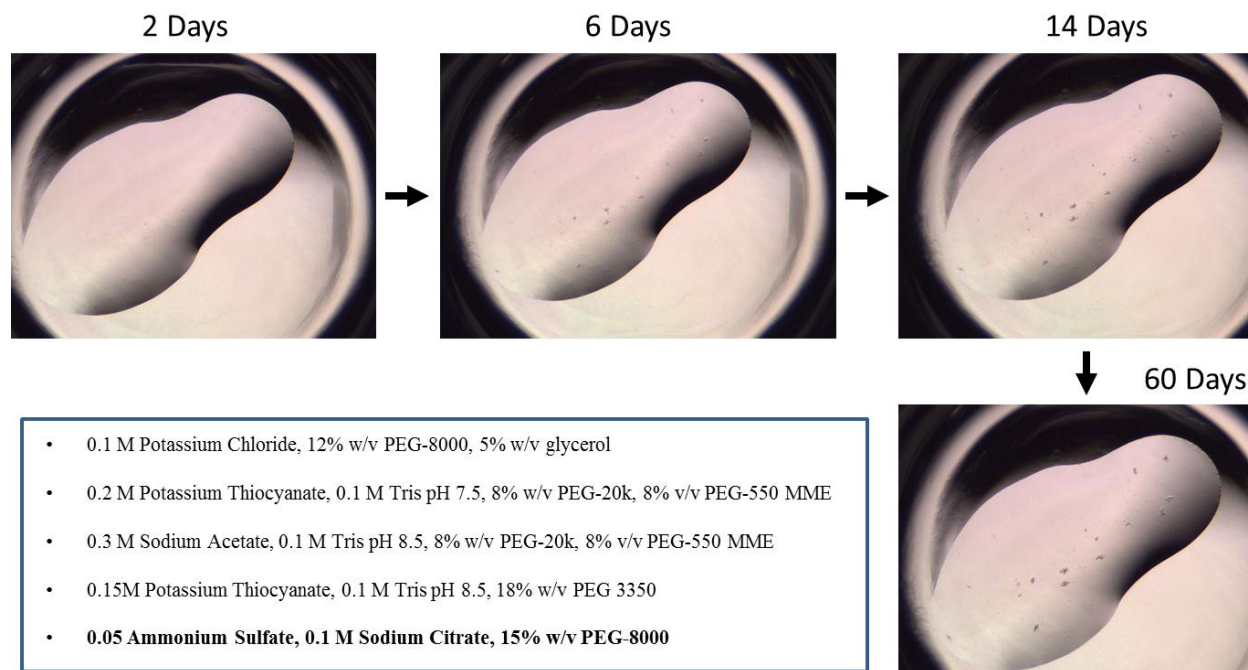
Figure 29. Microcrystals of methylated N-LptD$_{C173S, \Delta D26-G45}$-His$_8$. Images show growth of microcrystals over time in a representative crystallization condition. Inset: precipitant conditions that gave rise to these (bold) and similar crystals.

3.2.4. Discussion and future work

The work described here, while not leading to diffracting crystals, does suggest that N-LptD has the potential to be crystallized. It also provides a starting point for further refinement of the expression construct.

Going forward, it will be of the utmost importance to stabilize N-LptD such that it does not degrade appreciably over time. As is seen in Figure 25, degradation of each of these constructs represents a major problem that will most likely have to be better addressed before diffracting crystals are obtained. One way to stabilize the protein could be to find a better expression construct. Because of its interaction with LptA, it is also possible that co-purification

of N-LptD with LptA could lead to a stabilized complex. Here we explored N-terminal truncations, but truncations from the C-terminus might also be beneficial. Installation of a protease-cleavable His-tag or an N-terminal His-tag might lead to a protein that is more stable and/or forms crystals more readily.

Using N-LptD from other species would also be a good idea moving forward. While we have found *E. coli N-lptD* to overexpress much better than *P. aeruginosa N-lptD* (expressed heterologously in *E. coli*; data not shown), expressing *N-lptD* from various organisms, particularly thermophilic organisms, could produce a more stable N-LptD protein that is better suited to crystallographic studies.

While the conditions identified here (Figure 29) do not produce useful crystals, they may provide a starting point from which better crystals can be grown. This could be done through the use of additive screening or by attempting to crystallize the protein using precipitant screens that are similar to the conditions that were identified for LptA/LptC crystallization. It is worth noting that the fibril forming crystal-form of LptA was only observed when LptA was crystallized in the presence of LPS[117]. Similarly, it might be beneficial to screen for N-LptD crystallization in the presence of various purified LPS species.

3.3. Materials and methods

3.3.1. Strains and growth conditions

The strain BL21(λDE3) [*F⁻ dcm ompT hsdS(r⁻$_B$m⁻$_B$) gal(λDE3)*] (Novagen) was used for protein overexpression. Luria-Bertani (LB) broth and agar were prepared as described previously[135]. Antibiotics were used at 50 μg/ml unless otherwise indicated.

3.3.2. Overexpression and purification

Expression and purification of N-LptD proteins was modified from the previous reported protocol[105]. Briefly, N-LptD$_{CC}$-His$_8$, N-LptD$_{CC}$-His$_8$, and N-LptD$_{C173S, \Delta D26-G45}$-His$_8$ proteins were expressed and purified from BL21(λDE3) cells carrying the pET22/42*N-lptD$_{XX}$-His$_8$* plasmid. A 10 ml LB culture (supplemented with 50 µg/ml carbenicillin) was inoculated with the appropriate strain and grown at 37°C until OD$_{600}$ ~0.6. 10 ml of this culture was used to inoculate each 1.5 l LB culture (supplemented with 100 µg/ml carbenicillin). A typical experiment involved growing several 1.5 l cultures. The 1.5 l cultures were grown at 24°C until OD$_{600}$ ~0.6, at which point they were supplemented with 0.1 mM isopropyl-β-D-1-thiogalactopyranoside (IPTG) and grown for another 20 hours at 16°C. The cultures were centrifuged at 5,000 x g for 10 minutes, and the cells were resuspended in 40 ml of cold TBS (20 mM Tris-HCl, pH 8.0, 150 mM NaCl) (supplemented with 1 mM PMSF, 0.05 mg/ml DNase I, and 0.1 mg/ml lysozyme) per 1.5 l culture that was centrifuged. The resuspended cells were lysed by a single passage through a French Press (Thermo) at 16,000 psi. The lysate was centrifuged for 10 min at 3,000 x g to remove unlysed cells, and the supernatant was centrifuged for 30 min at 100,000 x g in an ultracentrifuge (Model XL-90, Beckman; Type 45-Ti rotor). The supernatant was supplemented with 20 mM imidazole. 3 ml of Ni-NTA resin (Qiagen), as a 50% slurry, was added directly to the supernatant per 1.5 l culture being processed. The resulting mixture was rocked at 4°C for 2 hr. The mixture was applied to a column and allowed to drain by gravity. The flow-through was reapplied to the column and drained again. The column was washed four times with five column volumes of TBS-A (20 mM Tris-HCl, pH 8.0, 300 mM NaCl, 20 mM imidazole). The protein was eluted in two column volumes of TBS-B (20 mM Tris-HCl, pH 8.0, 150 mM NaCl, 200 mM imidazole). Protein was concentrated in an ultrafiltration device (Amicon Ultra, Millipore, 10

kDa cut-off) and further purified by SEC using a pre-packed Superdex 200 column (GE

Healthcare), using 20 mM HEPES pH 7.5, 300 mM NaCl as the eluent. Protein concentration

was determined by NanoDrop spectrophotometer (Thermo, A280 measurement). Protein

concentration was calculated using extinction coefficients as determined by ExPASy ProtParam

tool (available at web.expasy.org/protparam/). ESI-MS was conducted using a micrOTOF-QII

mass spectrometer (Bruker) and was processed and deconvoluted using Bruker Compass

DataAnalysis 4.0. SDS-PAGE was performed using 4-20% Tris-HCl polyacrylamide gels as

previously published[140]. Gels were run at 150 V for 1 hr.

3.3.3. Limited protease digestion

Purified N-LptD$_{CC}$-His$_8$ or N-LptD$_{SS}$-His$_8$ was diluted to 1 mg/ml in TBS. The solution

was subdivided into 11 separate 20-µl reactions. Subtilisin (Sigma) was added to five these

reactions at concentrations of 4000, 800, 160, 32, and 6.4 ng/ml. Trypsin (Sigma) was added to

five of the remaining reactions at 4000, 800, 160, 32, and 6.4 ng/ml. The remaining reaction

contained no protease. Each reaction was incubated at 37°C for 1 hour and then quenched with 2

µl of 100 mM PMSF. Samples were analyzed by SDS-PAGE, as described above.

3.3.4. Lysine methylation

Methylation of exposed lysine residues was carried out as reported[139]. In brief, the protein

was concentrated to 1 mg/ml in 20 mM HEPES, 300 mM NaCl. 20 µl of freshly prepared 1 M

borane-dimethylamine complex (Sigma) and 40 µl 1 M formaldehyde (Sigma) were added per

ml of protein solution. The solution was gently rocked and incubated at 4°C for 2 hr. Another 20

µl 1 M borane-dimethylamine complex and 40 µl 1 M formaldehyde were added per ml of

solution, and the solution was gently rocked and incubated at 4°C for another 2 hr. Following

this incubation, a final 10 µl of 1 M borane-dimethylamine complex was added per ml of

solution, and the reaction was gently rocked and incubated at 4°C overnight. The next day, the

reaction was quenched by the addition of 20 mM Tris-HCl, pH 8.5 (from 1 M stock). Following

methylation, the sample was concentrated using an ultrafiltration device (Amicon Ultra,

Millipore, 10 kDa cut-off), subsequently diluted with 20 mM HEPES pH 7.5, 300 mM NaCl, and

concentrated again for at least three cycles until remaining formaldehyde/borane-dimethylamine

complex is confidently removed. The resulting protein was concentrated for use in crystallization

experiments.

3.3.4. Plasmid construction

Construction of pET22/42*N-lptD$_{CC}$-His$_8$* was previously reported[105]. To create the

cysteine-free variant, this plasmid was mutagenized twice with QuickChange site-directed

mutagenesis (Stratagene) using primers shown in Table 1. Primers C31S F and C31S R were

used to insert the C31S mutation, and primers C173S F and C173S R were used to insert the

C173S mutation, as previously reported[125]. Briefly, the template plasmid was amplified by PCR

using the indicated primers. The resulting PCR product was digested with DpnI (New England

Biolabs) for 1 hr at 37°C. 1 µl of the digested PCR product was used to transform NovaBlue

(Novagen) cells. The transformed cells were plated onto LB-agar plates that were supplemented

with carbenicillin. Mutagenesis was confirmed by sequencing.

Table 1. Primers used in this chapter.

Name	Sequence
C31S F	5'-GCCTCACAGTCAATGTTGGGCGTGCC-3'
C31S R	5'-GGCACGCCCAACATTGACTGTGAGGCG-3'
C173S F	5'-GCTTTACCTCCTCACTGCCGGGTTCTGACACC-3'
C173S R	5'-GGTGTCAGAACCCGGCAGTGAGGAGGTAAAGC-3'
ΔA25-N48 F	5'-CCGCCCTTTATAGTCAACAGGGACTGGCAGACTTACCCGTGACTATCAATGCTGACCACGC-3'
ΔA25-N48 R	5'-GCGTGGTCAGCATTGATAGTCACGGGTAAGTCTGCCAGTCCCTGTTGACTATAAAGGGCGG-3'
ΔD26-N48 F	5'-GCCCTTTATAGTCAACAGGGACTGGCAGCCGACTTACCCGTGACTATCAATGCTGACCACGC-3'
ΔD26-N48 R	5'-GCGTGGTCAGCATTGATAGTCACGGGTAAGTCGGCTGCCAGTCCCTGTTGACTATAAAGGGC-3'
ΔD26-G45 F	5'-GCCCTTTATAGTCAACAGGGACTGGCAGCCGATACCAATGACTTACCCGTGACTATCAATGCTG-3'
ΔD26-G45 R	5'-CAGCATTGATAGTCACGGGTAAGTCATTGGTATCGGCTGCCAGTCCCTGTTGACTATAAAGGGC-3'
ΔD26-L50 F	5'-GCCCTTTATAGTCAACAGGGACTGGCAGCCCCCGTGACTATCAATGCTGACCACGCGAAAG-3'
ΔD26-L50 R	5'-CTTTCGCGTGGTCAGCATTGATAGTCACGGGGGCTGCCAGTCCCTGTTGACTATAAAGGGC-3'
ΔA25-L50 F	5'-CCGCCCTTTATAGTCAACAGGGACTGGCACCCGTGACTATCAATGCTGACCACGCGAAAG-3'
ΔA25-L50 R	5'-CTTTCGCGTGGTCAGCATTGATAGTCACGGGTGCCAGTCCCTGTTGACTATAAAGGGCGG-3'

N-terminal N-LptD truncation mutants were made as described above using site-directed mutagenesis with p22/42*N-lptD$_{SS}$-His$_8$* as a template. Primers ΔA25-N48 F and ΔA25-N48 R were used to remove amino acids A25 through N48, and so on (Table 1).

3.3.5. Crystallization

For screening of crystallization conditions, purified N-LptD$_{SS}$-His$_8$ or N-LptD$_{C173S, ΔD26-G45}$-His$_8$ was prepared as above and concentrated to the indicated concentration (e.g. 10, 20, or 30 mg/ml). The protein sample was dispensed using an Art Robbins Instruments Phoenix drop-setting robot into 96-well sitting drop crystallization plates (Intelli-Plate 96-3 LVR, Art Robbins Instruments). Crystallization droplets contained 150 nl protein and 150 nl precipitant solution,

and the reservoir solution contained 70 µl of the precipitant solution. The following precipitant screens were used: Clear Strategy I (Molecular Dimensions), Clear Strategy II (Molecular Dimensions), JCSG+ (Qiagen), ComPAS (Qiagen), and ProComplex (Qiagen). Plates were stored at either 4°C or 18°C and imaged in a crystallization hotel (Formulatrix)

Larger scale crystallization was set by hand in 24-well sitting drop Cryschem crystallization plates (Hampton). The precipitant solution was made by hand from individual components. The reservoir of each well was filled with 750 µl of the precipitant solution. Various droplet volumes were used; 1 µl to 1 µl, 2 µl to 2 µl, 1 µl to 2 µl, 2 µl to 1 µl, 1 µl to 3 µl, and 3 µl to 1 µl of protein to precipitant were used.

Chapter 4: Crystallization of the LptD/E Complex

Part of this chapter is adapted from: Chimalakonda, G., Ruiz, N., Chng, S. S., Garner, R. A., Kahne, D., and Silhavy T. J. Lipoprotein LptE is required for the assembly of LptD by the β-barrel assembly machine in the outer membrane of *Escherichia coli*. *Proceedings of the National Academy of Sciences of the United States of America*, **108**, 2492-2497, (2011).

Collaborators: Goran Malojcic, Daniel Kahne

4.1 Introduction

An X-ray crystal structure of the LptD/E complex (*E. coli* LptD, amino acids 25-784, 87.1 kDa; *E. coli* LptE, amino acids 19-193, 19.4 kDa) will be necessary to ultimately confirm the plug-and-barrel model, answer a number of questions regarding the mechanism of LPS transport, and understand the structural significance of the translocon-activating disulfide bond rearrangement. Determination of this structure represents a challenging problem given that it is a complex of two membrane proteins. Several crystal and NMR structures of LptE alone are available (crystal structure from *Shewanella oneidensis*, PDB accession code 2R76; NMR structure from *Nitrosomonas europaea*, PDB accession code 2JXP; structure from *N. meningitidis*, PDB accession code 3BF2; crystal structure from *E. coli*, PDB accession code 4NHR), but only the structure from *E. coli* has been published[141]. These structures are all very similar, and they show that LptE contains a three-stranded β-sheet that is packed against two α-helices and a shorter β-strand (Figure 30A).
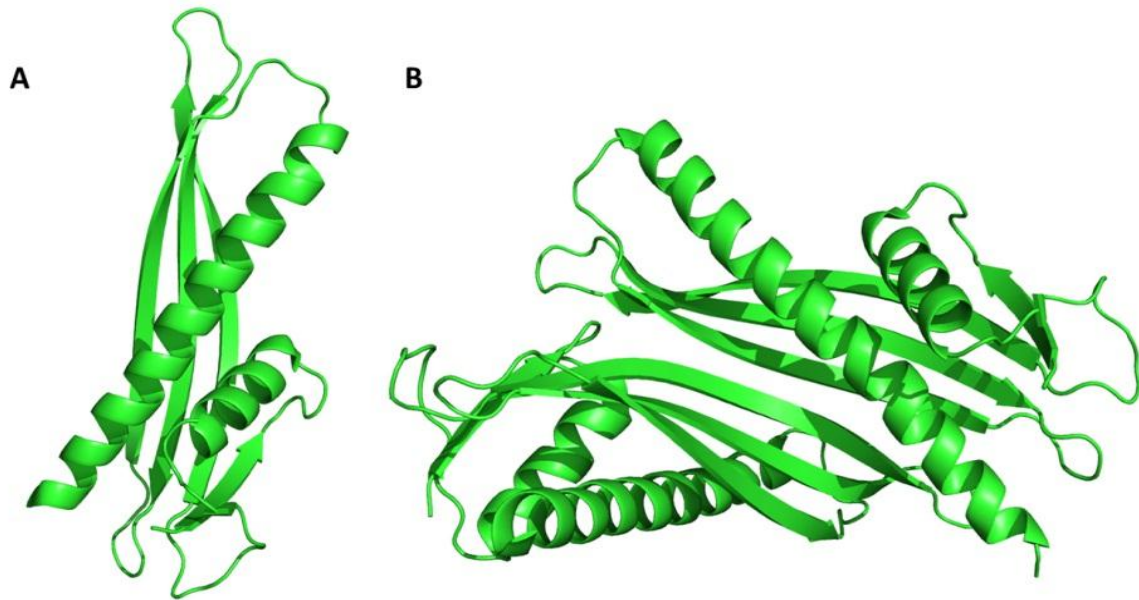
Figure 30. X-ray crystal structure of *Shewanella oneidensis* LptE (PDB accession number 2R76). (A) Monomer. (B) Dimer, as observed in the crystal structure.

While the plug-and-barrel model for the LptD/E structure is heavily supported by experimental evidence[106], it has not been completely confirmed, and its exact nature is unknown. While the basic model is that LptE is simply situated inside of the lumen of the LptD β-barrel, it also seems possible that LptD/E could form a β-barrel in which the β-strands of LptE contribute to the overall β-barrel architecture. This possibility is suggested because LptE and LptD form a nearly inseparable complex[105], because LptE is required for LptD β-barrel assembly[105,127] and oxidation[125], and because LptE contains a β-sheet that interacts with another molecule of LptE in the crystal structure to form a larger β-sheet (as in PDB assession code 2R76; see Figure 30B). Additionally, a crystal structure could be used to address the structural basis for phenotypes caused by the *lptD4213*, *lptD$_{Δ529-538}$* and *lptE6* mutant alleles that were described in Chapters 1 and 2. In particular, the phenotype caused by *lptD$_{Δ529-538}$* is proposed to be caused by a loss of a contact between LptE and a putative extracellular loop of LptD[106], and the *lptE6* phenotype is

proposed to be caused by a loss of affinity between LptD and LptE[127]. A crystal structure of LptD/E will likely clarify the cause of each of these phenotypes while also addressing the mechanisms behind their suppressors.

An LptD/E crystal structure would be useful in determining the path and mechanism by which LPS moves through LptD/E and into the membrane. While it has been proposed that four conserved proline residues in LptD (P214, P246, P483, and P510) create a lateral opening that enables LPS access to the OM[106], this has not been confirmed. In addition, questions remain regarding whether LptE plays a functional or purely structural role in LPS transport. In *N. meningitidis*, LptE is reported to be unnecessary for LPS transport[142]. In contrast, LptE from *E. coli* has been reported to bind LPS *in vitro*[105]. This has been supported by more recent work where LptE was shown to affect the aggregation state of LPS *in vitro* and where point mutations were identified in LptE that led to OM permeability *in vivo* and disrupted the ability of LptE to affect LPS aggregation *in vitro*[141]. While recent evidence suggests that LptE plays a functional role in LPS transport, its specific function is unknown, but could potentially be clarified with the aid of a crystal structure showing how LptD interacts with LptE. Such a structure might also reveal different conformations of the complex, which could provide clues as to how LptE is involved in the handling of LPS.

The structural significance of the disulfide bond rearrangement discussed in Chapter 2 remains unknown. First of all, it is unclear why the inter-domain disulfide bonds are essential. It could be that they are necessary to orient the two domains relative to one another to enable passage of LPS from one domain to the next, or it could be that the presence of these disulfides triggers a conformational change, or even an ordering, of the N-terminal domain such that it becomes capable of forming an interaction with LptA that is suitable for LPS transport. It is also

not clear why the disulfide bond rearrangement is used *in vivo* to activate the LPS exporter. It could be that this is to prevent mistargeting of LPS by disallowing misassembled LptD/E complexes from being incorporated into Lpt complexes, or it could be that the rearrangement step is simply the only possible way to form the necessary long-range disulfide bonds within the folded core of the LptD/E plug-and-barrel structure, which, given its complexity, might otherwise be inaccessible to DsbA. A crystal structure showing the locations of these disulfide bonds and their effects on the conformation of the LptD/E complex could help address these questions.

A protocol for the overexpression and purification of the LptD/E complex has been published[105], providing a starting point for efforts to obtain its crystal structure. In addition, it has been shown that the C-terminal β-barrel domain of LptD overexpresses and assembles with LptE in a stable complex that can be purified[105]. This may represent a construct that is better suited for crystallography given the troubles with N-LptD stability that were described in Chapter 3. While this construct would make it difficult to address questions about the disulfide bonds, it would still be useful for addressing questions regarding the mechanism of LPS transport and LptE's role in it.

4.2. Results and Discussion

4.2.1. Purified LptD/E contains identifiable impurities

LptD/LptE-His$_6$ were overexpressed from BL21(λDE3) cells harboring pET23/42*lptD* and pCDF*lptE-His$_6$* and purified via Ni-NTA affinity chromatography and SEC as previously reported[105]. The resulting protein preparation was analyzed by SDS-PAGE and found to contain significant amounts of several specific contaminants that co-eluted with LptD/E following SEC

(Figure 31A). Several of these contaminants were identified by MS analysis as being components of cytochrome o oxidase. The previously reported strategy for dealing with these impurities was to extract the isolated total membranes with *N*-lauroylsarcosine, a detergent that specifically solubilizes the IM but not the OM, prior to extraction with anzergent 3-14, which solubilizes both IM and OM[105]. We found this additional extraction step to be time consuming, dirty, and detrimental to protein yield, which was already quite low. Since cytochrome o oxidase is non-essential, we deleted the genes, *cyoA-E*, that encode the cytochrome o oxidase proteins in our expression strain. Neither cell growth nor protein yield was impaired by this deletion. LptD/E purified from the resulting strain lacked these contaminating proteins (Figure 31B). All expression strains used hereafter in this chapter contain the *cyoA-E::kan* allele.

In addition to contamination by cytochrome o oxidase, N-terminal degradation of LptD was observed in most batches of purified LptD/E, as determined by Edman degradation/MS sequencing. This issue was found to become more notable in batches of protein as they aged, as observed with purified N-LptD in Chapter 3 (Figure 25). Because of this, a construct that lacks the N-terminal domain will likely improve the chances obtaining a diffracting crystal.
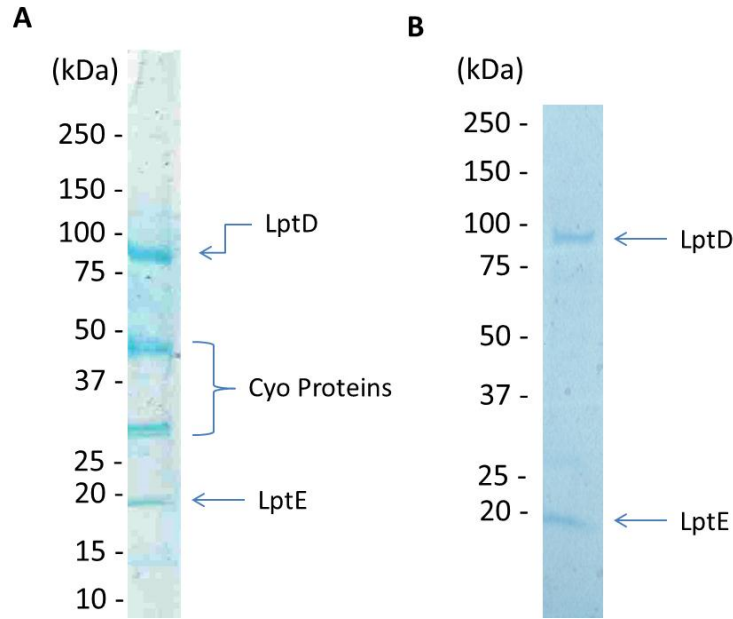
Figure 31. Contaminants present in purified LptD/E. (A) SDS-PAGE analysis of purified LptD/LptE-His$_6$ following SEC. Cyo proteins were identified by MS sequencing. (B) SDS-PAGE analysis of purified LptD/LptE-His$_6$, following SEC, from a *ΔcyoA-E::kan* strain.

4.2.2. Purification of LptD/LptE6-His$_6$ and LptD4213/LptE-His$_6$

LptD/LptE6-His$_6$ was overexpressed and purified in order to gauge its usefulness as a possible crystallography construct. Protein was obtained for this mutant, and the LptD/LptE6-His$_6$ and wild-type LptD/LptE-His$_6$ complexes were found to be similarly stable (Figure 32). Both complexes migrate similarly and in a heat-modifiable manner during seminative SDS-PAGE (Figure 32A). Both complexes also display similar susceptibility to trypsin digestion (Figure 32B). Based on these data, LptE6 containing complexes might be suitable for crystallization experiments.
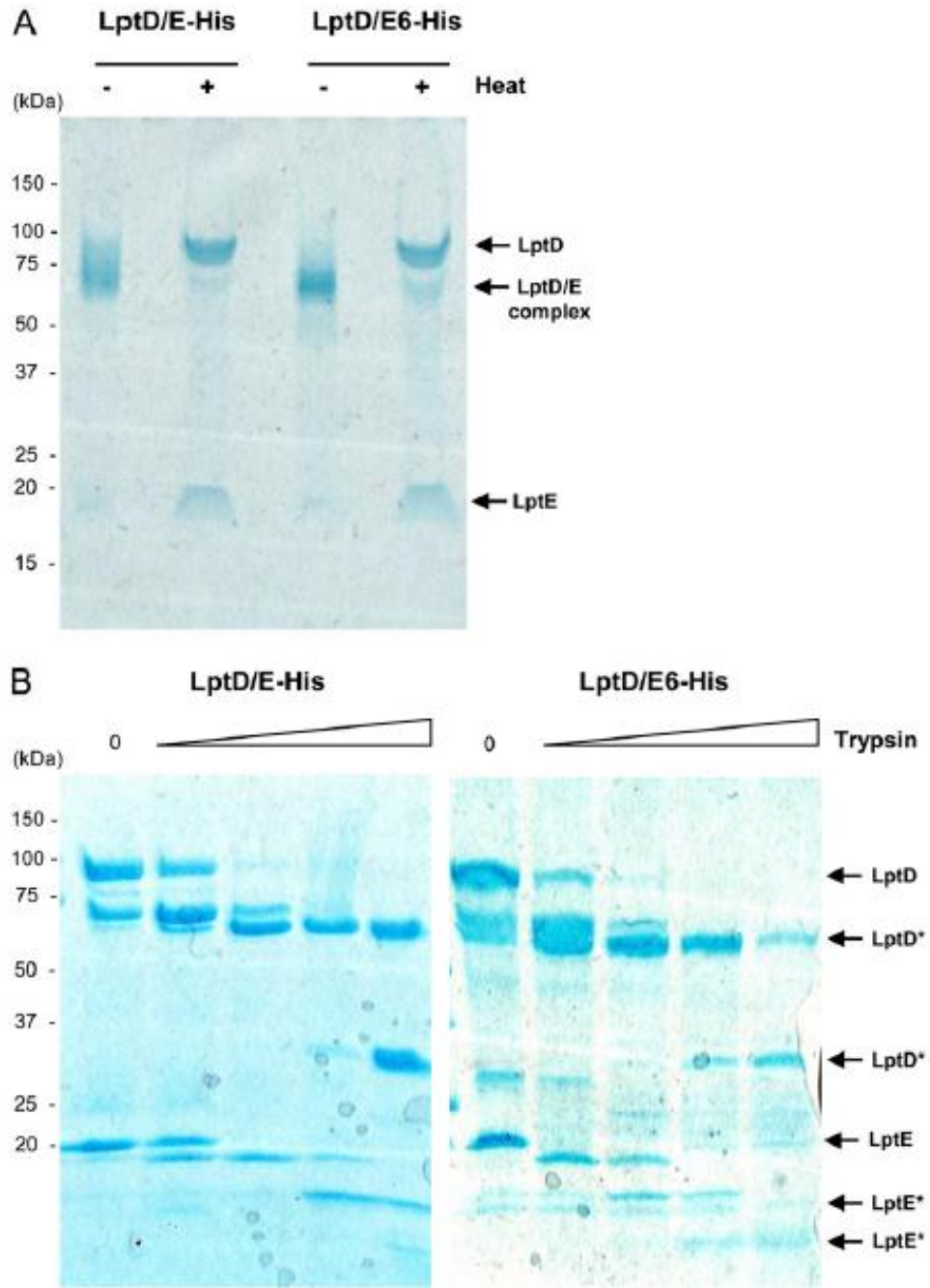
Figure 32. LptD/LptE-His$_6$ and LptD/LptE6-His$_6$ are similarly stable. (A) Seminative SDS-PAGE analysis of purified LptD/LptE-His$_6$ and LptD/LptE6-His$_6$. All samples were reduced with β-ME; samples were heated as indicated. (B) Limited trypsin digestion of purified LptD/LptE-His$_6$ and LptD/LptE6-His$_6$. Truncated proteins are indicated with an asterisk (*).

LptD4213/LptE-His$_6$ was also overexpressed and purified. This construct yielded lower amounts of protein, and heavy aggregation of the purified protein was observed. When analyzed by seminative SDS-PAGE, the complex migrates as expected when not heated (Figure 33A). When heated, however, much less LptD and LptE are observed than expected, and heavy aggregation was observed in the form of protein that fails to enter the gel. LptD4213/LptE-His$_6$ complex that is treated with trypsin displays the degradation pattern that is largely expected (Figure 33B, as compared to Figure 32B), but heavy aggregation was observed in each reaction, including the 0 mg/ml trypsin control. Additional bands that appear to correspond to previously unobserved LptD degradation are also seen for this mutant complex. While this complex is similarly stable to protease digestion, it seems to readily aggregate, and as such, it is likely a poor candidate for crystallography.
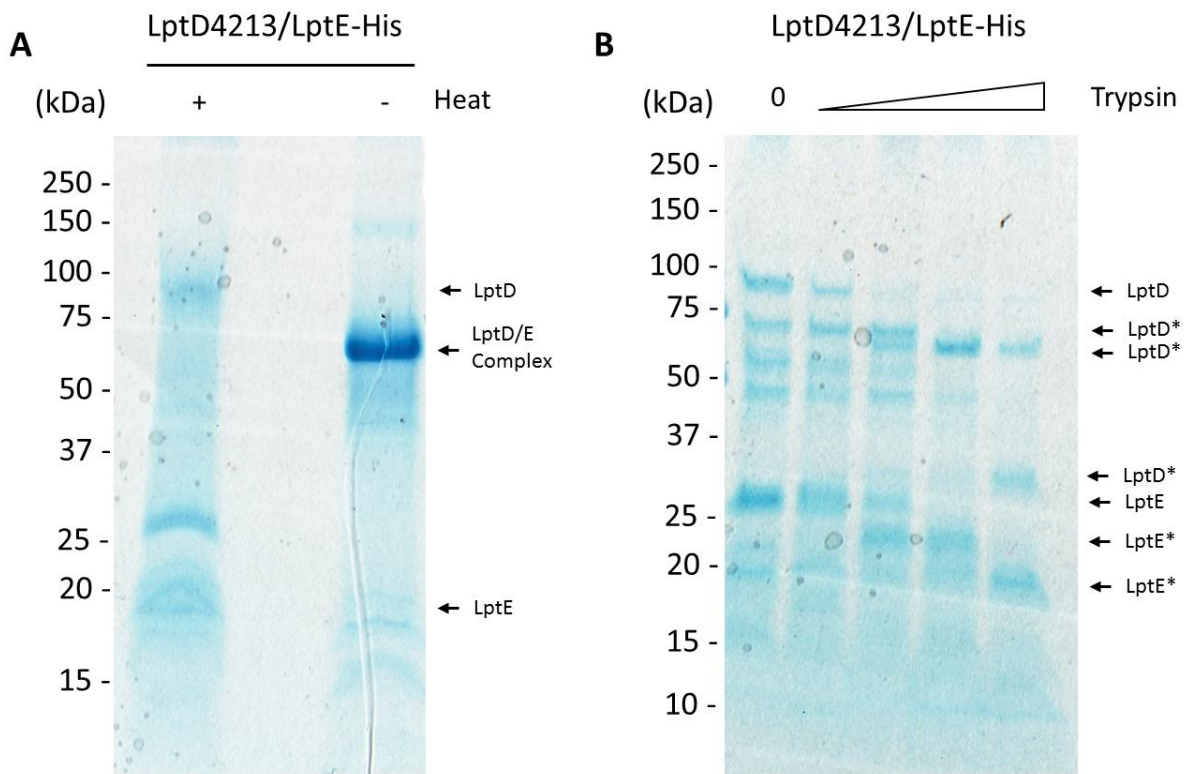
Figure 33. Stability of purified LptD4213/LptE-His$_6$. (A) Seminative SDS-PAGE analysis of purified LptD4213/LptE-His$_6$. All samples were reduced with β-ME; samples were heated as indicated. (B) Limited trypsin digestion of purified LptD4213/LptE6-His$_6$. Trypsin concentrations and digestion conditions are identical to Figure 32B. Truncated proteins are indicated with an asterisk (*).

4.2.3. Purification of C-LptD/LptE-His$_6$ and C-LptD-His$_8$/LptE

C-LptD/LptE-His$_6$ was overexpressed and purified. Because *lptD* is overexpressed at low levels, and since wild-type *lptD* is still present in the cell since *C-lptD* is not sufficient for viability, preparations of C-LptD/LptE-His$_6$ are often contaminated with significant quantities of LptD/LptE-His$_6$. This is due to the placement of the His-tag used for affinity purification on LptE, which can form a complex with either C-LptD or wild-type LptD. While of different sizes,

these complexes are not completely resolvable by SEC (Figure 34A); as a result, preparations of

C-LptD/LptE-His$_6$ are more heterogeneous than is preferred for crystallography. Movement of

the affinity tag to C-LptD from LptE enables direct pull-down of C-LptD/LptE during affinity

purification, removing wild-type LptD contamination (Figure 34B). In general, we believe this

construct represents a better candidate for crystallization.
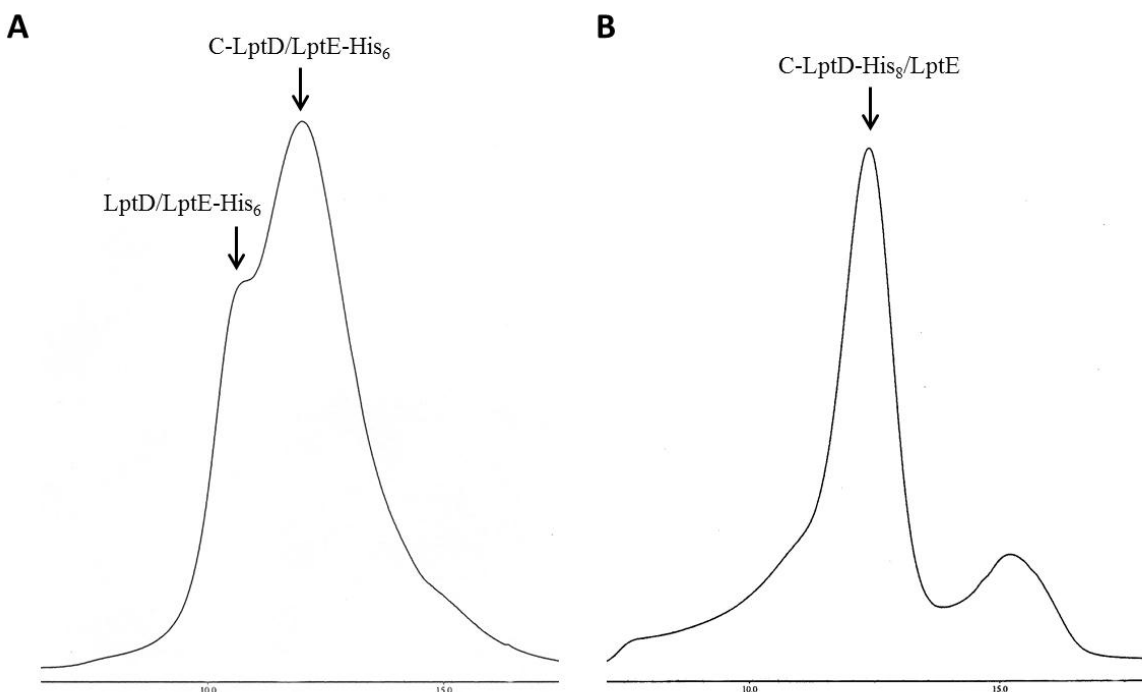
Figure 34. SEC chromatograms of C-LptD/LptE-His$_6$ and C-LptD-His$_8$/LptE preparations. (A)

SEC chromatogram of C-LptD/LptE-His$_6$ following affinity purification. Unresolved

LptD/LptE-His$_6$ peak is indicated. Retention volumes for the wild-type and C-LptD complexes

are consistent with published values[105]. (B) SEC chromatogram of C-LptD-His$_8$/LptE.

4.2.4. Optimization of the purification protocol to increase protein yield

The extremely low yield of LptD/LptE is the principal limiting factor in obtaining

crystals. As discussed earlier, the removal of the initial *N*-lauroylsarcosine extraction was critical

for increasing protein yield. In addition, we screened different solubilization conditions and found that using LDAO (n-dodecyl-*N*,*N*-dimethylamine-*N*-oxide or n-lauryldimethylamine-*N*-oxide) to solubilize isolated membranes at room temperature provided the best yield of protein (Figure 35). These changes together improved protein yield by roughly 50-100%, depending on batch-to-batch variation. Despite these improvements, protein yield is still extremely low and is limiting to this work, with typical yields of ~0.1 to 0.15 mg of protein per liter of culture. These expression levels are just high enough that the growth of large volumes of culture can be performed to make crystallography feasible.
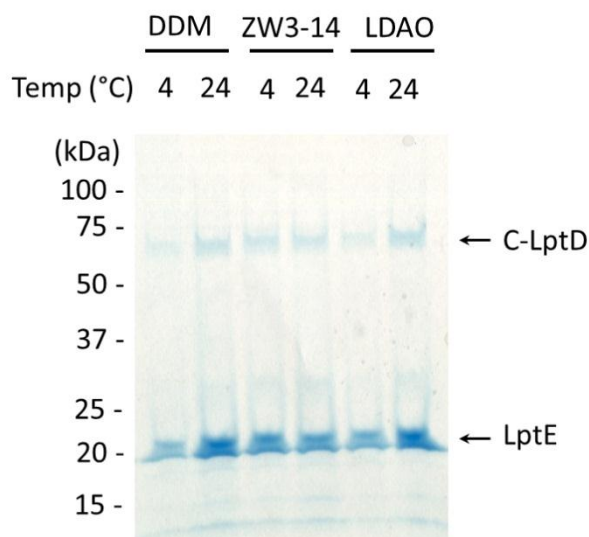
Figure 35. Screening of C-LptD/LptE solubilization conditions. DDM (n-dodecyl-β-D-maltopyranoside), ZW3-14 (anzergent 3-14), and LDAO (n-lauryldimethylamine-*N*-oxide) were used to solubilize membranes isolated from cells overexpressing *C-lptD/lptE-His$_6$*. Extraction was performed at either 4°C or 24°C.

4.2.5. Screening of C-LptD/LptE-His$_6$ crystallization conditions

Despite contamination by wild-type LptD, purified C-LptD/LptE-His$_6$, solubilized with 1% OG (n-octyl-β-D-glucoside), was exhaustively screened for conditions that produce crystals. Most available precipitant screens were utilized, including MemGold, ProComplex, ComPAS, PEGs I & II, Clear Strategy Screen I & II, JCSG+, Crystal Screen I & II, MemPlus, MemFac, and MemSys (all from either Qiagen or Molecular Dimensions). All screening was done with OG solubilized protein. Screens were also conducted at both 4°C and 18°C. Images of the most promising crystals and the conditions from which they were obtained are shown (Figure 36A, C, and D). These crystals were observed in 96-well plates, and when these crystals were grown again on a larger scale, only the crystals from Figure 36A grew. These crystals were analyzed for X-ray diffraction and diffracted to 10-13 Å (Figure 36B). While diffraction of this resolution is not sufficient to solve the structure, it does provide promise of better diffraction under different conditions or with different constructs.
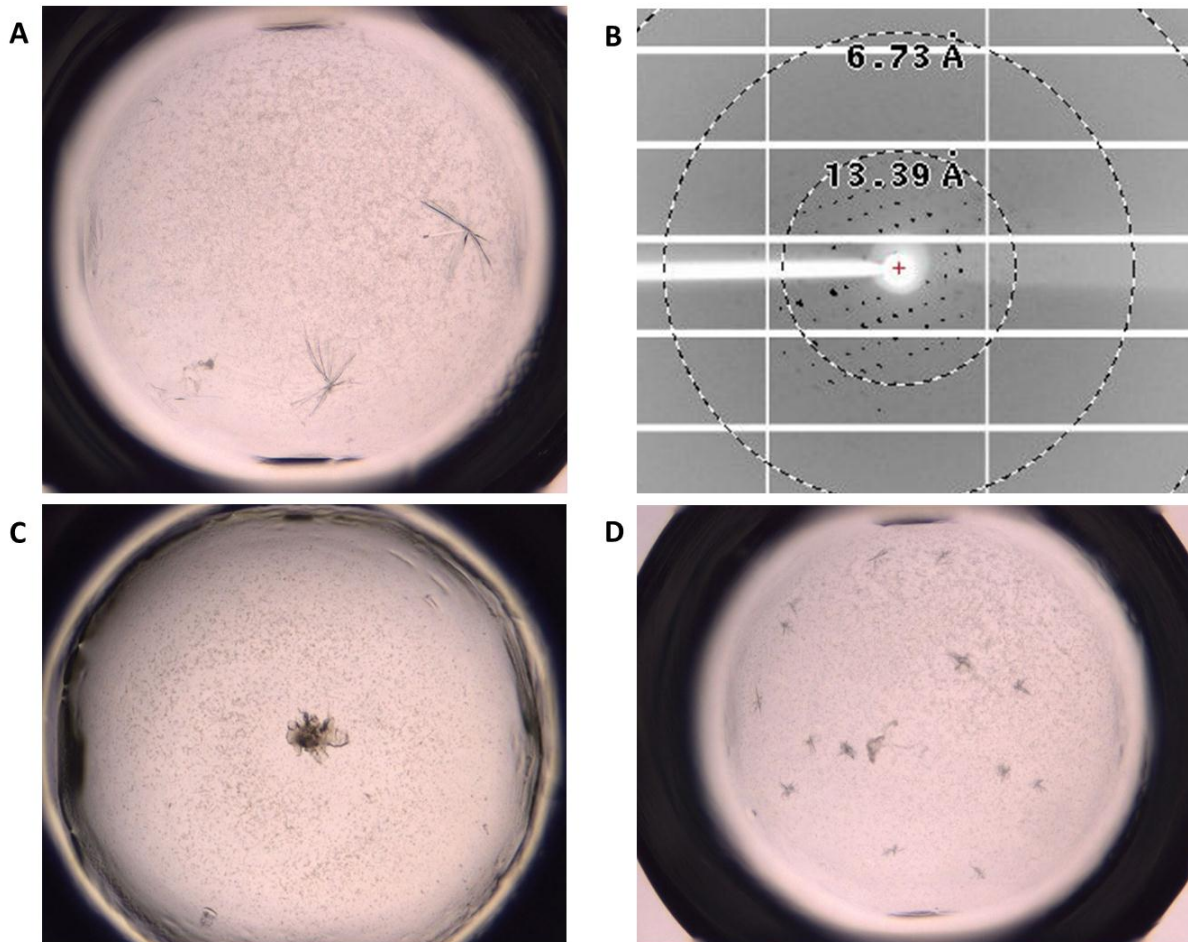
Figure 36. C-LptD/LptE-His$_6$ crystals and X-ray diffraction. (A) C-LptD/LptE-His$_6$ crystals obtained from OG solubilized protein at a 3:1 ratio of protein to precipitant, where 0.1 M MgCl$_2$, 0.1 M NaCl, 0.1 M Tris-HCl pH 8.5, 33% v/v PEG 400 is the precipitant. (B) Example of X-ray diffraction pattern resulting from the crystals from (A). (C) C-LptD/LptE-His$_6$ crystals obtained from OG solubilized protein at a 3:1 ratio of protein to precipitant, where 0.1 M NaCl, 0.1 M sodium phosphate pH 7.0, 33% v/v PEG 300 is the precipitant. (D) C-LptD/LptE-His$_6$ crystals obtained from OG solubilized protein at a 1:1 ratio of protein to precipitant, where 0.01 M calcium acetate, 0.1 M Tris-HCl pH 8.5, 3% w/v PEG-3000 is the precipitant.

4.2.6. Screening of C-LptD-His$_8$/LptE crystallization conditions

Purified C-LptD-His$_8$/LptE was also screened extensively for conditions that produce crystals. Unlike the previously described screening, emphasis was placed on screening using a variety of detergents, not just OG. Glucoside detergents have not widely been reported in OM β-barrel protein structures, so we decided to focus on detergent classes that have historically been more successful for proteins of this class. In particular, polyoxyethylene detergents, such as C$_8$E$_4$ (n-octyltetraoxyethylene) and C$_8$E$_5$ (n-octylpentaoxyethylene), have been used in crystallization for approximately half of the reported monomeric and dimeric OM β-barrel protein structures. Many of the remaining structures utilized LDAO and related detergents. Virtually none have reported success with maltosides. As such, we systematically screened for crystallization conditions using the same five precipitant screens (MemGold I & II, Clear Strategy I & II, MemPlus; all from Molecular Dimensions) at both 4°C and 19°C, with and without lysine methylation, in combination with 1% OG, 0.1% LDAO, 0.8% C$_8$E$_4$, 0.75% C$_8$E$_5$, 0.14% Fos-12 (n-dodecylphosphocholine), 0.1% LDAO + 0.8% C$_8$E$_4$, and 0.05% LDAO + 1.67% heptane-1,2,3-triol solubilized C-LptD-His$_8$/LptE. Crystals were obtained from many conditions, especially from LDAO, OG, and C$_8$E$_4$ solubilized protein preparations. Representative crystals are shown (Figure 37). No significant diffraction was obtained from any of these crystals.

0.15 M KSCN, 0.1 M Tris pH 8.5,
18% w/v PEG 5K MME

0.15 M KSCN, 0.1 M NaOAc pH 5.5,
20% v/v PEG 500

0.2 M KSCN, 0.1 M Tris pH 8.5, 25% PEG 2K MME

0.2 M Ca(OAc)$_2$, 0.1 M Tris pH 8.5,
8% w/v PEG 20K, 8% v/v PEG 550 MME
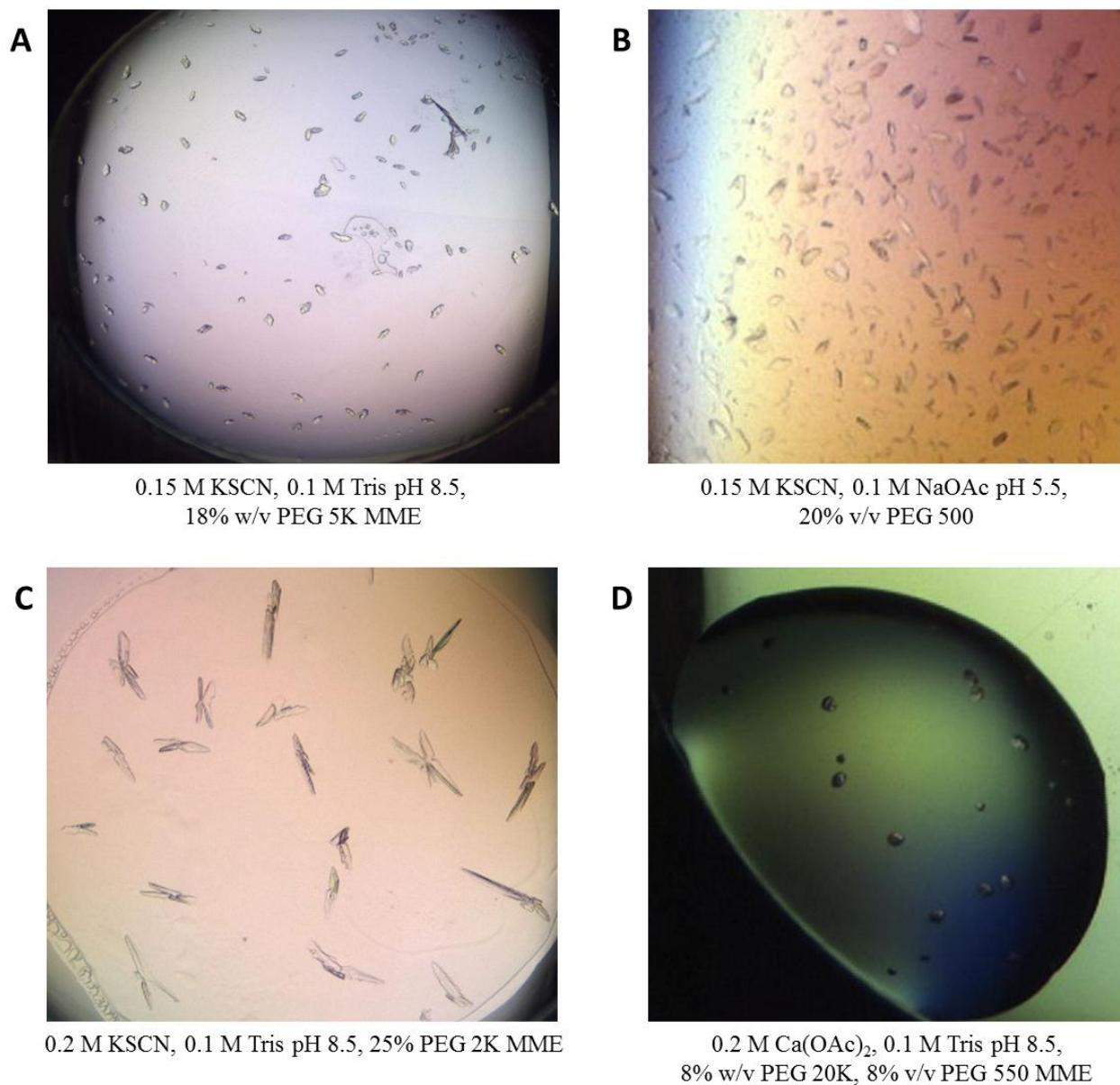
Figure 37. C-LptD-His$_8$/LptE crystals obtained from detergent screening. Representative crystals are shown for protein solubilized with (A-B) C$_8$E$_4$, (C) OG, and (D) Fos-12. Crystals in (B) were obtained with methylated protein, while the others were not. All crystals shown were obtained at 19°C. The precipitant condition is indicated.

Given the lack of diffraction obtained from traditional *in surfacto* crystallization, we screened for crystallization conditions using bicelle solubilized protein. This was also partly

86

motivated by several recently reported β-barrel membrane protein structures that were obtained

through the use of bicelles, including BamA[58]. While the detergents mentioned previously form

micelles in solution, bicelles form membrane-like discs that are intended to better emulate the

membrane environment in which the protein natively resides. They also better allow lateral

contacts between proteins in the membrane, making them useful for crystallizing proteins

without large hydrophilic domains that could otherwise mediate crystal contacts. Bicelles also

have the advantage of being easy to use and generally compatible with our existing screening

systems. Unfortunately, bicelles tend to generate false-positive lipid crystals and the resulting

protein crystals are often two-dimensional. False-positive crystals can typically be detected by

screening crystals for UV fluorescence, which is a property of protein, but not lipid, crystals. In

general, bicelles are composed of a mixture of two lipids, one that forms a membrane bilayer and

one that forms a micelle. The two types of lipids are arranged in such a way that the bilayer-

forming lipid assembles into membrane-like bilayer whose edges are capped by the micelle

forming lipid. The typical lipids that are used are DMPC (dimyristoylphosphatidyl choline) and

CHAPSO (3-[(3-cholamidopropyl)dimethylammonio]-2-hydroxy-1-propanesulfonate), which

form bilayers and micelles, respectively[143].

Purified C-LptD-His$_8$/LptE that was solubilized in either C_8E_4 or OG was mixed 4:1 with

a range of concentrations of bicelles (40%, 35%, 30%, or 25% 2.8:1 DMPC:CHAPSO) and

screened using the five precipitant screens discussed above. All screening was done at 19°C, as

bicelles are incompatible with screening at 4°C. No crystals were obtained with OG solubilized

samples, but many conditions produced crystals with the C_8E_4 solubilized samples. The most

reliably reproducible condition produced the crystals shown below (Figure 38).
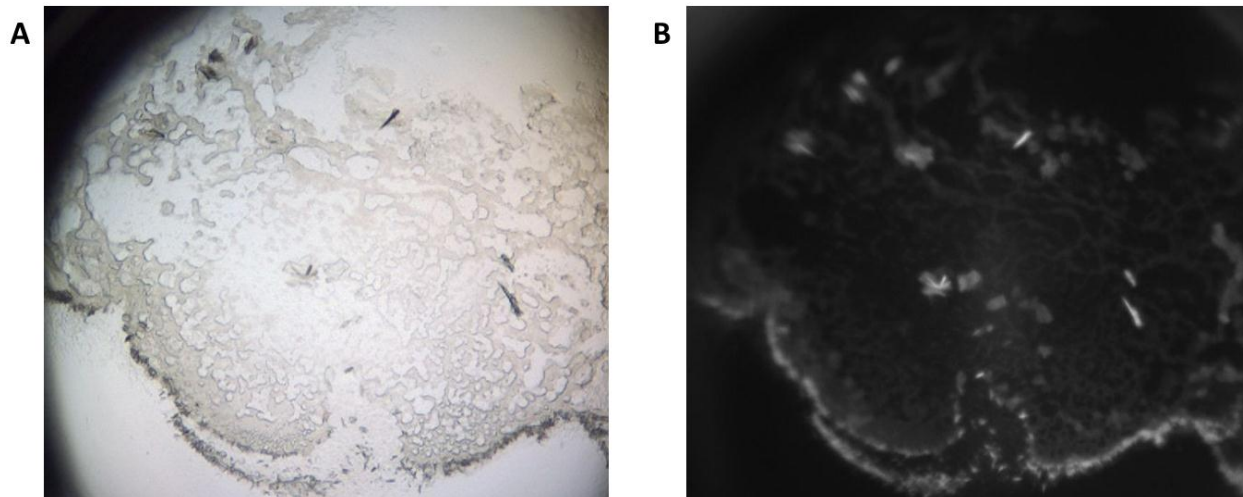
Figure 38. Crystals of C-LptD-His$_8$/LptE obtained using bicelles. The precipitant used was 400 mM KSCN, 100 mM sodium acetate, pH 4.5, 11% w/v PEG 4K. (A) Bright field; (B) UV.

The crystals shown in Figure 38 did not diffract particularly well (>20 Å resolution), so we used this condition as a starting point from which to screen for additives. Many additive conditions were found to produce crystals, and a number of varied crystal morphologies were observed. The resulting crystals were repeated on a larger scale and screened for diffraction. Of the identified additives, 200 mM NaSCN had the greatest effect on diffraction. Crystals grew reliably from this condition and are shown below (Figure 39). While the crystals shown here largely form needles, the best diffracting crystals occurred as two-dimensional plates. No well-formed three-dimensional crystals were observed for this condition. Diffraction quality seems to track well with crystal size, with only the larger crystals showing reasonable diffraction. Seeding of these crystals to produce larger crystals was attempted, but was not successful.
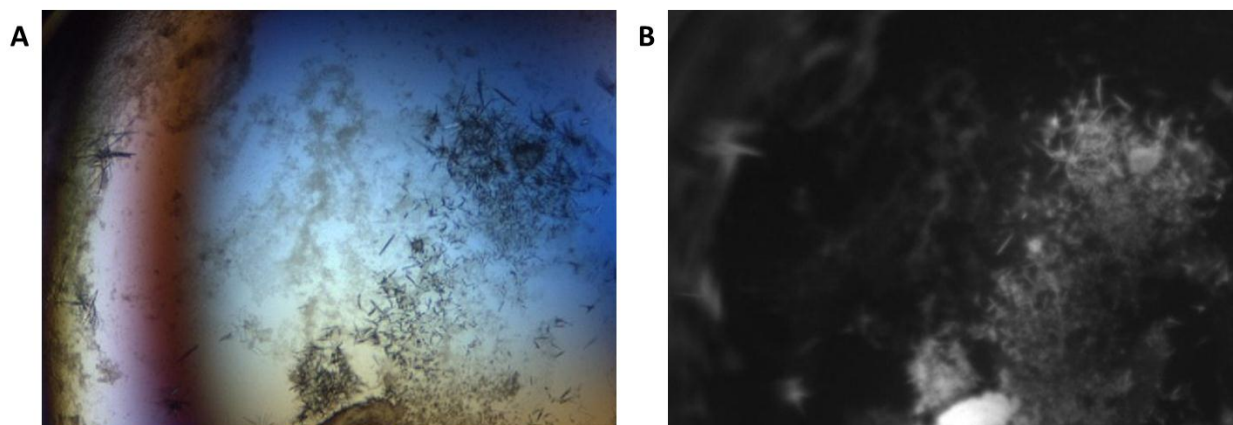
Figure 39. C-LptD-His$_8$/LptE crystals obtained from additive screening. The precipitant condition is as described in Figure 38, but with an added 200 mM NaSCN. (A) Bright field; (B) UV.

A complete 360° data set was obtained from these crystals. Exemplary diffractograms from the dataset are shown below (Figure 40). The diffraction limit for the data set was 3.85 Å. These data processed into the space group P22$_1$2$_1$ (#18), with unit cell parameters of a=108.42 Å, b=128.86 Å, c=136.73 Å, and α=β=γ=90° (Table 2). These data are anisotropic, possibly a result of the two-dimensional crystal morphology. The crystal also suffered from radiation damage. Another partial data set was collected from a different crystal in which the diffraction limit was 3.2 Å, but radiation damage prevented the collection of a complete data set. Assuming a molecular weight of 80 kDa, there appear to be two molecules in the asymmetric unit, with a V_M of 2.98 Å^3/Da, corresponding to a solvent percentage of 58.82%. The presence of a bicelle or detergent micelle may contribute significantly such that only one molecule is present in the asymmetric unit.
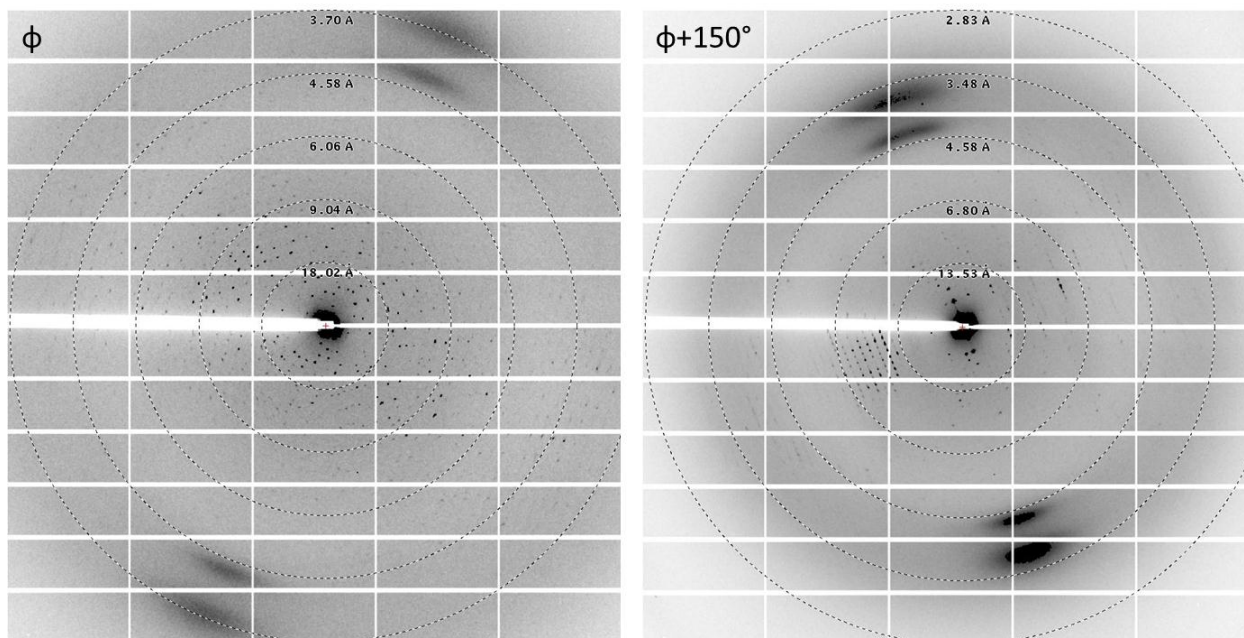
Figure 40. Exemplary diffractograms from a 3.85Å data set obtained from C-LptD-His$_8$/LptE crystals. Images are shown at two angles, φ and φ+150°.

Table 2. Crystallographic parameters and statistics associated with data shown in Figure 40.

Resolution (Å)	136.73-3.85 (4.06-3.85)
Space Group	$P22_12_1$
Cell Dimensions	
a, b, c (Å)	108.42, 128.86, 136.73
$\alpha=\beta=\gamma$ (°)	90
R_{merge}	0.379 (1.632)
R_{meas}	0.400 (1.723)
R_{pim}	0.127 (0.541)
Total number of observations	184212 (27703)
Total number of unique	18706 (2681)
Mean $I/\sigma(I)$	5.3 (2.0)
$CC_{1/2}$	0.997 (0.661)
Completeness (%)	99.7 (99.8)
Multiplicity	9.8 (10.3)
Average mosaicity (°)	1.18

Values in parentheses are for highest resolution shell.

4.2.7. Phasing of C-LptD-His$_8$/LptE diffraction data

Phasing of the 3.85Å C-LptD-His$_8$/LptE data set was attempted using molecular

replacement. A number of structures were used as search models, including *E. coli* LptE and a

number of large Gram-negative β-barrel proteins, including FhuA (1QJQ), FimD (3OHN), AlgE

(4AFK), and PapC (3FIP). Of these, only LptE and FimD returned solutions. The solution

provided by LptE showed only LptE in isolation, while the FimD solution shows a large β-barrel

with an area of unassigned electron density at its center, possibly suggesting the presence of

LptE. Both of the resulting electron density maps are noisy and difficult to interpret; refinement

does not improve the electron density map or the model, and the resulting R factors are significantly worse than what can be tolerated at this resolution.

Since a suitable molecular replacement model was not available, we pursued experimental methods of phasing. First, SeMet (L-selenomethionine) derivatized C-LptD-His$_8$/LptE was overexpressed, purified in C_8E_4, and crystallized as above. Crystals grew under these conditions, but were generally smaller. The smaller size of these crystals is likely a result of the lower protein concentrations used when setting up crystallization experiments with SeMet labeled protein. The lower concentration was largely necessitated by the lower yields obtained for SeMet labeled protein (roughly 50% that of native protein). Diffraction obtained from these crystals has so far been too weak to be useful, with resolutions of 10-20 Å.

Next, we screened for heavy atom compounds that can derivatize purified C-LptD-His$_8$/LptE by using a gel shift assay (Figure 41). In this experiment, purified C-LptD-His$_8$/LptE was incubated with various heavy atom containing molecules and then analyzed by native PAGE to look for changes in migration speed that are due to the additional positive charge from the heavy atom. While difficult to interpret due to poor resolution of the bands, this experiment seems to indicate that C-LptD-His$_8$/LptE is modified by two mercury containing compounds, $HgCl_2$ and K_2HgI_4. Labeling with mercury is consistent with the presence of two cysteine residues in C-LptD, which were reduced with dithiothreitol (DTT) prior to heavy metal incubation in order to allow for possible mercury derivatization. Protein incubated with these two compounds migrated slightly slower than unlabeled protein in the gel shift assay, signifying the presence of additional positive charge on these proteins. Unfortunately, there is no control in this experiment to verify that this band is LptD/LptE (since migration speed is not proportional to protein size in this type of gel), and upon staining, it was evident that there was a significant

amount of protein that aggregated and never entered the gel. Therefore, it is possible that the observed band is simply a small impurity that happens to be labeled by these mercury compounds. We think this is unlikely though, since heavy aggregation is expected when using this type of gel.
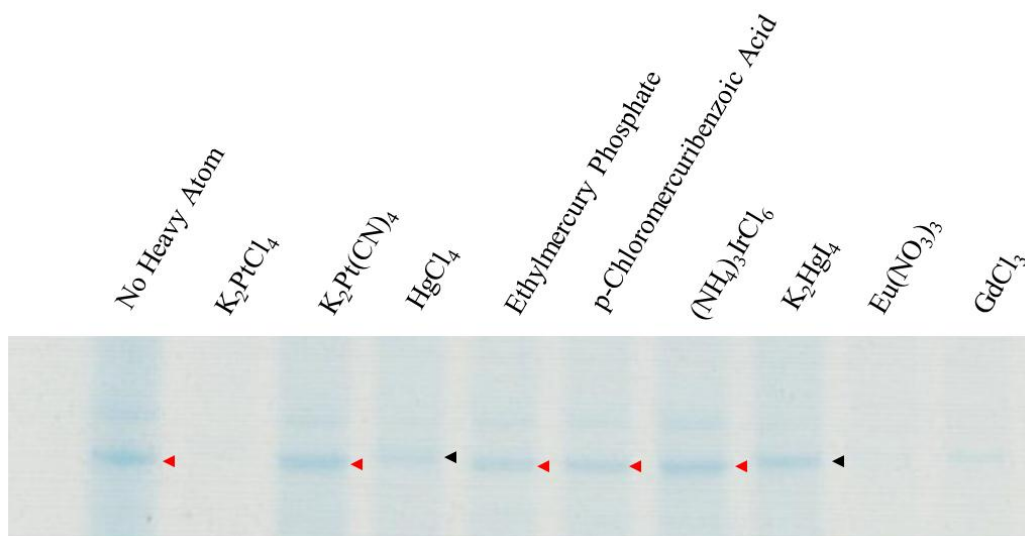
Figure 41. Gel shift assay screening for heavy atom derivatization. Native PAGE analysis of C-LptD-His$_8$/LptE incubated with various heavy atom compounds. Red arrowhead shows migration of native protein (as judged by control); black arrowhead indicates slower migration.

Given these results, we soaked C-LptD-His$_8$/LptE crystals with HgCl$_2$ and screened them for diffraction. So far, the best data set that we have collected is at roughly 6 Å, but this was not sufficient to use for phasing the native data set.

4.2.8. Crystallization with LPS additives

Given data showing that LPS may bind to LptE, we decided to co-crystallize C-LptD-His$_8$/LptE with a variety of purified LPS variants. These LPS variants were purified by Dorothee Andres and Carolin Doering from *E. coli* strains in which various LPS biosynthesis genes are

93

knocked out. The structures of the LPS molecules used and the genes that are knocked out in the strains that produce them are shown below (Figure 42). When used as an additive in the condition that gave rise to the 3.85 Å data set, LPS from *ΔlpxL* and *ΔrfaC* strains led to crystals, but these crystals did not diffract well. While this strategy was not effective here, it might be worth revisiting if new conditions or constructs are found to give rise to diffracting crystals. It might also be worthwhile to screen for new conditions in the presence of these lipids.
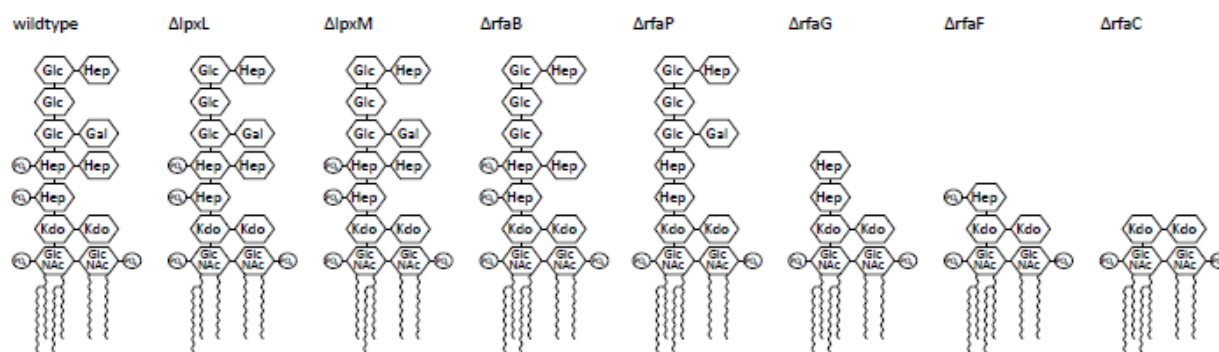
Figure 42. LPS additives used for co-crystallization screens. Crystals grew in the presence of LPS from *ΔlpxL* and *ΔrfaC* strains. Figure credit: Carolin Doering and Dorothee Andres.

4.2.9. Discussion and future work

While the X-ray crystal structure of LptD/LptE has not yet been solved, we have made great progress in obtaining it. We modified the published purification protocol to obtain a purer sample in roughly double the yield. Then we identified a stable expression construct and used it to screen crystallization detergents under thousands of conditions. Once crystals were identified, we screened for additives that improved diffraction such that a useable data set could be obtained. Then we adopted two parallel strategies for obtaining phasing information. At this point a complete data set at 3.85 Å and a partial data set at 3.2 Å have been obtained, but phasing information is still missing.

Our top priority is to obtain phasing information for the data that we have. As such, we are primarily focusing on overexpressing SeMet substituted protein. We feel that the poor diffraction that was previously observed was due to the small size of the protein crystals as opposed to innately poor diffraction of the crystals. We previously observed a reliable correlation between LptD/LptE concentration and the size of the resulting protein crystal. Because of the low yield of SeMet substituted protein, we have been forced to set up crystallization experiments with protein concentrations of ~17 mg/ml, versus 30 mg/ml for native protein. We believe that by expressing more SeMet substituted protein we can overcome the yield issue and, hopefully, grow larger crystals. In addition to pursuing SeMet methods of phasing, we also plan to do additional screening with heavy atoms. The initial screening that was conducted lacked a control to ensure that the protein we were observing was LptD/LptE. This could be easily addressed by performing an α-LptD immunoblot using the native gel from the gel shift assay.

In addition to obtaining phasing information, it will likely be necessary to obtain a better diffracting data set. To do this, it will probably be necessary to find a better expression construct. One approach is to examine C-terminal truncations of LptE. As reported[105], *E. coli* LptE contains a C-terminal extension that is predicted to be unstructured. It was necessary to remove this region in order obtain diffracting crystals of *E. coli* LptE, and as such, its removal may benefit LptD/LptE crystallization and diffraction as well. Additionally, truncations at the LptD C-terminus should also be explored since LptD secondary structure predictions suggest that there is likely an unstructured region at the LptD C-terminus as well. Removal of this extension could benefit both diffraction and crystallization. We have produced and purified several of these constructs already; conservative truncations such as C-LptD$_{\Delta760\text{-}784}$ overexpressed and purified well, while the more liberal truncation C-LptD$_{\Delta714\text{-}784}$ overexpressed but could not be pulled

down with LptE-His$_6$, suggesting that a portion of the β-barrel had been deleted, preventing interaction with LptE. It is worth noting that simultaneous removal of these C-terminal extensions from both LptE and LptD has the potential of interfering with affinity purification by causing the His-tag to be hidden. I have already observed this when trying to overexpress and purify C-LptD/LptE$_{\Delta168-193}$-His$_6$. This construct overexpresses well, but only LptE is obtained following affinity purification, suggesting that either an unstable complex is formed or that interaction with C-LptD hides the affinity tag on LptE.

Another strategy that we have pursued is selective mutation of specific residues to reduce surface entropy in order to promote crystallization. According to software predictions (available at services.mbi.ucla.edu/SER/), mutation of K711 and Q712 to alanine is the change most critical to reducing surface entropy. We have generated this construct, but its expression has not yet been a priority.

We are also interested in crystallizing LptD/LptE homologues from species other than *E. coli*. LptD/LptE from *P. aeruginosa* is the most obvious choice as it is the target of an antibiotic. We have been able to overexpress and purify this protein complex, but its yield does not make its use in crystallography feasible at this point in time. We are also interested in trying to express LptD/LptE from other organisms as well, particularly from thermophilic organisms.

Overall, future efforts will initially focus on obtaining phasing information for our current data set and will then likely shift towards the screening of additional constructs, detergent mixtures, and conditions in order to obtain larger, better diffracting crystals.

4.3. Materials and Methods

4.3.1. Strains and growth conditions

The strain BL21(λDE3) [F^- *dcm ompT hsdS($r^-_B m^-_B$) gal(λDE3)*] (Novagen) was initially used for protein overexpression. This strain was later modified to delete *cyoA-E*, as described below. Luria-Bertani (LB) broth and agar were prepared as described previously[135]. Antibiotics were used at 50 µg/ml unless otherwise indicated. The strains primarily used for overexpression in this chapter are summarized in Table 3.

Table 3. LptD/E expression strains used in this chapter.

Strain	Plasmid 1	Plasmid 2
BL21(λDE3)	pET23/42*lptD*	pCDF*lptE-His₆*
BL21(λDE3) *ΔcyoA-E::Kan*	pET23/42*lptD*	pCDF*lptE-His₆*
BL21(λDE3) *ΔcyoA-E::Kan*	pET23/42*ClptD*	pCDF*lptE-His₆*
BL21(λDE3) *ΔcyoA-E::Kan*	pET23/42*ClptD-His₈*	pCDF*lptE*
BL21(λDE3) *ΔcyoA-E::Kan*	pET23/42*lptD*	pCDF*lptE6-His₆*
BL21(λDE3) *ΔcyoA-E::Kan*	pET23/42*lptD4213*	pCDF*lptE-His₆*

4.3.2. Deletion of *cyoA-E*

The genes *cyoA-E* were removed from the overexpression strain using a previously reported method of gene inactivation[144]. Briefly, the kanamycin resistance gene, *kan*, was amplified via PCR from the pKD4 plasmid using primers CyoA-N-P1 and CyoE-C-P2 (Table 4). The resulting PCR product was gel purified and transformed via electroporation into BL21(λDE3) cells already bearing the plasmid pKD46. Cells of the resulting strain, bearing the

cyoA-E::kan allele, were lysed with P1 phage, and the resulting lysate was used to transduce BL21(λDE3) cells, which were then subjected to kanamycin selection. Primers CyoA-F and CyoE-R (Table 4) were used in a test PCR to ensure the loss of *cyoA-E*.

Table 4. Primers used in *cyoA-E* inactivation.

Name	Sequence
CyoA-N-P1	5'-CTTTAAACGCCACCAGATCCCGTGGAATTGAGGTCGTTAAGTGTAGGCTGGAGCTGCTTC-3'
CyoE-C-P2	5'-AGGTCGCGCGCCTCTCACCTGGCGTCATTTTATAATCGTTCATATGAATATCCTCCTTAG-3'
CyoA-F	5'-CTTCCCGTAAAATGCCCACAC-3'
CyoE-R	5'-ACGAGAATACGGTCCCTAAAC-3'

4.3.3. Overexpression and purification of LptD/LptE

The appropriate overexpression strain (summarized in Table 3) was grown on LB-agar (supplemented with 50 µg/ml carbenicillin, 50 µg/ml streptomycin, 25 µg/ml kanamycin, and 0.2% glucose) overnight at 37°C. Colonies from the plate were used to inoculate an appropriate number of 10 ml starter cultures (LB supplemented with 50 µg/ml carbenicillin, 50 µg/ml streptomycin, 25 µg/ml kanamycin, and 0.2% glucose), which were grown at 37°C until OD_{600} ~ 0.6. At this point, 10 ml of starter culture was used to inoculate each 1.5 l culture (LB supplemented with 100 µg/ml carbenicillin, 50 µg/ml streptomycin, 25 µg/ml kanamycin, and 0.2% glucose). The 1.5 l cultures were grown at 37°C with shaking at 220 rpm until OD_{600} ~ 0.15, at which point the temperature was reduced to 26°C and the shaking speed was reduced to 180 rpm. At OD_{600} ~ 0.6, 0.1 mM IPTG was added to each culture. The cultures were then grown for 20 hr. Cells were collected by centrifugation at 5,250 x *g* for 10 minutes, and the cells were resuspended in 30 ml of cold TBS (20 mM Tris-HCl, pH 8.0, 150 mM NaCl)

(supplemented with 1 mM PMSF, 0.05 mg/ml DNase I, and 0.1 mg/ml lysozyme) per 1.5 l culture that was centrifuged. The resuspended cells were lysed by a single passage through a French Press (Thermo) at 16,000 psi, or by two passes through a cell disruptor (Avestin). The lysate was centrifuged for 10 min at 3,000 x g to remove unlysed cells, and the supernatant was centrifuged for 30 min at 100,000 x g in an ultracentrifuge (Model XL-90, Beckman; Type 45-Ti rotor). The supernatant was discarded, and the membrane pellet was resuspended in TBS-A (20 mM Tris-HCl, pH 8.0, 300 mM NaCl, 20 mM imidazole) at a volume equal to half of what was centrifuged. Resuspended membranes were flash-frozen with liquid nitrogen and stored at -80°C for future use. To solubilize LptD/LptE, the frozen membranes were thawed, supplemented with 1% LDAO (Anatrace, Sol-grade), and stirred at room temperature for 1.5 hr. Prior to screening for better solubilization conditions, 1% ZW3-14 (Anatrace) at 4°C was used instead. The solubilized membranes were then centrifuged again for 30 min at 100,000 x g in an ultracentrifuge (Model XL-90, Beckman; Type 45-Ti rotor). The supernatant was retained. For a purification that started with 45 l of culture, 16 ml of Ni-NTA resin (Qiagen), as a 50% slurry, was used for affinity purification. The resin slurry was applied to a column, allowed to drain by gravity, and washed with 100 ml of TBS-A supplemented with 0.1% LDAO. The supernatant from the membrane solubilization was applied to the column and allowed to drain by gravity. The flow-through was reapplied to the column and drained again. The column was washed four times with a total of 200 ml of TBS-A (supplemented with the detergent to be used for crystallization, typically either 0.8% C_8E_4 (Bachem) or 1% OG (Antrace)). Other detergents/additives were used on occasion, and include C_8E_5 (Anatrace), Fos-12 (Anatrace), DDM (Anatrace), and heptane-1,2,3-triol (Sigma). The protein was eluted in 40 ml of TBS-B (20 mM Tris-HCl, pH 8.0, 150 mM NaCl, 200 mM imidazole) (supplemented with the same

detergent present in the wash buffer). Protein was concentrated in an ultrafiltration device (Amicon Ultra, Millipore, 50 kDa cut-off) and further purified by SEC using a pre-packed Superdex 200 column (GE Healthcare), using 10 mM HEPES pH 7.5, 150 mM NaCl, supplemented with the appropriate detergent, as the eluent. Protein concentration was determined by NanoDrop spectrophotometer (Thermo, A280 measurement). Protein concentration was calculated using extinction coefficients as determined by ExPASy ProtParam tool (available at web.expasy.org/protparam/). SDS-PAGE was performed using 4-20% Tris-HCl polyacrylamide gels as previously published[140]. Gels were run at 150 V for 1 hr. Lysine methylation, when performed, was done as described in Chapter 3.

4.3.4. Overexpression and purification of LptD/E mutants

LptD4213 and LptE6 were overexpressed from the appropriate strains, as described in Table 3. Overexpression and purification for these mutants was carried out as described above. These complexes were solubilized with ZW3-14 and ultimately purified in 1% OG, as described earlier. Seminative SDS-PAGE was conducted using 4-20% Tris-HCl polyacrylamide gels. These samples were either heated or not. The gel was ran at 4°C for 2 hr at 120 V.

Trypsin digestion was performed in five separate 20 µl reactions containing 1 mg/ml purified protein and either 0, 0.05, 0.5, 5, or 50 µg/ml trypsin. The digestion reactions were incubated at room temperature for 3 hr, after which time 20 µl of 2x SDS loading dye was added to each reaction and the sample was immediately heated. The reactions were then analyzed by SDS-PAGE, as described above.

4.3.5. Plasmid construction

pET23/42*lptD*, pET23/42*ClptD*, pET23/42*ClptD-His$_8$*, pCDF*lptE*, and pCDF*lptE-His$_6$* have been previously reported[105]. Site-directed mutagenesis was used to generate LptD C-terminal truncation and LptD surface entropy reduction constructs using primers from Table 5 and pET23/42*ClptD* as the initial template. Briefly, the entire template was amplified by PCR and the resulting PCR product mixture digested with DpnI for >1 h at 37°C. NovaBlue (Novagen) cells were transformed with 1 μl of digested PCR product and plated onto LB plates containing 50 μg/ml carbenicillin. For each construct, plasmids from six colonies were isolated and sequenced.

Table 5. Primers used to construct plasmids encoding C-terminally truncated *lptD* and surface entropy reduction mutants of *lptD*.

Name	Sequence
LptDΔ760-784 F	5'-CATCGAACTTCGCGGCTAGAGCTCCAACTACGGTC-3'
LptDΔ760-784 R	5'-GACCGTAGTTGGAGCTCTAGCCGCGAAGTTCGATG-3'
LptDΔ714-784 F	5'-CACCAATGCTAACAAGCAAGCCTAATCTATGTTAGGTGTGC-3'
LptDΔ714-784 R	5'-GCACACCTAACATAGATTAGGCTTGCTTGTTAGCATTGGTG-3'
LptD K711A/Q712A F	5'-CTACGACACCAATGCTAACGCGGCAGCCGACTCTATGTTAGG-3'
LptD K711A/Q712A R	5'-CCTAACATAGAGTCGGCTGCCGCGTTAGCATTGGTGTCGTAG-3'

4.3.6. Crystallization

For screening of crystallization conditions, purified protein was prepared as above and concentrated to an appropriate concentration (generally 10-35 mg/ml). The protein sample was dispensed using a Formulatrix NT8 drop-setting robot into 96-well sitting drop crystallization

plates (MRC 3 well crystallization plate, Swissci). Crystallization droplets contained 150 nl

protein and 150 nl precipitant solution, and the reservoir solution contained 30 µl of the

precipitant solution. The following crystallization screens were routinely used: Clear Strategy I

and II, MemGold I and II, and MemPlus (all from Molecular Dimensions). Plates were stored at

either 4°C or 19°C and imaged in a crystallization hotel (Formulatrix).

Larger scale crystallization was set by hand in 24-well sitting drop Cryschem

crystallization plates (Hampton). The precipitant solution was made by hand from individual

components. The reservoir of each well was filled with 750 µl of the precipitant solution.

Various droplet volumes were used; 1 µl to 1 µl, 2 µl to 2 µl, 1 µl to 2 µl, 2 µl to 1 µl, 1 µl to 3

µl, and 3 µl to 1 µl of protein to precipitant were used. Grid-like variation of the precipitant

condition was typically done when scaling up crystallization experiments (e.g. using more or less

PEG in 1% steps).

Additive screening was conducted using an additive screen from Hampton Research in a

96 well fashion, as described above. The additive screen was mixed 1:10 with 400 mM KSCN,

100 mM sodium acetate, pH 4.5, and either 11% or 15% PEG 4K to form the precipitant for the

condition being screened. When LPS molecules were used as additives, they were added at

concentration of 10 mM, with the exception of Lipid A (1 mM), wild-type LPS (10 mg/ml), and

LPS from *ΔlpxL* (1 mM).

The MemMagic Bicelle Screen Kit (Molecular Dimensions) was used when screening

bicelle solubilized protein. In short, OG or C_8E_4 solubilized protein was mixed 4:1 with either

40%, 35%, 30%, or 25% DMPC:CHAPSO (2.8:1) and incubated on ice for at least 30 minutes

prior to pipetting. 25% bicelles was used for the crystals that yielded the 3.85 Å data set.

Crystals were cryoprotected by gradual addition of a cryoprotectant solution consisting of 1% C_8E_4, 70 mM acid acid/NaOH pH 4.5, 0.42 M KSCN, 7% PEG 4K, and 30% glycerol. Crystals were mounted into loops and frozen by direct immersion into liquid nitrogen.

4.3.7. Collection of diffraction data

Screening for X-ray diffraction and collection of diffraction data occurred at Brookhaven National Laboratory National Synchrotron Light Source II (NSLS-II), Argonne National Laboratory Advanced Photon Source (APS), and Lawrence Berkeley National Laboratory Advanced Light Source (ALS).

4.3.8. Data processing and molecular replacement

X-ray diffraction data were integrated using MOSFLM[145] and scaled using SCALA[146]. Subsequently, molecular replacement was run using Phaser[147] within the CCP4 crystallographic software suite[148].

4.3.9. Production of selenomethionine labeled protein

M9 minimal media was used for overexpression of selenomethionine labeled protein. It is prepared by first preparing 5x M9 salts by dissolving 256 g $Na_2HPO_4 \cdot 7H_2O$, 60 g KH_2PO_4, 10 g NaCl, and 20 g NH_4Cl in 4 l deionized water. 300 ml of 5x M9 salts is diluted to 1.5 l in a 4 l flask and autoclaved. Once cool, and when ready for use, it is supplemented with 0.4% glucose, 2 mM $MgSO_4$, 0.1 mM $CaCl_2$, vitamins, and trace metals. The vitamin solution is prepared as a 1000x stock solution by dissolving 0.5 g riboflavin, 0.5 g niacin, 0.5 pyridoxine monohydrate, and 0.5 g thiamine in 500 ml water. The trace metals solution is prepared as a 100x stock by

dissolving 5 g EDTA, 0.8 g $FeCl_3$, 0.05 g $ZnCl_2$, 0.01 g $CuCl_2$, 0.01 g $CoCl_2$, 0.01 g HBO_3, 1.6 g $MnCl_2$, 0.01 g Ni_2SO_4, and 0.01 g molybdic acid in 1 l deionized water (in that order) and adjusting the pH to 7.0 with NaOH. Glucose, $CaCl_2$, $MgSO_4$, vitamins, and trace metal stock solutions all must be sterile filtered prior to use.

The overexpression of selenomethionine labeled protein was adapted from previously reported protocols[149]. The BL21(λDE3) *ΔcyoA-E::kan* pET23/42*ClptD-His$_8$* pCDF*lptE* strain was grown on LB-agar (supplemented with 50 µg/ml carbenicillin, 50 µg/ml streptomycin, 25 µg/ml kanamycin, and 0.2% glucose) overnight at 37°C. Colonies from the plate were used to inoculate an appropriate number of 10 ml starter cultures (M9 minimum medium, supplemented with glucose, $MgSO_4$, vitamins, trace metals, $CaCl_2$, 50 µg/ml carbenicillin, 50 µg/ml streptomycin, and 25 µg/ml kanamycin), which were grown at 37°C until OD_{600} ~ 0.6. At this point, 10 ml of starter culture was used to inoculate each 1.5 l culture (M9 minimum medium, supplemented with glucose, $MgSO_4$, vitamins, trace metals, $CaCl_2$, 100 µg/ml carbenicillin, 50 µg/ml streptomycin, and 25 µg/ml kanamycin). The 1.5 l cultures were grown at 37°C with shaking at 220 rpm until OD_{600} ~ 0.15, at which point the temperature was reduced to 26°C and the shaking speed was reduced to 180 rpm. At OD_{600} ~ 0.3, 0.15 g L-lysine (Sigma), 0.15 g L-threonine (Sigma), 0.15 g L-phenylalanine (Sigma), 0.075 g L-leucine (Sigma), 0.075 g L-isoleucine (Sigma), 0.075 g L-valine (Sigma), and 0.075 g L-selenomethonine (Tokyo Chemical Industry Co., TCI) were individually added to each 1.5 l culture. At OD_{600} ~ 0.6, and at least 30 minutes following amino acid addition, 0.1 mM IPTG was added to each culture. The cultures were then grown for 20 hr and processed as usual.

4.3.10. Heavy atom screening

The gel shift assay was conducted as previously reported[150]. In brief, 35 mg/ml protein was incubated in 10 μl reactions with 5 mM heavy atom compound in the dark for 2 hr. The heavy atom compounds were prepared freshly as a 50 mM stock solution in the same buffer as the protein. All heavy atom compounds were from heavy atom screens available from Hampton Research. 1 mM DTT was added to reactions containing mercury in order to assure that the cysteine residues were reduced. 4 μl from each reaction was combined with 4 μl native gel loading buffer (62 mM Tris-HCl, pH 6.8, 1% bromophenol blue, 25% glycerol, 0.8% C_8E_4). The samples were run on 4-20% gradient acrylamide gels for 3 hours at 150 V at 4°C. The gel running buffer was supplemented with detergent (25 mM Tris-base, 192 mM Glycine, 0.8% C_8E_4).

Heavy atom derivatives of LptD/E crystals were produced by adding a solution containing 1 mM TCEP for 5 min followed by 5 mM $HgCl_2$ for 15 minutes. Both solutes were freshly prepared and were dissolved in a cryoprotectant solution consisting of 1% C8E4, 70 mM acetic acid/NaOH pH 4.5, 0.42 mM KSCN, 7% PEG 4K, and 30% glycerol. Crystals were then mounted into loops and frozen by direct immersion in liquid nitrogen.

References

1   Gan, L., Chen, S. & Jensen, G. J. Molecular organization of Gram-negative peptidoglycan. *Proceedings of the National Academy of Sciences of the United States of America* **105**, 18953-18957, doi:10.1073/pnas.0808035105 (2008).

2   Vollmer, W. & Holtje, J. V. The architecture of the murein (peptidoglycan) in gram-negative bacteria: vertical scaffold or horizontal layer(s)? *Journal of bacteriology* **186**, 5978-5987, doi:10.1128/JB.186.18.5978-5987.2004 (2004).

3   Nikaido, H. Molecular Basis of Bacterial Outer Membrane Permeability Revisited. *Microbiology and Molecular Biology Reviews* **67**, 593-656, doi:10.1128/mmbr.67.4.593-656.2003 (2003).

4   Raetz, C. R. & Whitfield, C. Lipopolysaccharide endotoxins. *Annual review of biochemistry* **71**, 635-700, doi:10.1146/annurev.biochem.71.110601.135414 (2002).

5   Plesiat, P. & Nikaido, H. Outer membranes of Gram-negative bacteria are permeable to steroid probes. *Molecular microbiology* **6**, 1323-1333 (1992).

6   Plesiat, P., Aires, J. R., Godard, C. & Köhler, T. Use of steroids to monitor alterations in the outer membrane of Pseudomonas aeruginosa. *Journal of bacteriology* **179**, 7004-7010 (1997).

7   Raetz, C. R. Biochemistry of endotoxins. *Annual review of biochemistry* **59**, 129-170 (1990).

8   Poltorak, A. Defective LPS Signaling in C3H/HeJ and C57BL/10ScCr Mice: Mutations in Tlr4 Gene. *Science* **282**, 2085-2088, doi:10.1126/science.282.5396.2085 (1998).

9   Hoshino, K. *et al.* Cutting edge: Toll-like receptor 4 (TLR4)-deficient mice are hyporesponsive to lipopolysaccharide: evidence for TLR4 as the Lps gene product. *The Journal of Immunology* **162**, 3749-3752 (1999).

10   MÜHLRADT, P. F. & GOLECKI, J. R. Asymmetrical distribution and artifactual reorientation of lipopolysaccharide in the outer membrane bilayer of Salmonella typhimurium. *European Journal of Biochemistry* **51**, 343-352 (1975).

11   Kamio, Y. & Nikaido, H. Outer membrane of Salmonella typhimurium: accessibility of phospholipid head groups to phospholipase c and cyanogen bromide activated dextran in the external medium. *Biochemistry* **15**, 2561-2570 (1976).

12   Funahara, Y. & Nikaido, H. Asymmetric localization of lipopolysaccharides on the outer membrane of Salmonella typhimurium. *Journal of bacteriology* **141**, 1463-1465 (1980).

13   Bos, M. P., Robert, V. & Tommassen, J. Biogenesis of the gram-negative bacterial outer membrane. *Annual review of microbiology* **61**, 191-214, doi:10.1146/annurev.micro.61.080706.093245 (2007).

14   Suzuki, H. *et al.* Murein-lipoprotein of Escherichia coli: a protein involved in the stabilization of bacterial cell envelope. *Molecular and General Genetics MGG* **167**, 1-9 (1978).

15   Cascales, E., Bernadac, A., Gavioli, M., Lazzaroni, J. C. & Lloubes, R. Pal Lipoprotein of Escherichia coli Plays a Major Role in Outer Membrane Integrity. *Journal of bacteriology* **184**, 754-759, doi:10.1128/jb.184.3.754-759.2002 (2002).

16   Ruiz, N., Kahne, D. & Silhavy, T. J. Transport of lipopolysaccharide across the cell envelope: the long road of discovery. *Nature reviews. Microbiology* **7**, 677-683, doi:10.1038/nrmicro2184 (2009).

17   Schulz, G. E. The structure of bacterial outer membrane proteins. *Biochimica et Biophysica Acta (BBA) - Biomembranes* **1565**, 308-317, doi:http://dx.doi.org/10.1016/S0005-2736(02)00577-1 (2002).

18   Malinverni, J. C. & Silhavy, T. J. An ABC transport system that maintains lipid asymmetry in the gram-negative outer membrane. *Proceedings of the National Academy of Sciences of the United States of America* **106**, 8009-8014, doi:10.1073/pnas.0903229106 (2009).

19   Lugtenberg, E. & Peters, R. Distribution of lipids in cytoplasmic and outer membranes of< i> Escherichia coli</i> K12. *Biochimica et Biophysica Acta (BBA)-Lipids and Lipid Metabolism* **441**, 38-47 (1976).

20   ISHINAGA, M. & KANAMOTO, R. Distribution of phospholipid molecular species in outer and cytoplasmic membranes of Escherichia coli. *Journal of biochemistry* **86**, 161-165 (1979).

21   White, D. A., Lennarz, W. & Schnaitman, C. A. Distribution of lipids in the wall and cytoplasmic membrane subfractions of the cell envelope of Escherichia coli. *Journal of bacteriology* **109**, 686-690 (1972).

22   Tefsen, B., Geurtsen, J., Beckers, F., Tommassen, J. & de Cock, H. Lipopolysaccharide transport to the bacterial outer membrane in spheroplasts. *The Journal of biological chemistry* **280**, 4504-4509, doi:10.1074/jbc.M409259200 (2005).

23   Jones, N. C. & Osborn, M. Translocation of phospholipids between the outer and inner membranes of Salmonella typhimurium. *Journal of Biological Chemistry* **252**, 7405-7412 (1977).

24   Langley, K., Hawrot, E. & Kennedy, E. Membrane assembly: movement of phosphatidylserine between the cytoplasmic and outer membranes of Escherichia coli. *Journal of bacteriology* **152**, 1033-1041 (1982).

25   Donohue-Rolfe, A. M. & Schaechter, M. Translocation of phospholipids from the inner to the outer membrane of Escherichia coli. *Proceedings of the National Academy of Sciences* **77**, 1867-1871 (1980).

26   Papanikou, E., Karamanou, S. & Economou, A. Bacterial protein secretion through the translocase nanomachine. *Nature reviews. Microbiology* **5**, 839-851, doi:10.1038/nrmicro1771 (2007).

27   Tokuda, H. Biogenesis of Outer Membranes in Gram-Negative Bacteria. *Bioscience, Biotechnology, and Biochemistry* **73**, 465-473, doi:10.1271/bbb.80778 (2009).

28   Yamaguchi, K., Yu, F. & Inouye, M. A single amino acid determinant of the membrane localization of lipoproteins in E. coli. *Cell* **53**, 423-432 (1988).

29   Gennity, J. M. & Inouye, M. The protein sequence responsible for lipoprotein membrane localization in Escherichia coli exhibits remarkable specificity. *Journal of Biological Chemistry* **266**, 16458-16464 (1991).

30   Seydel, A., Gounon, P. & Pugsley, A. P. Testing the '+ 2 rule' for lipoprotein sorting in the Escherichia coli cell envelope with a new genetic selection. *Molecular microbiology* **34**, 810-821 (1999).

31   Terada, M., Kuroda, T., Matsuyama, S. I. & Tokuda, H. Lipoprotein sorting signals evaluated as the LolA-dependent release of lipoproteins from the cytoplasmic membrane of Escherichia coli. *The Journal of biological chemistry* **276**, 47690-47694, doi:10.1074/jbc.M109307200 (2001).

32   Matsuyama, S., Tajima, T. & Tokuda, H. A novel periplasmic carrier protein involved in the sorting and transport of Escherichia coli lipoproteins destined for the outer membrane. *The EMBO journal* **14**, 3365 (1995).

33   Matsuyama, S. i., Yokota, N. & Tokuda, H. A novel outer membrane lipoprotein, LolB (HemM), involved in the LolA (p20)-dependent localization of lipoproteins to the outer membrane of Escherichia coli. *The EMBO journal* **16**, 6947-6955 (1997).

34   Yakushi, T. LolA-dependent Release of a Lipid-modified Protein from the Inner Membrane of Escherichia coli Requires Nucleoside Triphosphate. *Journal of Biological Chemistry* **273**, 32576-32581, doi:10.1074/jbc.273.49.32576 (1998).

35   Yakushi, T., Masuda, K., Narita, S.-i., Matsuyama, S.-i. & Tokuda, H. A new ABC transporter mediating the detachment of lipid-modified proteins from membranes. *Nature cell biology* **2**, 212-218 (2000).

36   Masuda, K., Matsuyama, S. & Tokuda, H. Elucidation of the function of lipoprotein-sorting signals that determine membrane localization. *Proceedings of the National Academy of Sciences of the United States of America* **99**, 7390-7395, doi:10.1073/pnas.112085599 (2002).

37   Hara, T., Matsuyama, S. & Tokuda, H. Mechanism underlying the inner membrane retention of Escherichia coli lipoproteins caused by Lol avoidance signals. *The Journal of biological chemistry* **278**, 40408-40414, doi:10.1074/jbc.M307836200 (2003).

38   Fukuda, A. *et al.* Aminoacylation of the N-terminal cysteine is essential for Lol-dependent release of lipoproteins from membranes but does not depend on lipoprotein sorting signals. *The Journal of biological chemistry* **277**, 43512-43518, doi:10.1074/jbc.M206816200 (2002).

39   Yokota, N., Kuroda, T., Matsuyama, S.-i. & Tokuda, H. Characterization of the LolA-LolB system as the general lipoprotein localization mechanism of Escherichia coli. *Journal of Biological Chemistry* **274**, 30995-30999 (1999).

40   Takeda, K. *et al.* Crystal structures of bacterial lipoprotein localization factors, LolA and LolB. *The EMBO journal* **22**, 3199-3209 (2003).

41   Okuda, S. & Tokuda, H. Model of mouth-to-mouth transfer of bacterial lipoproteins through inner membrane LolC, periplasmic LolA, and outer membrane LolB. *Proceedings of the National Academy of Sciences of the United States of America* **106**, 5877-5882, doi:10.1073/pnas.0900896106 (2009).

42   Taniguchi, N., Matsuyama, S. & Tokuda, H. Mechanisms underlying energy-independent transfer of lipoproteins from LolA to LolB, which have similar unclosed {beta}-barrel structures. *The Journal of biological chemistry* **280**, 34481-34488, doi:10.1074/jbc.M507388200 (2005).

43   Knowles, T. J., Scott-Tucker, A., Overduin, M. & Henderson, I. R. Membrane protein architects: the role of the BAM complex in outer membrane protein assembly. *Nature reviews. Microbiology* **7**, 206-214, doi:10.1038/nrmicro2069 (2009).

44   Kim, K. H., Aulakh, S. & Paetzel, M. The bacterial outer membrane beta-barrel assembly machinery. *Protein science : a publication of the Protein Society* **21**, 751-768, doi:10.1002/pro.2069 (2012).

45   Sklar, J. G., Wu, T., Kahne, D. & Silhavy, T. J. Defining the roles of the periplasmic chaperones SurA, Skp, and DegP in Escherichia coli. *Genes & development* **21**, 2473-2484, doi:10.1101/gad.1581007 (2007).

46   Volokhina, E. B. *et al.* Role of the periplasmic chaperones Skp, SurA, and DegQ in outer membrane protein biogenesis in Neisseria meningitidis. *Journal of bacteriology* **193**, 1612-1621, doi:10.1128/JB.00532-10 (2011).

47   Wu, T. *et al.* Identification of a Multicomponent Complex Required for Outer Membrane Biogenesis in< i> Escherichia coli</i>. *Cell* **121**, 235-245 (2005).

48   Voulhoux, R., Bos, M. P., Geurtsen, J., Mols, M. & Tommassen, J. Role of a highly conserved bacterial protein in outer membrane protein assembly. *Science* **299**, 262-265 (2003).

49   Werner, J. & Misra, R. YaeT (Omp85) affects the assembly of lipid-dependent and lipid-independent outer membrane proteins of Escherichia coli. *Molecular microbiology* **57**, 1450-1459 (2005).

50   Doerrler, W. T. & Raetz, C. R. Loss of outer membrane proteins without inhibition of lipid export in an Escherichia coli YaeT mutant. *Journal of Biological Chemistry* **280**, 27679-27687 (2005).

51   Bos, M. P., Tefsen, B., Geurtsen, J. & Tommassen, J. Identification of an outer membrane protein required for the transport of lipopolysaccharide to the bacterial cell surface. *Proceedings of the National Academy of Sciences of the United States of America* **101**, 9417-9422 (2004).

52   Sánchez-Pulido, L., Devos, D., Genevrois, S., Vicente, M. & Valencia, A. POTRA: a conserved domain in the FtsQ family and a class of β-barrel outer membrane proteins. *Trends in biochemical sciences* **28**, 523-526 (2003).

53   Kim, S. *et al.* Structure and function of an essential component of the outer membrane protein assembly machine. *Science* **317**, 961-964 (2007).

54   Knowles, T. J. *et al.* Fold and function of polypeptide transport-associated domains responsible for delivering unfolded proteins to membranes. *Molecular microbiology* **68**, 1216-1227 (2008).

55   Hagan, C. L., Kim, S. & Kahne, D. Reconstitution of outer membrane protein assembly from purified components. *Science* **328**, 890-892, doi:10.1126/science.1188919 (2010).

56   Hagan, C. L., Westwood, D. B. & Kahne, D. Bam lipoproteins assemble BamA in vitro. *Biochemistry* **52**, 6108-6113 (2013).

57   Hagan, C. L. & Kahne, D. The reconstituted Escherichia coli Bam complex catalyzes multiple rounds of β-barrel assembly. *Biochemistry* **50**, 7444-7446 (2011).

58   Noinaj, N. *et al.* Structural insight into the biogenesis of [bgr]-barrel membrane proteins. *Nature* **501**, 385-390 (2013).

59   Anderson, M. S. & Raetz, C. Biosynthesis of lipid A precursors in Escherichia coli. A cytoplasmic acyltransferase that converts UDP-N-acetylglucosamine to UDP-3-O-(R-3-hydroxymyristoyl)-N-acetylglucosamine. *Journal of Biological Chemistry* **262**, 5159-5169 (1987).

60   Anderson, M. S., Bulawa, C. E. & Raetz, C. The biosynthesis of gram-negative endotoxin. Formation of lipid A precursors from UDP-GlcNAc in extracts of Escherichia coli. *Journal of Biological Chemistry* **260**, 15536-15541 (1985).

61   Anderson, M. *et al.* UDP-N-acetylglucosamine acyltransferase of Escherichia coli. The first step of endotoxin biosynthesis is thermodynamically unfavorable. *Journal of Biological Chemistry* **268**, 19858-19865 (1993).

110

62	Anderson, M. S., Robertson, A. D., Macher, I. & Raetz, C. R. Biosynthesis of lipid A in Escherichia coli: identification of UDP-3-O-[(R)-3-hydroxymyristoyl]-. alpha.-D-glucosamine as a precursor of UDP-N2, O3-bis [(R)-3-hydroxymyristoyl]-. alpha.-D-glucosamine. *Biochemistry* **27**, 1908-1917 (1988).

63	Young, K. *et al.* The envA permeability/cell division gene of Escherichia coli encodes the second enzyme of lipid A biosynthesis UDP-3-O-(R-3-hydroxymyristoyl)-N-acetylglucosamine deacetylase. *Journal of Biological Chemistry* **270**, 30384-30391 (1995).

64	Kelly, T., Stachula, S., Raetz, C. & Anderson, M. The firA gene of Escherichia coli encodes UDP-3-O-(R-3-hydroxymyristoyl)-glucosamine N-acyltransferase. The third step of endotoxin biosynthesis. *Journal of Biological Chemistry* **268**, 19866-19874 (1993).

65	Babinski, K. J., Kanjilal, S. J. & Raetz, C. R. Accumulation of the lipid A precursor UDP-2, 3-diacylglucosamine in an Escherichia coli mutant lacking the lpxH gene. *Journal of Biological Chemistry* **277**, 25947-25956 (2002).

66	Babinski, K. J., Ribeiro, A. A. & Raetz, C. R. The Escherichia coli gene encoding the UDP-2, 3-diacylglucosamine pyrophosphatase of lipid A biosynthesis. *Journal of Biological Chemistry* **277**, 25937-25946 (2002).

67	Metzger IV, L. E. & Raetz, C. R. Purification and characterization of the lipid A disaccharide synthase (LpxB) from Escherichia coli, a peripheral membrane protein. *Biochemistry* **48**, 11559-11571 (2009).

68	Ray, B. & Raetz, C. The biosynthesis of gram-negative endotoxin. A novel kinase in Escherichia coli membranes that incorporates the 4'-phosphate of lipid A. *Journal of Biological Chemistry* **262**, 1122-1128 (1987).

69	Garrett, T. A., Kadrmas, J. L. & Raetz, C. R. Identification of the Gene Encoding the Escherichia coli Lipid A 4′-Kinase FACILE PHOSPHORYLATION OF ENDOTOXIN ANALOGS WITH RECOMBINANT LpxK. *Journal of Biological Chemistry* **272**, 21855-21864 (1997).

70	Clementz, T. & Raetz, C. A gene coding for 3-deoxy-D-manno-octulosonic-acid transferase in Escherichia coli. Identification, mapping, cloning, and sequencing. *Journal of Biological Chemistry* **266**, 9687-9696 (1991).

71	Belunis, C. & Raetz, C. Biosynthesis of endotoxins. Purification and catalytic properties of 3-deoxy-D-manno-octulosonic acid transferase from Escherichia coli. *Journal of Biological Chemistry* **267**, 9988-9997 (1992).

72	Six, D. A., Carty, S. M., Guan, Z. & Raetz, C. R. Purification and Mutagenesis of LpxL, the Lauroyltransferase of Escherichia coli Lipid A Biosynthesis†. *Biochemistry* **47**, 8623-8637 (2008).

73   Brozek, K. A. & Raetz, C. Biosynthesis of lipid A in Escherichia coli. Acyl carrier protein-dependent incorporation of laurate and myristate. *Journal of Biological Chemistry* **265**, 15410-15417 (1990).

74   Meredith, T. C., Aggarwal, P., Mamat, U., Lindner, B. & Woodard, R. W. Redefining the requisite lipopolysaccharide structure in Escherichia coli. *ACS chemical biology* **1**, 33-42 (2006).

75   Mamat, U. *et al.* Single amino acid substitutions in either YhjD or MsbA confer viability to 3-deoxy-d-manno-oct-2-ulosonic acid-depleted Escherichia coli. *Molecular microbiology* **67**, 633-648 (2008).

76   Klein, G., Lindner, B., Brabetz, W., Brade, H. & Raina, S. Escherichia coli K-12 Suppressor-free Mutants Lacking Early Glycosyltransferases and Late Acyltransferases MINIMAL LIPOPOLYSACCHARIDE STRUCTURE AND INDUCTION OF ENVELOPE STRESS RESPONSE. *Journal of biological chemistry* **284**, 15369-15389 (2009).

77   Wang, X. & Quinn, P. J. Lipopolysaccharide: Biosynthetic pathway and structure modification. *Progress in lipid research* **49**, 97-107, doi:10.1016/j.plipres.2009.06.002 (2010).

78   Roncero, C. & Casadaban, M. J. Genetic analysis of the genes involved in synthesis of the lipopolysaccharide core in Escherichia coli K-12: three operons in the rfa locus. *Journal of bacteriology* **174**, 3250-3260 (1992).

79   Schnaitman, C. A. & Klena, J. D. Genetics of lipopolysaccharide biosynthesis in enteric bacteria. *Microbiological reviews* **57**, 655-682 (1993).

80   Brozek, K. A., Hosaka, K., Robertson, A. & Raetz, C. Biosynthesis of lipopolysaccharide in Escherichia coli. Cytoplasmic enzymes that attach 3-deoxy-D-manno-octulosonic acid to lipid A. *Journal of Biological Chemistry* **264**, 6956-6966 (1989).

81   Whitfield, C. & Amor, P. A. Modulation of the surface architecture of Gram-negative bacteria by the action of surface polymer: lipid A–core ligase and by determinants of polymer chain length. *Molecular microbiology* **23**, 629-638 (1997).

82   Abeyrathne, P. D., Daniels, C., Poon, K. K., Matewish, M. J. & Lam, J. S. Functional characterization of WaaL, a ligase associated with linking O-antigen polysaccharide to the core of Pseudomonas aeruginosa lipopolysaccharide. *Journal of bacteriology* **187**, 3002-3012 (2005).

83   Wösten, M. M., Kox, L. F., Chamnongpol, S., Soncini, F. C. & Groisman, E. A. A signal transduction system that responds to extracellular iron. *Cell* **103**, 113-125 (2000).

84   Guo, L. *et al.* Regulation of lipid A modifications by Salmonella typhimurium virulence genes phoP-phoQ. *Science* **276**, 250-253 (1997).

85   Soncini, F. C., Vescovi, E. G., Solomon, F. & Groisman, E. A. Molecular basis of the magnesium deprivation response in Salmonella typhimurium: identification of PhoP-regulated genes. *Journal of bacteriology* **178**, 5092-5099 (1996).

86   Gunn, J. S., Ryan, S. S., Van Velkinburgh, J. C., Ernst, R. K. & Miller, S. I. Genetic and Functional Analysis of a PmrA-PmrB-Regulated Locus Necessary for Lipopolysaccharide Modification, Antimicrobial Peptide Resistance, and Oral Virulence of Salmonella entericaSerovar Typhimurium. *Infection and immunity* **68**, 6139-6146 (2000).

87   Breazeale, S. D., Ribeiro, A. A. & Raetz, C. R. Oxidative Decarboxylation of UDP-Glucuronic Acid in Extracts of Polymyxin-resistant Escherichia coli ORIGIN OF LIPID A SPECIES MODIFIED WITH 4-AMINO-4-DEOXY-l-ARABINOSE. *Journal of Biological Chemistry* **277**, 2886-2896 (2002).

88   Gatzeva-Topalova, P. Z., May, A. P. & Sousa, M. C. Crystal structure of Escherichia coli ArnA (PmrI) decarboxylase domain. A key enzyme for lipid A modification with 4-amino-4-deoxy-L-arabinose and polymyxin resistance. *Biochemistry* **43**, 13370-13379 (2004).

89   Groisman, E. A., Kayser, J. & Soncini, F. C. Regulation of polymyxin resistance and adaptation to low-Mg2+ environments. *Journal of bacteriology* **179**, 7040-7045 (1997).

90   Roland, K. L., Martin, L. E., Esther, C. R. & Spitznagel, J. K. Spontaneous pmrA mutants of Salmonella typhimurium LT2 define a new two-component regulatory system with a possible role in virulence. *Journal of bacteriology* **175**, 4154-4164 (1993).

91   Wang, X., Ribeiro, A. A., Guan, Z., Abraham, S. N. & Raetz, C. R. Attenuated virulence of a Francisella mutant lacking the lipid A 4′-phosphatase. *Proceedings of the National Academy of Sciences* **104**, 4136-4141 (2007).

92   Ahn, V. E. *et al.* A hydrocarbon ruler measures palmitate in the enzymatic acylation of endotoxin. *The EMBO journal* **23**, 2931-2941 (2004).

93   Kawasaki, K., Ernst, R. K. & Miller, S. I. 3-O-deacylation of lipid A by PagL, a PhoP/PhoQ-regulated deacylase of Salmonella typhimurium, modulates signaling through Toll-like receptor 4. *Journal of Biological Chemistry* **279**, 20044-20048 (2004).

94   Gibbons, H. S., Lin, S., Cotter, R. J. & Raetz, C. R. Oxygen Requirement for the Biosynthesis of theS-2-Hydroxymyristate Moiety in Salmonella typhimurium Lipid A FUNCTION OF LpxO, A NEW Fe2+/α-KETOGLUTARATE-DEPENDENT DIOXYGENASE HOMOLOGUE. *Journal of Biological Chemistry* **275**, 32940-32949 (2000).

95   Doerrler, W. T., Gibbons, H. S. & Raetz, C. R. MsbA-dependent translocation of lipids across the inner membrane of Escherichia coli. *Journal of Biological Chemistry* **279**, 45102-45109 (2004).

96   Karow, M. & Georgopoulos, C. The essential Escherichia coli msbA gene, a multicopy suppressor of null mutations in the htrB gene, is related to the universally conserved family of ATP-dependent translocators. *Molecular microbiology* **7**, 69-79 (1993).

97   Zhou, Z., White, K. A., Polissi, A., Georgopoulos, C. & Raetz, C. R. Function of Escherichia coli MsbA, an essential ABC family transporter, in lipid A and phospholipid biosynthesis. *Journal of Biological Chemistry* **273**, 12466-12475 (1998).

98   Doerrler, W. T. & Raetz, C. R. ATPase activity of the MsbA lipid flippase of Escherichia coli. *Journal of Biological Chemistry* **277**, 36697-36705 (2002).

99   Ward, A., Reyes, C. L., Yu, J., Roth, C. B. & Chang, G. Flexibility in the ABC transporter MsbA: Alternating access with a twist. *Proceedings of the National Academy of Sciences* **104**, 19005-19010 (2007).

100   Zou, P. & Mchaourab, H. S. Alternating access of the putative substrate-binding chamber in the ABC transporter MsbA. *Journal of molecular biology* **393**, 574-585 (2009).

101   Zou, P., Bortolus, M. & Mchaourab, H. S. Conformational cycle of the ABC transporter MsbA in liposomes: detailed analysis using double electron–electron resonance spectroscopy. *Journal of molecular biology* **393**, 586-597 (2009).

102   Ruiz, N., Gronenberg, L. S., Kahne, D. & Silhavy, T. J. Identification of two inner-membrane proteins required for the transport of lipopolysaccharide to the outer membrane of Escherichia coli. *Proceedings of the National Academy of Sciences of the United States of America* **105**, 5537-5542, doi:10.1073/pnas.0801196105 (2008).

103   Freinkman, E., Okuda, S., Ruiz, N. & Kahne, D. Regulated assembly of the transenvelope protein complex required for lipopolysaccharide export. *Biochemistry* **51**, 4800-4806 (2012).

104   Wu, T. *et al.* Identification of a protein complex that assembles lipopolysaccharide in the outer membrane of Escherichia coli. *Proceedings of the National Academy of Sciences of the United States of America* **103**, 11754-11759, doi:10.1073/pnas.0604744103 (2006).

105   Chng, S. S., Ruiz, N., Chimalakonda, G., Silhavy, T. J. & Kahne, D. Characterization of the two-protein complex in Escherichia coli responsible for lipopolysaccharide assembly at the outer membrane. *Proceedings of the National Academy of Sciences of the United States of America* **107**, 5363-5368, doi:10.1073/pnas.0912872107 (2010).

106   Freinkman, E., Chng, S.-S. & Kahne, D. The complex that inserts lipopolysaccharide into the bacterial outer membrane forms a two-protein plug-and-barrel. *Proceedings of the National Academy of Sciences* **108**, 2486-2491 (2011).

107   Sampson, B. A., Misra, R. & Benson, S. A. Identification and characterization of a new gene of Escherichia coli K-12 involved in outer membrane permeability. *Genetics* **122**, 491-501 (1989).

108   Braun, M. & Silhavy, T. J. Imp/OstA is required for cell envelope biogenesis in Escherichia coli. *Molecular microbiology* **45**, 1289-1302 (2002).

109   Steeghs, L. *et al.* Meningitis bacterium is viable without endotoxin. *Nature* **392**, 449-449 (1998).

110   Moffatt, J. H. *et al.* Colistin resistance in Acinetobacter baumannii is mediated by complete loss of lipopolysaccharide production. *Antimicrobial agents and chemotherapy* **54**, 4971-4977 (2010).

111   Zhang, G., Meredith, T. C. & Kahne, D. On the essentiality of lipopolysaccharide to Gram-negative bacteria. *Current opinion in microbiology* **16**, 779-785 (2013).

112   Chiu, H. C., Lin, T. L. & Wang, J. T. Identification and characterization of an organic solvent tolerance gene in Helicobacter pylori. *Helicobacter* **12**, 74-81 (2007).

113   Serina, S. *et al.* Scanning the< i> Escherichia coli</i> chromosome by random transposon mutagenesis and multiple phenotypic screening. *Research in microbiology* **155**, 692-701 (2004).

114   Sperandeo, P., Pozzi, C., Dehò, G. & Polissi, A. Non-essential KDO biosynthesis and new essential cell envelope biogenesis genes in the< i> Escherichia coli yrbG–yhbG</i> locus. *Research in microbiology* **157**, 547-558 (2006).

115   Sperandeo, P. *et al.* Characterization of lptA and lptB, two essential genes implicated in lipopolysaccharide transport to the outer membrane of Escherichia coli. *Journal of bacteriology* **189**, 244-253 (2007).

116   Sperandeo, P. *et al.* Functional analysis of the protein machinery required for transport of lipopolysaccharide to the outer membrane of Escherichia coli. *Journal of bacteriology* **190**, 4460-4469 (2008).

117   Suits, M. D., Sperandeo, P., Deho, G., Polissi, A. & Jia, Z. Novel structure of the conserved gram-negative lipopolysaccharide transport protein A and mutagenesis analysis. *Journal of molecular biology* **380**, 476-488, doi:10.1016/j.jmb.2008.04.045 (2008).

118   Tran, A. X., Dong, C. & Whitfield, C. Structure and functional analysis of LptC, a conserved membrane protein involved in the lipopolysaccharide export pathway in Escherichia coli. *The Journal of biological chemistry* **285**, 33529-33539, doi:10.1074/jbc.M110.144709 (2010).

119   Chng, S.-S., Gronenberg, L. S. & Kahne, D. Proteins required for lipopolysaccharide assembly in Escherichia coli form a transenvelope complex. *Biochemistry* **49**, 4565-4567 (2010).

120   Sperandeo, P. *et al.* New insights into the Lpt machinery for lipopolysaccharide transport to the cell surface: LptA-LptC interaction and LptA stability as sensors of a properly assembled transenvelope complex. *Journal of bacteriology* **193**, 1042-1053 (2011).

121   Gronenberg, L. S. & Kahne, D. Development of an activity assay for discovery of inhibitors of lipopolysaccharide transport. *Journal of the American Chemical Society* **132**, 2518-2519 (2010).

122   Sherman, D. J., Okuda, S., Denny, W. A. & Kahne, D. Validation of inhibitors of an ABC transporter required to transport lipopolysaccharide to the cell surface in Escherichia coli. *Bioorganic & Medicinal Chemistry* **21**, 4846-4851, doi:http://dx.doi.org/10.1016/j.bmc.2013.04.020 (2013).

123   Sherman, D. J. *et al.* Decoupling catalytic activity from biological function of the ATPase that powers lipopolysaccharide transport. *Proceedings of the National Academy of Sciences* **111**, 4982-4987 (2014).

124   Okuda, S., Freinkman, E. & Kahne, D. Cytoplasmic ATP hydrolysis powers transport of lipopolysaccharide across the periplasm in E. coli. *Science* **338**, 1214-1217 (2012).

125   Ruiz, N., Chng, S.-S., Hiniker, A., Kahne, D. & Silhavy, T. J. Nonconsecutive disulfide bond formation in an essential integral outer membrane protein. *Proceedings of the National Academy of Sciences* **107**, 12245-12250 (2010).

126   Kadokura, H., Tian, H., Zander, T., Bardwell, J. C. & Beckwith, J. Snapshots of DsbA in action: detection of proteins in the process of oxidative folding. *Science* **303**, 534-537 (2004).

127   Chimalakonda, G. *et al.* Lipoprotein LptE is required for the assembly of LptD by the beta-barrel assembly machine in the outer membrane of Escherichia coli. *Proceedings of the National Academy of Sciences of the United States of America* **108**, 2492-2497, doi:10.1073/pnas.1019089108 (2011).

128   Ruiz, N., Falcone, B., Kahne, D. & Silhavy, T. J. Chemical conditionality: A geneticstrategy to probe organelle assembly. *Cell* **121**, 307-317 (2005).

129   Ruiz, N., Wu, T., Kahne, D. & Silhavy, T. J. Probing the barrier function of the outer membrane with chemical conditionality. *ACS chemical biology* **1**, 385-395 (2006).

130   Srinivas, N. *et al.* Peptidomimetic antibiotics target outer-membrane biogenesis in Pseudomonas aeruginosa. *Science* **327**, 1010-1013, doi:10.1126/science.1182749 (2010).

131   Fischbach, M. A. & Walsh, C. T. Antibiotics for emerging pathogens. *Science* **325**, 1089-1093, doi:10.1126/science.1176667 (2009).

132   Onishi, H. R. *et al.* Antibacterial agents that inhibit lipid A biosynthesis. *Science* **274**, 980-982 (1996).

133   Barb, A. W. *et al.* Inhibition of lipid A biosynthesis as the primary mechanism of CHIR-090 antibiotic activity in Escherichia coli. *Biochemistry* **46**, 3793-3802, doi:10.1021/bi6025165 (2007).

134   Ureta, A. R., Endres, R. G., Wingreen, N. S. & Silhavy, T. J. Kinetic analysis of the assembly of the outer membrane protein LamB in Escherichia coli mutants each lacking a secretion or targeting factor in a different cellular compartment. *Journal of bacteriology* **189**, 446-454 (2007).

135   Silhavy, T. J., Berman, M. L. & Enquist, L. W. Experiments with gene fusions. (1984).

136   Kadokura, H. & Beckwith, J. Detecting folding intermediates of a protein as it passes through the bacterial translocation channel. *Cell* **138**, 1164-1173 (2009).

137   Kadokura, H. & Beckwith, J. Four cysteines of the membrane protein DsbB act in concert to oxidize its substrate DsbA. *The EMBO journal* **21**, 2354-2363 (2002).

138   Paxman, J. J. *et al.* The structure of the bacterial oxidoreductase enzyme DsbA in complex with a peptide reveals a basis for substrate specificity in the catalytic cycle of DsbA enzymes. *Journal of biological chemistry* **284**, 17835-17845 (2009).

139   Walter, T. S. *et al.* Lysine methylation as a routine rescue strategy for protein crystallization. *Structure* **14**, 1617-1622, doi:10.1016/j.str.2006.09.005 (2006).

140   Laemmli, U. K. Cleavage of structural proteins during the assembly of the head of bacteriophage T4. *Nature* **227**, 680-685 (1970).

141   Malojcic, G. *et al.* LptE binds to and alters the physical state of LPS to catalyze its assembly at the cell surface. *Proc Natl Acad Sci U S A (In Press)* (2014).

142   Bos, M. P. & Tommassen, J. The LptD chaperone LptE is not directly involved in lipopolysaccharide transport in Neisseria meningitidis. *The Journal of biological chemistry* **286**, 28688-28696, doi:10.1074/jbc.M111.239673 (2011).

143   Ujwal, R. & Bowie, J. U. Crystallizing membrane proteins using lipidic bicelles. *Methods* **55**, 337-341 (2011).

144   Datsenko, K. A. & Wanner, B. L. One-step inactivation of chromosomal genes in Escherichia coli K-12 using PCR products. *Proceedings of the National Academy of Sciences of the United States of America* **97**, 6640-6645, doi:10.1073/pnas.120163297 (2000).

145   Leslie, A. Integration of macromolecular diffraction data. *Acta Crystallographica Section D: Biological Crystallography* **55**, 1696-1702 (1999).

146   Evans, P. Data reduction. *CCP4 Daresbury Study Weekend DL/SCI/R34*, 114-122 (1993).

147   McCoy, A. J. *et al.* Phaser crystallographic software. *Journal of applied crystallography* **40**, 658-674 (2007).

148   Winn, M. D. *et al.* Overview of the CCP4 suite and current developments. *Acta Crystallographica Section D: Biological Crystallography* **67**, 235-242 (2011).

149   Van Duyne, G. D., Standaert, R. F., Karplus, P. A., Schreiber, S. L. & Clardy, J. Atomic structures of the human immunophilin FKBP-12 complexes with FK506 and rapamycin. *Journal of molecular biology* **229**, 105-124 (1993).

150   Boggon, T. J. & Shapiro, L. Screening for phasing atoms in protein crystallography. *Structure* **8**, R143-R149 (2000).